# Expedition 379T Preliminary Report

# Digging Deeper with the JR100: Extending high resolution paleoclimate records from the Chilean Margin to the Eemian

20 July–18 August 2019

**Samantha Bova, Yair Rosenthal, Laurel Childress,**

**and**

**Expedition 379T Scientists**

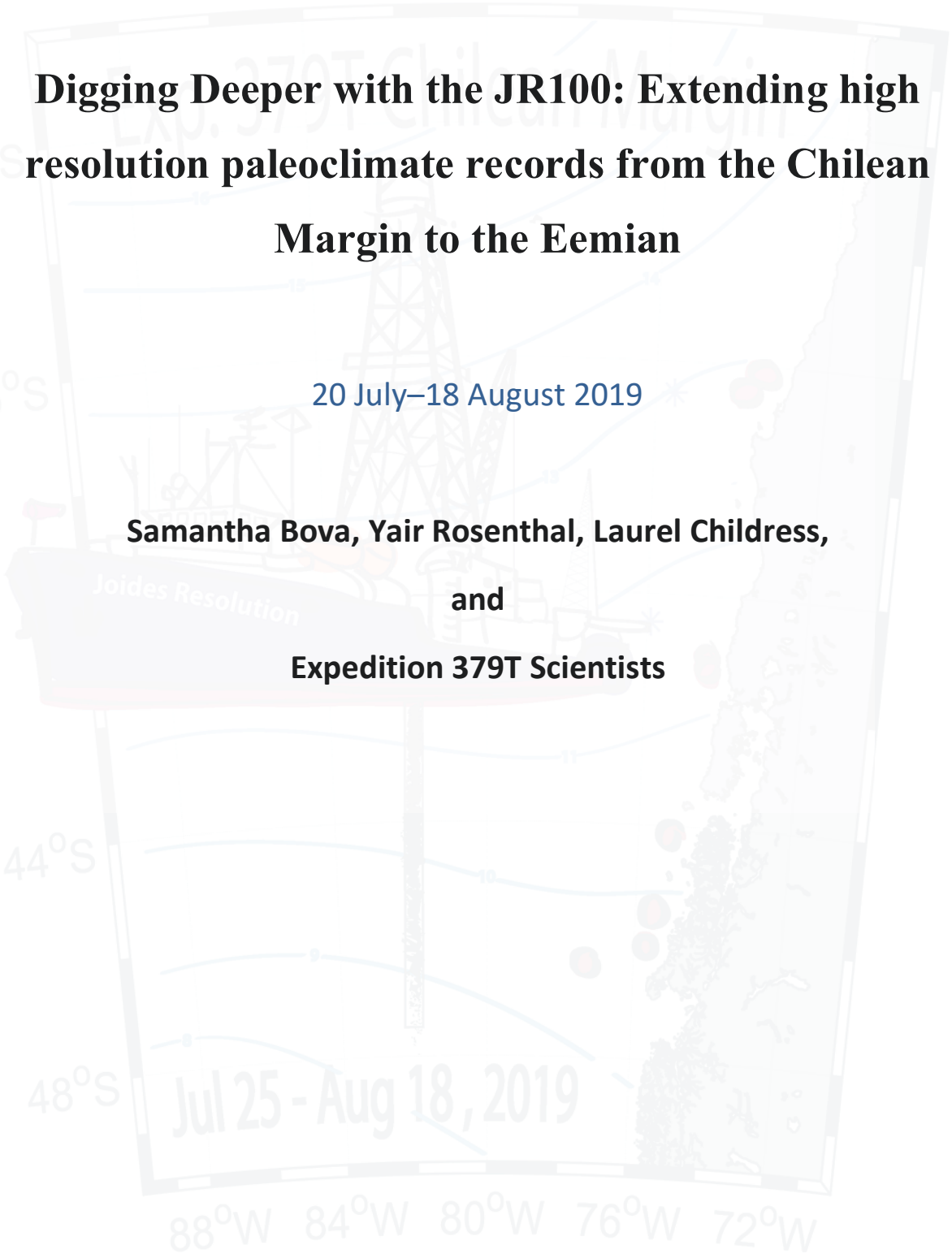

## Table of Contents

*Expedition Participants* ..... 5
*Abstract* ..... 6
*Introduction* ..... 7
**Oceanographic Setting** ..... 9
**Motivation for coring the Chilean Margin** ..... 10
Investigating (sub)millennial-scale climate variability along the Chilean Margin and its relation to equatorial Pacific and Northern Hemisphere climate ..... 11
Evaluating the sensitivity of the Patagonia icefields to regional and global climate change ..... 13
Assessing the density structure of the southeast Pacific during the LGM ..... 15
**Specific scientific objectives** ..... 16
**Specific outreach and education objectives** ..... 16
*J1001 Site Summary* ..... 17
**Background and Objectives** ..... 17
**Operations** ..... 19
Hole J1001A ..... 19
Hole J1001B ..... 20
Hole J1001C ..... 20
Hole J1001D ..... 21
Hole J1001E ..... 21
**Principal results** ..... 22
*J1002 Site Summary* ..... 27
**Background and Objectives** ..... 27
**Operations** ..... 28
Hole J1002A ..... 28
Hole J1002B ..... 29
Hole J1002C ..... 29
**Principal results** ..... 30
*J1003 Site Summary* ..... 35
**Background and Objectives** ..... 35
**Operations** ..... 36
Hole J1003A ..... 36
Hole J1003B ..... 37
**Principal results** ..... 38
*J1004 Site Summary* ..... 42
**Background and Objectives** ..... 42
**Operations** ..... 43
Hole J1004A ..... 43
Hole J1004B ..... 44
Hole J1004C ..... 45

**Principal results** ..... **45**

***J1005 Site Summary*** ..... ***49***

**Background and Objectives** ..... **49**

**Operations** ..... **50**
Hole J1005A ..... 51
Hole J1005B ..... 51
Hole J1005C ..... 52

**Principal results** ..... **52**

***J1006 Site Summary*** ..... ***57***

**Background and Objectives** ..... **57**

**Operations** ..... **58**
Hole J1006A ..... 58
Hole J1006B ..... 59
Hole J1006C ..... 59

**Principal results** ..... **60**

***J1007 Site Summary*** ..... ***64***

**Background and Objectives** ..... **64**

**Operations** ..... **65**
Hole J1007A ..... 65
Hole J1007B ..... 66
Hole J1007C ..... 66

**Principal results** ..... **67**

***J1008 Site Summary*** ..... ***71***

**Background and Objectives** ..... **71**

**Operations** ..... **72**
Hole J1008A ..... 72
Hole J1008B ..... 73
Hole J1008C ..... 73

**Principal results** ..... **73**

***Tables and Figures*** ..... ***79***

***References*** ..... ***99***

## Table of Figures:

*Figure F1. Map of sites cored during Expediton 379T/JR100.* 80
*Figure F2. Water mass cross section with coring locations.* 81
*Figure F3. Summary of coring operations and temporal resolution of Expedition 379T/JR100 core sites.* 82
*Figure F4. Location map of Sites J1001, J1002, J1003, and J1004.* 83
*Figure F5. Summary of Site J1001 results.* 84
*Figure F6. Age-depth plot for Site J1001.* 85
*Figure F7. Summary of Site J1002 results.* 86
*Figure F8. Summary of J1003 results.* 87
*Figure F9. Seismic Line near site J1003 showing prominent bottom seismic reflector.* 88
*Figure F10. Summary of J1004 results.* 89
*Figure F11. Location map of Sites J1005 and J1006.* 90
*Figure F12. Digital parasound data used to target sites J1005 and J1006.* 91
*Figure F13. Summary of J1005 results.* 92
*Figure F14. Summary of J1006 results.* 93
*Figure F15. Location map of Sites J1007 and J1008.* 94
*Figure F16. Summary of J1007 results.* 95
*Figure F17. Summary of J1008 results.* 96
*Figure F18. Age-depth plot for Site J1008.* 97
*Figure F19. Headspace methane concentrations at all eight sites cored during Expedition 379T.* 98

## Expedition Participants

**Co-chiefs:**

- Samantha Bova (postdoc, Rutgers, USA; samantha.bova@rutgers.edu)
- Yair Rosenthal (professor, Rutgers, USA; rosentha@marine.rutgers.edu)

**Expedition Project Manager:**

- Laurel Childress (JRSO/TAMU, USA; childress@iodp.tamu.edu)
- Emily Estes (JRSO/TAMU, USA; estes@iodp.tamu.edu)

**Sedimentologists:**

- Ivano Aiello (professor, Moss Landing Marine Labs, USA; iaiello@mlml.calstate.edu)
- Hailey Riechelson (graduate student, Rutgers, USA; hriechelson@marine.rutgers.edu)
- Chen Li (graduate student, Tongji U., China; 1532983@tongji.edu.en)
- Mark Yu (graduate student, Rutgers, USA; sdy10@eps.rutgers.edu)
- Julia Hagemann (graduate student, AWI, Germany; julia.hagemann@web.de)
- Beryl DeLong (graduate student, UCSC, USA; kimberly.delong@gmail.com)
- Sarah McGrath (graduate student, Brown, USA; sarah_mcgrath@brown.edu)
- Vincent Clementi (graduate student, Rutgers, USA; clementi@marine.rutgers.edu)
- Alejandro Avila (Lab Technician, U. of Concepcion, Chile; aavila@udec.cl)
- Yusuke Yokoyama (U. of Tokyo, Japan; yokoyama@aori.u-tokyo.ac.jp)
- Steve Goldstein (professor, LDEO, USA; steveg@ldeo.columbia.edu)

**Stratigraphic Correlation:**

- Jim Wright (professor, Rutgers, USA; jdwright@eps.rutgers.edu)
- Chris Charles (professor, UCSD-SIO, USA; ccharles@ucsd.edu)

**Physical Properties:**

- Jonathan Lambert (graduate student, LDEO, USA; lambert@ldeo.columbia.edu)
- Xiaojing Du (graduate student, U. of Michigan, USA; xjdu@umich.edu)
- Anya Hess (graduate student, Rutgers, USA; anya.hess@rutgers.edu)
- Shawn Taylor (graduate student, SUNY Binghamton, USA; staylor5@binghamton.edu)

**Inorganic geochemists:**

- Anson Cheung (graduate student, Brown, USA; anson_cheung@brown.edu)
- Adam Sproson (postdoc, U. of Tokyo, Japan; sproson@aori.u-tokyo.ac.jp)
- Yael Kiro (professor, Weizmann Institute, IL; ykiro@ldeo.columbia.edu or yael.kiro@weizmann.ac.il)
- Laura Haynes (postdoc, Rutgers, USA, llh131@gmail.com)

**Organic geochemists:**

- William Longo (postdoc, WHOI, USA; wlongo@whoi.edu)
- Becky Robinson (professor, URI, USA; rebecca_r@uri.edu)

**Micropaleontologists:**

- **Diatoms:** Isabel Dove (graduate student, URI; isabel_dove@my.uri.edu)
- **Nannofossils:** John Sarao (graduate student, TAMU, USA; john.sarao@tamu.edu)
- **Foraminifers:** Minda Monteagudo (graduate student, Georgia Tech, USA; minda.monteagudo@gatech.edu), Nil Irvali (postdoc, U. of Bergen, Norway; Nil.Irvali@uib.no)

**Paleomagnetics:**

- Rob Hatfield (professor, UFl, USA; rhatfield1@ufl.edu)
- Cristina Garcia Lasanta (Research Scientist, Western Washington Univ., USA; garcia52@wwu.edu)

**Apprentice marine techs:**

- Anna Golub (undergraduate student, Lafayette, USA; goluba@lafayette.edu)
- William Biggs (undergraduate student, Rutgers, USA; willbiggs@me.com)

**Chilean Observer:**

- Ursula Fuentes (SHOA, Chile; ursu.hauser.f@gmail.com)

## Abstract

Expedition 379T of the D/V JOIDES Resolution was the first in the new NSF funded JR100 program, intended to provide the US paleoceanographic community a new way for recovering long sediment records (up to 100 meters below seafloor) outside of the IODP program. As such, it bridges between the conventional coring capability on UNOLS ships and the deep sea drilling program. The primary objective of the expedition was to investigate links between oceanographic changes at the northern margin of the Antarctic Circumpolar Current and climate variability on the South American continent over the past few glacial-interglacial cycles, with a special emphasis on obtaining high-resolution records of the Eemian interval and the last two glacial terminations. Given very high sedimentation rates along the Chilean margins, the new cores will enable reconstruction of surface and intermediate water variability at centennial-to-millennial resolution, which will extend available records from previous coring expeditions (ODP Expedition 202), thus permitting comparison of Southern Hemisphere records of the Holocene and last interglacial (LIG- Eemian), terminations I and II, and the MIS 5e-5d glacial inception.

Eight sites were cored during Expedition 379T, recovering a total of 2232 m of sediment cores in 670–3055 m water depth with an average recovery of 101.8% during 14.62 days of on-site operations (Table T1). Despite delayed departure at Punta Arenas and several bad weather days that prevented us from coring some of the planned sites, we have achieved almost all the expedition objectives. The eight sites extend over a wide latitudinal distance (46-36°S) covering the modern transition from the Antarctic subpolar to the subtropical zones (Figure F1) as well as spanning water depths intersecting the Antarctic Intermediate Water (AAIW), Pacific Deep Water (PDW) and Circumpolar deep water (CPDW) water masses (Figure F2). Six of the sites are located on the Chilean margins at intermediate water depths (670-1534 mbsl) and the other

two sites are situated in deep water off the shelf (2032 and 3055 mbsl). Three holes were APC cored in all but one site (J1003 has only two holes) allowing for compositing complete splices for paleoceanographic reconstructions (Figure F3). Shipboard analyses of the sediment cores included determining properties including magnetic susceptibility (MS), gamma ray attenuation (GRA), natural gamma radiation (NGR), visual description and imaging, paleomagnetic measurements, and micropaleontology (foraminifers, nannofossil and diatoms). Low-resolution (1 per core) interstitial water samples were collected for shipboard elemental analysis at each site. In addition, high-resolution interstitial water samples (1 per section) were collected at each site for further shore-based isotopic and elemental investigations totaling 472 IW samples.

Of the 30 science-party members we had 15 graduate students and 7 postdocs, assisted by 6 senior scientists. All members of the science-party were trained in and carried out the shipboard analyses, and contributed to the interpretations and report writing. We adopted the report format used on IODP expeditions to ensure future users of the cores have all the necessary information to interpret the wealth of data collected onboard; we recommend that this be done on future JR100 expeditions. Finally, two undergraduate students were trained by the technical staff, and two Chilean observers both fully participated in the shipboard analyses. It is our opinion that the educational component is another important strength of the JR100 program.

## Introduction

The southeast Pacific is a complex and climatically important region. It is home to the largest temperate ice masses in the SH, the Northern and Southern Patagonia Icefields (NPI, SPI), which contribute a disproportionate amount to modern sea level rise relative to other mountain glaciers (Rignot et al., 2003; Glasser et al., 2011). Icefield loss is expected to continue into the future; global climate model simulations with double $CO_2$ predict a 2 to 4°C increase in regional air

temperatures by 2030-2050 and a decrease in precipitation (Carrasco et al., 2002; Vera et al., 2006; Cabre et al., 2010). The climate impacts of future ice loss from the Patagonia icefield remain uncertain, but will likely lead to significant variations in this region of the SH (Glasser et al., 2016), with potential implications to ocean circulation and the global climate.

Surface ocean conditions in the southeast Pacific exert primary control on southern South American climate and impact many other parts of the globe via oceanic and atmospheric teleconnections. Strong latitudinal gradients in sea surface temperature (SST) and sea surface salinity (SSS) (Figure F1) impact the strength and position of the Southern Westerly Winds (SWWs), which are linked to key modes of variability such as the Southern Annular Mode (SAM) and the El Niño Southern Oscillation (ENSO) (e.g. Hall and Visbek, 2002). SWWs variability driven by these mode changes or by large-scale shifts in global climate background state have far-reaching consequences for many climate modulators, including the strength of the Atlantic Meridional Overturning Circulation (AMOC) (Toggwelier and Samuels 1993; 1995, Russell et al., 2006a; 2006b; Sijp and England 2009), Southern Ocean stratification affecting the deep ocean carbon storage and hence atmospheric $pCO_2$ (e.g. Toggweiler et al., 2006, Anderson et al., 2009), pole-to-equator heat transport and interior ocean heat storage (Kalansky et al., 2015, Roemmich et al., 2015; Rosenthal et al., 2013, 2017) and nutrient supply to the equatorial regions (e.g. Hayes et al., 2011). The SWWs are also largely responsible for precipitation patterns on the western side of the Andes; north-south precipitation gradients are severe in southern South America transitioning from a semi-arid, winter-rain climate in central Chile to persistent hyper-humid conditions in the fjord region of southern Chile (Garreaud, 2007).

Rainfall and meltwater fluxes along the southern Chilean Margin may impact the temperature and salinity of key subsurface water masses Subantarctic Mode Water (SAMW) and Antarctic

Intermediate Water (AAIW) form from surface waters in the southeast Pacific and are responsible for ventilating the low latitude thermocline (Bostock et al., 2010; 2013). Change in their buoyancy via surface temperature and salinity variations in their formation zones will therefore lead to changes to the strength of upper ocean vertical stratification across vast areas of the global ocean (Bova et al., 2015; 2018 Schmidtko and Johnson, 2012; Graham et al., 2011). In turn, these changes can alter the ability of the ocean to sequester heat and carbon in the subsurface and thus to mitigate future climate change (Bova et al., 2015, Kalansky et al., 2015; Rosenthal et al., 2013, 2017, Schmidtko and Johnson, 2012; Umling and Thunnell, 2017). Periods of apparent high variability in these water masses detected in the eastern equatorial Pacific (EEP) during the Holocene have been attributed to strong eddy activity (Bova et al., 2016), but could also be explained by large influxes of freshwater to the surface ocean in the water mass source regions.

Extending over a large latitudinal gradient, the Chilean Margin is an ideal location to study variations in regional climate, expressed by changes in sea surface temperature and salinity as related to shifts in the position of the SWWs and its effects on regional precipitation and glacial stability (Figure F1). Additionally, the water depths of the cores collected during the expedition intersect the main water masses (Figure F2), which will allow us to assess the links between surface processes and changes in intermediate and deep water circulation and their extratropical effects.

## Oceanographic Setting

Sediment cores were collected along the Chilean Margin near the northern boundary of the Antarctic Circumpolar Current (ACC). The ACC is a key oceanographic feature that connects the ocean basins of the southern hemisphere and plays an important role in regional and global

climate. The ACC migrates seasonally, moving between ~50°S in summer and ~40-45°S in winter, following the N-S migration of the Southern Westerly Winds. At present, the ACC bifurcates at ~46°S sending Subantarctic surface water north via the Peru-Chile Current and south via the Cape Horn Current, which continues through the Drake Passage. This circulation sets up a series of sea surface fronts along the Chilean Margin characterized by strong latitudinal gradients in sea surface temperature (SST) and sea surface salinity (SSS), including the Polar, Subantarctic, and Subtropical Fronts located at 58°, 56°, and 35°S, respectively. The eight sites collected during the expedition are located between ~46 and 36°S and span the region between the ACC and the Subtropical Front (Figure F1).

Beneath the surface waters, the southeast Pacific is characterized by interweaving layers of northern and southern sourced waters characterized by relatively low and high oxygen levels, respectively. Just beneath the surface layer, the Gunther Undercurrent (GUC) flows poleward between ~100 and 400 m water, carrying low oxygen equatorial sourced water poleward. From 400 to 1200 m water depth, Antarctic Intermediate Water (AAIW) carries well-oxygenated Subantarctic surface waters equatorward. Beneath AAIW, we find another northern sourced low-oxygen water mass, Pacific Deep Water (PDW) and finally Circumpolar Deep Water occurs below ~2500 m water depth. The eight sites collected during the expedition intersect three of these water masses: AAIW, PDW, and CPDW (Figure F2).

## Motivation for coring the Chilean Margin

Paleoceanographic records from previous coring cruises to the Chilean Margin have uniquely contributed to our understanding of SH climate because they provide exceptional time resolution, not captured at most SH locations. However, the records from these cores are limited; while the exceptionally high sedimentation rates along the Chilean Margin provide excellent temporal

resolution, this comes at the expense of record length and foraminifer abundances. The JR100 provided the unique opportunity to capitalize on these "limitations". By coring multiple 100 m-long holes with the JOIDES Resolution at each location we obtained records ranging from ~15 to 800 ka, while maximizing foraminiferal abundances to enable stable isotope and trace metal studies so far not possible with single hole piston coring in this region. Sites targeted during the expedition lie between 36 and 46°S near the northern margin of the ACC and SWWs belt, mostly south of those collected during ODP Leg 202 and north of those collected on IODP Leg 383. These sites will allow us to address the following research themes.

### *Investigating (sub)millennial-scale climate variability along the Chilean Margin and its relation to equatorial Pacific and Northern Hemisphere climate*

One of the primary findings from ODP Leg 202 is the clear Antarctic timing in sea surface conditions along the Chilean Margin over the last 70 ky (Lamy et al., 2004; Kaiser et al., 2005; 2008; Caniupan et al., 2011). High sedimentation rates combined with excellent age control enabled millennial- and even centennial-scale direct comparisons to high latitude ice core records. Prior to ODP Leg 202, SH climate was considered an important global climate modulator on orbital timescales but millennial-scale climate variability was attributed almost exclusively to Northern Hemisphere (NH) ice sheet instabilities (e.g. Clark et al., 1999) and the associated impacts on the AMOC (Ganopolski and Rahmstorf, 2001; Clark et al., 2002; McManus et al., 2004). Results from Chilean Margin sediment core archives changed this view by providing some of the first and best evidence for millennial-scale climate change originating from the south.

Sediment cores from the southeast Pacific also demonstrate a close coupling between surface waters and subsurface mode / intermediate waters on millennial to centennial timescales. Euler

and Ninnemann (2010) find that SSTs at 41°S covary with temperatures at 851 m, within the heart of AAIW, over the past 1300 yr. The magnitude of the observed subsurface variability, though smaller than at the surface, suggests southeast Pacific surface anomalies can be transferred into the subsurface far faster than previously anticipated. Oxygenation and preformed nutrient content of these water masses are also highly sensitive to Subantarctic surface ocean conditions and Antarctic climate (Martinez et al., 2006; Robinson et al., 2007; Muratli et al., 2010b; De Pol-Holz et al., 2007). Finally, Robinson et al. (2007) found that denitrification rates in the southeast Pacific are in phase with Antarctic temperatures based on bulk sediment $\delta_{15}N$ records. This finding is supported by a subsequent study using redox sensitive metal concentrations at intermediate depths (Muratli et al., 2010b).

Oceanographic conditions along the Chilean Margin are not only sensitive to Southern Ocean climate variability but also effectively communicate these climate anomalies through ocean tunneling and/or via their impact on atmospheric circulation (Liu and Alexander, 2007). A clear correspondence to Antarctic climate can be seen in Eastern Equatorial Pacific (EEP) Mg/Ca sea surface temperature estimates over at least the last 275 ky (Pena et al., 2008; Lea et al., 2006). Thermocline and intermediate depth temperature estimates are in phase with Antarctic temperature change (Bova et al., unpublished; 2015; Moffa-Sanchez et al. 2019), with the earliest and largest increases occurring at 1000 m depth before propagating up towards the surface ocean (Bova et al., 2015). Furthermore, thermocline carbon isotopes in the EEP (Shackleton and Pisias, 1985; Spero and Lea, 2002; Pena et al., 2008) and equatorial Atlantic (Curry and Crowley, 1987) exhibit strong isotopic minima during Antarctic warm events of the last ~300 ky that can be directly correlated to surface records from the Subantarctic Pacific (Ninnemann and Charles, 1997). The most likely conduit for transporting high latitude change

into the EEP are Southern Ocean mode and intermediate waters, which form from surface waters in the southeast Pacific, just south of our proposed coring region and propagate northward. Change in their buoyancy via surface temperature and salinity variations along the Chilean Margin will therefore lead to changes to the strength of upper ocean vertical stratification that may feedback to local tropical dynamics (i.e. ENSO) on orbital and perhaps shorter timescales in intriguing ways (Pena et al., 2008).

Although we have excellent sub-millennial-scale records of the surface ocean in the southeast Pacific during the Holocene and last deglaciation (i.e. Lamy et al., 2001; 2002; 2004; 2010; Siani et al., 2010; Muralti et al., 2010a; Caniupan et al., 2011; Mohtadi et al., 2008; Robinson et al., 2009; Kim et al., 2002; Euler and Ninnemann, 2010; Collins et al., 2019), many important questions cannot be addressed with this material because the records are short and limited by foraminiferal abundances (Hebbeln et al., 2001; Mix et al., 2002; 2003; Kissel et al., 2007). High-resolution records of subsurface waters are particularly limited due to low benthic foraminifer abundances. It is therefore difficult to assess the role of the oceanic tunneling system in driving change in the equatorial Pacific even during the last deglaciation, let alone termination II and the MIS 5e to 5d transition. An outstanding question remains as to whether meltwater input from the Patagonia Icefields during deglaciations impacts the buoyancy of SAMW and AAIW. High resolution records from the EEP are available but we lack surface and subsurface records from the southeast Pacific at adequate resolution for comparison (e.g. Pena et al., 2008).

### *Evaluating the sensitivity of the Patagonia icefields to regional and global climate change*

Previous work on land (Lowell et al., 1995; Denton et al., 1999; Moreno et al., 2001; 2015; Shakun et al., 2015; Bendle et al, 2019), in the fjord systems (Bertrand et al., 2012a; 2012b), and using marine sediment records document chronologically well-constrained PIS meltwater events

during the last deglaciation and Holocene. Most importantly, they show that conditions over Patagonia during the last deglaciation and Holocene are in phase with offshore SSTs and thus Antarctic climate (Kim et al., 2002; Lamy et al., 2001; 2004; 2010; Pisias et al., 2006; Kaiser et al., 2005; 2007; 2008). This is shown most vividly by comparing marine SST records with records of vegetative change and weathering intensity on land. Pollen records indicate systematic latitudinal shifts in the zones of cool, mesic rainforests and warm, xeric vegetation in response to north-south movement of offshore frontal systems and associated shifts in the SWWs (Heusser et al., 2006; Kaiser et al., 2008). Grain size, clay mineralogy, and sediment geochemistry analyses of margin sediments indicate large changes in provenance and weathering intensity on the continent in phase with Antarctic ice core temperature records. These sedimentological changes are likely related to rainfall (aka the intensity and position of the SWWs) and/or fluctuations in the size and extent of the PIS (Lamy et al., 1998; 2001; 2002; 2004; 2010; Kaiser et al., 2007; Muratli et al., 2010a; Siani et al., 2010; Chase et al., 2014). Finally, foraminifer trace metal ratios are also sensitive to freshwater discharge; Rosenthal reconstructed the sea surface conditions during the last millennium from a high-resolution core MD07-3094, recovered at the same location as J1004, using Mg/Ca in *N. incompta* as a temperature proxy and Ba/Ca and Nd/Ca as proxies of riverine discharge to the coastal zone (Rosenthal – unpublished data). The records show a strong covariance between the hydrologic proxies (Ba/Ca and Nd/Ca), Mg/Ca-derived SST and the reconstruction of terrestrial temperature in southern Chile (PAGES 2k, 2013) all exhibiting a different pattern from the NH temperature reconstruction (Mann et al., 2008). This suggests high-sensitivity of the Patagonia glaciers to the regional climate conditions, although at this point we cannot rule out that changes in rainfall are the cause. Furthermore, although the Holocene is presently our only example for interglacial conditions along the Chilean Margin,

many studies find it is unique among past interglacials possibly due to anthropogenic affects (e.g. Ruddiman, 2003).

### *Assessing the density structure of the southeast Pacific during the LGM*

It has been three decades since the potential role of the polar ocean in controlling atmospheric $CO_2$ and thus global climate has been highlighted using simple model studies (Knox and and McElroy, 1984; Sarmiento and Toggweiler, 1984; Siegenthaler and Wenk, 1984), but the mechanisms behind it are still debated. Paleoceanographic records show strong synchroneity in climate variability in the EEP and in Antarctica and the Southern Ocean suggesting that the region plays a key role in both glacial inception and decay processes (e.g. Knorr and Lohmann, 2003; Anderson et al., 2009; Shakun et la., 2012; Adkins et al., 2013; Ferrari et al., 2014). However, this coupling cannot be explained solely by the radiative effect of $CO_2$ because Southern Ocean and EEP SST lead the change in atmospheric $CO_2$ during glacial inception (e.g. MIS 5e-5d) and terminations (e.g. Terminations I and II). Nevertheless, it has been suggested that cooling of Antarctic surface water might have contributed to establishing glacial climates by regulating the carbon uptake and storage capabilities of the deep ocean (Adkins et al., 2013; Ferrari et al., 2014). Pore water [$Cl^-$] and $\delta^{18}O$ combined with benthic foraminifer $\delta^{18}O$ data from the South Atlantic imply a stark change in deep water temperature and salinity properties that indicate Antarctic Bottom Water (AABW) was volumetrically expanded, colder, saltier and more isolated during the LGM relative to today (Adkins et al., 2002). Whether driven by equatorward movement of the permanent sea ice edge as suggested by Ferrari et al., (2014) or the temperature of upwelled deep water around the coast of Antarctica (Adkins et al., 2013), this configuration would act to draw down $CO_2$ from the atmosphere and cool climate globally. However, it remains to be determined if the LGM stratification documented in the South Atlantic was also a

feature of the South Pacific, reflecting a fundamentally different mode of deep ocean circulation than today, and what processes caused the reversal to interglacial circulation and the termination of glacial conditions.

## Specific scientific objectives

The objectives of the JR100-Expedition 379T include the following:

- Evaluate the sensitivity of the Patagonia icefield to regional and global climate change under different climate background conditions. For example, Holocene vs. Eemian climate records will highlight the icefield sensitivity to differences in orbital configuration and possible anthropogenic effects in the late Holocene.
- Reconstruct the evolution of sea surface temperature and salinity along the Chilean Margin and the impact of SWW variations and Patagonia icefield melt on regional surface ocean conditions
- Examine the impact of Southeast Pacific surface ocean temperature and salinity change on Southern Ocean intermediate water structure and dynamics.
- Document variations in intermediate and deep-water temperatures, heat content, and carbonate chemistry over the late Pleistocene glacial interglacial cycles
- Assess the links between southeast Pacific and equatorial Pacific climate change on millennial and orbital time scales and their relation to Northern Hemisphere records.
- Determine the density structure of the southeast Pacific Ocean during the LGM relative to the south Atlantic.

## Specific outreach and education objectives

The objectives of the JR100 expedition include the following:

- Provide early career participants seagoing experience and training in making and interpreting standard shipboard analyses

# J1001 Site Summary

## Background and Objectives

Site J1001 (proposed site CM-12) is located on the abyssal plane ~130 km offshore the coast of Chile at 46° 24.3180'S, 77° 19.4499'W and 3067 mbsl (Figure F4). The site is located on a seismic reflection profile collected during MR16-9 Leg 2 off of the Taitao Peninsula. A 17.53 m piston core, collected at the site location in 2017, is dominantly composed of dark olive grey to grey silt- and diatom-bearing clay with some thin silt and sandy layers (Murata et al., 2017). The upper and lower three meters of the core contain greater abundances of biogenic material, most likely deposited during interglacial periods, likely the Holocene and last interglacial Marine Isotope State 5, respectively, implying sedimentation rates of ~15 cm/ky. The seismic record exhibits well-developed stratification down to at least 100 mbsf.

Site J1001 is located in a tectonically complex region west of the Peru-Chile Trench on oceanic crust. The trench east of J1001, at 46°S, is intersected by the Chile Rise, an active spreading center of the Nazca and Antarctic Plates. This intersection, known as the Chile Triple Junction, is an example of an actively spreading mid-ocean ridge being subducted under continental lithosphere. Onshore, the Southern Volcanic Zone of the Andes spanning 33 to 46°S, contains at least 60 active volcanoes, including three giant caldera systems (Stern, 2010). Numerous historical eruptions have been documented, including recent eruptions in 2010, 2011, and 2015. The geology on land can be split into two units: the Coastal Range and the Andean Cordillera. The Coastal Range lies within ~150 km of the coast and is composed of metamorphic basement, ophiolite, and plutonic rocks with some sedimentary and volcanic units. The Andean Cordillera lies further inland and is composed predominantly of granites, in many cases overlain

by volcanic material. The Cordillera lies at altitudes higher than ~3000 km and is covered by glaciers within the Southern and Northern Patagonia icefield regions.

The climatology and oceanography of southern Chile is strongly influenced by the seasonal migration of the Southern Westerly Winds and the Southern Polar Front, which move between ~50°S in summer and 40-45°S in winter. Precipitation in the region is on the order of 3000 mm on the western side of the Andes (Fujiyoshi et al., 1987) and is almost entirely controlled by the Southern Westerly Winds (Garreaud et al., 2013). Thus, the band of maximum precipitation also migrates north and south with the seasonal cycle. The oceanography of the region is dominated by the northernmost extent of the Antarctic Circumpolar Current, which bifurcates at 45°S and carries Subantarctic surface water into the Cape Horn Current flowing to the south and the Peru-Chile Current (aka Humboldt Current) flowing to the north. In the subsurface, Antarctic Intermediate Water flows northward at depths of ~500-1000 m. At 3067 mbsl, the sediment is bathed by Circumpolar Deep Water.

Site J1001 is our southern-most and deepest site, providing the potential to reconstruct climate variability in the southeast Pacific and Patagonia over multiple glacial-interglacial cycles. The relatively modest sedimentation rates at Site J1001 of about 12-15 cm/ky means that this record is temporally the longest record collected during the JR100 expedition. This site will enable us to reconstruct changes in sea surface conditions and shifts in the sub-Antarctic polar front zone as well as variations in CPDW physiochemical properties. We expect the site is sensitive to changes in weathering and erosion in Patagonia and will provide a record of Patagonia icefield activity over the past ~ 0.8 Myr.

## Operations

Hole locations, water depths, and the number of cores recovered are listed in (Table T1). All times are local ship time (UTC -03 h) unless otherwise noted. Site J1001 (proposed Site CM-12) was the first site occupied during Expedition 379T. The plan for Site J1001 was to advanced piston corer (APC) triple core to ~100 mbsf while using stratigraphic correlation to construct a complete splice for a 100% record over the 100 m interval. Temperature measurements with the advanced piston corer temperature tool (APCT-3) were scheduled to be completed on the first hole.

### *Hole J1001A*

After a 664 nmi transit from Punta Arenas, Chile, averaging 10.5 knots, the ship arrived at Site J1001 at 1020 h (UTC -03 h) on 28 July 2019. The thrusters were lowered and secured, and the dynamic positioning system was engaged. At 1106 h the drill floor was cleared for operations, beginning Hole J1001A. We did not deploy an acoustic positioning beacon, but prepared one for immediate deployment if required.

The APC bottom-hole assembly (BHA) was made up and deployed. When the BHA reached 650.0 meters below rigfloor (mbrf), operations were halted when vessel motion made operations on the drill floor too dangerous for personnel and equipment. After a 2.75 h wait, the motions were sufficiently reduced to resume operations. The drill string was run to 3040.9 mbrf and all tubulars were strapped (measured) and drifted for an inside diameter check. The top drive was picked up, and a wiper “pig” was pumped through the drill string. The calculated precision depth recorder (PDR) depth for the site was 3066.4 mbrf. Based on the PDR, 3061.0 mbrf was selected as the shoot depth for the first core. A non-magnetic core barrel was run to bottom and the first attempt at spudding Site J1001 resulted in a water core. The bit was lowered 5 m to 3066.0 mbrf

and another attempt was made to secure a mudline core. Hole J1001A was spudded at 0420 h on 29 July 2019. Unfortunately, this attempt resulted in 9.66 m of core recovered with no evidence of a mudline thus, Hole J1001A was terminated.

### *Hole J1001B*

After moving the vessel 20 m east, the drill pipe was spaced out to 3063.5 mbrf and Hole J1001B was spudded at 0545 h on 29 July. Non-magnetic core barrels were used for all cores and temperature measurements were taken with the APCT-3 on Cores J1001B-4H, 6H, 8H and 10H with mixed results due to high vessel heave. Coring continued through Core J1001B-10H to a depth of 91.2 meters below seafloor (mbsf) when the coring line parted. The coring line was pulled back to the surface and became lodged in the oil saver above the top drive. The coring line was cut, the damaged piece of wire was removed, and after 7.5 h Core J1001B-10H was recovered. Hole J1001B was terminated at 100.7 mbsf with Core J1001B-11H, recovering a total of 101.25 m of sediment (101%). Hole J1001B ended at 0300 h on 30 July 2019 after clearing the seafloor and the vessel was offset 20 m south to begin Hole J1001C.

### *Hole J1001C*

The drill string was spaced out to 3062.0 mbrf and the first attempt to spud Hole J1001C resulted in an empty core barrel. The bit was lowered 1 m to 3063.0 mbrf and another attempt was made to secure a mudline core. Hole J1001C was spudded at 0515 h on 30 July 2019. The mudline core recovered 4.56 m of sediment and sea floor was calculated to be 3068.0 mbrf. Non-magnetic core barrels were used for APC coring and coring continued through Core J1001C-12H to a depth of 102.5 mbsf. The bit was tripped back and cleared the seafloor at 1615 h ending Hole J1001C. There was one drilled interval of 3.0 m from 23.5-26.5 mbsf for stratigraphic correlation purposes, resulting in 99.5 m of cored sediments and recovery of 102.61 m of

sediment (103%). Hole J1001C ended at 1615 h on 30 July, the vessel was offset 20 m to the west.

### *Hole J1001D*

At Hole J1001D the drill pipe was spaced out to 3064.5 mbrf in an attempt to recover at least 7.5 m of core for stratigraphic correlation of the splice. Hole J1001D was spudded at 1715 h on 30 July, however the mudline core recovered was only 6.13 m and Hole J1001D was abandoned after failing to recover a mudline core >7.5 m long.

### *Hole J1001E*

After clearing the seafloor from Hole J1001D at 1715 h on 30 July, the vessel was repositioned 20 m west for the start of Hole J1001E. The shoot depth was adjusted to 3065.5 mbrf and Hole J1001E began with a mudline core with 9.48 m recovered. Non-magnetic core barrels were used for APC coring and coring continued to final depth of 90.9 mbsf. There were two drilled intervals for correlation of the splice. The first interval drilled was from 18.9 mbsf to 20.90 mbsf. The second drilled interval was from 77.9 mbsf to 81.4 mbsf, again for correlation of the splice. In Hole J1001E 87.76 m of sediment were recovered through 85.4 m of cored interval (103%). At 1200 h on 31 July the drill floor was secured ending Hole J1001E and Site J1001.

A total of 33 cores were recorded for Site J1001. Only the APC coring system was used, with a 102.1% recovery over the 301.2 m cored. The five holes at Site J1001 consumed 3.04 days of expedition time. Of that time, 2.75 hours were lost due to weather related vessel motion and ~7.5 h were lost when the core wire failed.

## Principal results

All depth references in meters in this section refer to the CSF-A depth scale.

The sediment cored at Site J1001 is assigned to a single lithologic unit composed of ~103 m of middle Pleistocene to recent ash-rich clay with varying amounts of calcareous nannofossils, diatoms, and silt-sized siliciclastics (Figure F5). A ~20 cm brown ash layer is present at ~8 m CSF-A. In general, sediments containing larger amounts of biogenic particles are observed in the upper ~75 m of Site J1001, whereas biogenic particles are less abundant in the lower ~25 m (i.e., from ~75 – 100 m) where clay and silt-sized siliciclastics dominate. Nannofossils comprise most of the observed biogenic particles, while foraminifer tests and diatom frustules are generally present but sparse. Several of the cores collected at Site J1001 exhibit moderate to severe drilling disturbance, mainly concentrated in the top sections of the cores.

Planktonic foraminifers, benthic foraminifers, and calcareous nannofossils are present and generally exhibit excellent preservation throughout the succession at Site J1001. Planktonic foraminifers are generally more abundant than benthic forms; planktonic/benthic ratios range from 83:17 to 99:1, except for one sample at ~75 m where benthic foraminifera become more abundant than planktonics (36:64). The age model for Site J1001 is largely based on calcareous nannofossil biostratigraphy (Figure F6). At ~54 m, a distinct acme event of *Gephyrocapsa sp.* small was noted, corresponding to ~200 ka. The first appearance datum (FAD) of E. huxleyi was observed at ~63 m and corresponds to the base the NN21 nannofossil biozone. The last appearance datum (LAD) of *Pseudoemiliania lacunosa* was identified at ~73.5 m and corresponds to the top of the NN19 nannofossil biozone. *Reticulofenestra asanoi* (LAD) was observed in multiple spot samples between ~92 and 99 m suggesting an age of approximately 875 ka. No older age diagnostic nannofossils were observed through the base of Hole J1001B.

Diatoms exhibit good to moderate preservation and the flora is dominated by *Chaetoceros* spp. vegetative valves and resting spores, which are indicative of productivity associated with upwelling. Relative abundance of *Fragilariopsis kerguelensis*, a species associated with the Antarctic Circumpolar Current (ACC), increases in Samples J1001B-3H-CC, -5H-CC, and J1001C-9H-2A, possibly indicating northward shifts of the ACC during glacial periods. In general, planktonic foraminiferal assemblages of these samples were characterized by subpolar to transitional fauna, such as *N. incompta*, *T. quinqueloba*, *G. bulloides*, *G. glutinata* and *G. inflata,* with the rare occurrence of (usually ≤ 5%) subtropical-tropical species, e.g., *Globorotalia hirsuta*, *Globorotalia crassaformis* and *Globorotalia truncatulinoides* indicating temperate conditions. The benthic foraminiferal assemblage is dominated mainly by *Cibicidoides wuellerstorfi*, *Cibicidoides sp.*, *Melonis pumpiloides*, *Oridorsalis umbonatus*, *Pullenia bulloides*, *Uvigerina peregrina* and *Uvigerina sp*.

Paleomagnetic investigations on the recovered materials from Site J1001 involved the measurement of the natural remanent magnetization (NRM) of APC archive-half cores from Holes J1001A, J1001B, J1001C, J1001D and J1001E before and after alternating field (AF) demagnetization. The drill string overprint is relatively soft and is effectively removed after AF demagnetization in a 5–15 mT field. In addition, two discrete samples per core were generally taken in Sections 3 and 6 (one in Core 379T-J1001B-1H) from Hole J1001B (21 samples) to more fully characterize the NRM demagnetization behavior and to investigate the rock magnetic properties of the sediment, including anisotropy of magnetic susceptibility (AMS). Inclination and declination measured on discrete samples are generally in excellent agreement with those measured on the archive-half sections. SRM- and discrete-measured inclination plot around the expected values of -65° for the site latitude assuming the geocentric axial dipole (GAD) field

model (e.g. Opdyke and Channel, 1996 and references therein). NRM demagnetization behavior and rock magnetism results are consistent with [titano]magnetite being the primary magnetic remanence-carrying mineral in sediments deposited at Site J1001. Such conditions are optimal for the preservation of a paleogeomagnetic signal and for the reconstruction of reliable and robust paleomagnetic records (e.g. Stoner and St-Onge, 2007).

Inclination values shift from largely negative values to positive values between 90.85 to 91.5 m CSF-A in Hole J1001B and 92.3 to 92.9 m CSF-A in Hole J1001C. This shift is interpreted as the Matuyama/Brunhes polarity reversal (0.781 Ma) (GPTS; Cande and Kent, 1995). At 29.5 m CSF-A in Hole J1001B and 29.2 m CSF-A in Hole J1001C a large inclination anomaly accompanied by large shifts in declination and low NRM intensity values is observed (Figures J1001-F-F3 and J1001-F-F4). The remarkable repeatability of this inclination, declination, and intensity anomaly across Holes J1001B and J1001C (Figure J1001-F-F6) and the lack of evidence that lithologic change or drilling disturbance could be responsible for driving this variability leads us to conclude that this anomaly reflects an excursion of the geomagnetic field. This anomaly could be the Iceland Basin excursion (194 ka; Channell et al., 2009), or the Pringle Falls excursion (211 ka; Channell et al., 2009). Combining this stratigraphic point with the nannofossils biohorizon ages suggest > 10 cm/ky sedimentation rates in the upper ~ 75 meters of the core decreasing to < 10 cm/ky in the deeper part of the core (Figure F6).

The physical property data collected for Site J1001 includes gamma ray attenuation (GRA) bulk density, magnetic susceptibility (MS), and natural gamma ray (NGR) counts collected on whole-round cores and additional measurements on split cores and discrete samples including P-wave velocity; porosity; thermal conductivity; and bulk, dry, and grain densities. The physical properties of Site J1001 indicate high frequency variability (decimeter scale) in MS, NGR, and

bulk density, but do not display obvious long-term trends. Thermal conductivity decreases with depth, but variability increases, possibly due to small-scale fluctuations between terrigenous, biogenic, and ash layers in the core, contributing to a heterogeneous lithology. Formation temperature measurements made with the advanced piston corer temperature tool (APCT-3) indicate a strong geothermal gradient of 163°C/km for the upper ~100 m CSF-A, consistent with the young age of the underlying crust.

Despite the unfavorable sea state at the start of Site J1001 operations, a complete stratigraphic section was recovered from the mudline in Core 379T-J1001D-1H to the base of Core 379T-J1001C-12H at 107.04 m CCSF-A. Sequences from all holes were composited in near-real-time using magnetic susceptibility data from the Whole-Round Multisensor Logger measured at 2.5 cm resolution. Correlation was challenging due to substantial core disturbance, particularly at the top of Hole 379T-J1001B, resulting from large swell (~ 5 m). In a couple of instances, guaranteeing complete stratigraphic coverage required the drilling operations to advance without coring (Table T1; Figure F3). Final compositing in preparation for splice construction used a combination of magnetic susceptibility data from the WRMSL, NGR (10 cm resolution), and RGB channels (1–2 cm resolution). The relative depth offset of each core was determined by the optimized correlation of these 3 variables, with the top of Hole J1001D serving as the anchor (0 m CCSF). Once the composite depth scale was created, selected sequences from Holes J1001C and J1001E, with minor contributions from Hole J1001B, were spliced together to create a complete and representative stratigraphic section. Inspection of the spliced magnetic susceptibility, RGB, and NGR records demonstrates that the splice-tie boundaries do not create gaps or repeated intervals within the spliced section. Confidence in the splice ties is high because of the rich structure of the magnetic susceptibility records.

We collected 59 interstitial water samples from Hole J1001B (one per section) and mudline water samples from all holes. We measured routine shipboard analyses on one sample per core and each mudline sample, totaling 16 samples. The rest of the samples were collected for high-resolution isotope and chlorinity measurements. Routine shipboard analyses included chloride (by titration and ion chromatography; IC), alkalinity (by titration), major and minor elements (by Inductively Coupled Plasma-Optical Emission Spectroscopy; ICP-OES), major cations and anions (by IC), and ammonium and phosphate (by UV/vis spectrophotometry). Chemical gradients at this site reflect the influence of microbially mediated oxidation of organic matter, authigenic mineralization reactions, water-rock interaction related to clay alteration, and diffusive processes on interstitial water composition.

Methane concentrations were very low (~4 ppmV in Core 1 to 19 ppmV at the base of the Hole; Figure F19). The presence of methane and the absence of higher molecular weight hydrocarbon gases indicate that the methane is of biogenic origin.

Calcium carbonate ($CaCO_3$) contents are relatively low, < 15 %, in the upper ~60 m CCSF. Several intervals with >30 % CaCO3 occur between 56 and 103 m CCSF, but they are interspersed with sediments containing near zero %CaCO3. The more carbonate bearing intervals occur in low magnetic susceptibility sediments where RGB color shifts toward high green and blue, indicating significant lithologic variations, potentially driven by changes in dilution of biogenic materials by siliciclastic sediment or in surface productivity.

# J1002 Site Summary

## Background and Objectives

Site J1002 (proposed Site CM-5) is located at 46° 4.2964'S, 75° 41.2300'W offshore of the Taitao Peninsula to the east of the Chile Triple Junction on a bench in the continental slope at 1534 m water depth (Figure F4). Acoustic records obtained aboard the R/V Marion Dufresne and R/V Mirai MR16-09_2 cruise (Frank Lamy – personal communication) demonstrate well-developed stratification down to 70 mbsf. At present the core is located at the northern extent of the Antarctic Circumpolar Current (ACC) and thus sensitive to meridional shifts in the location of the polar fronts. Surface water at this site is influenced by the meltwater flow from the Patagonia ice sheet as reflected in the relative freshening of the surface at this location (Figure F1). At depth, the site is situated within the nutrient-rich, northern sourced Pacific deep-water mass (PDW), characterized by relatively low oxygen content compared with the overlying Antarctic intermediate water (AAIW) (Figure F2). A 18.9 m piston core collected by the R/V Marion Dufresne at this site suggests it will provide well-resolved records of glacial erosion from the NPI as well as PDW temperature and salinity (Kissel & Leau, 2007). The upper 6 m of the core is composed of olive black to greyish olive diatom and silt-bearing clay. The bottom 12.9 m of sediment is greyish olive to grey silty clay with numerous silt/sand layers. These silt/sand layers are unlikely to be turbidite layers (Siani et al., 2010).

At this site, sedimentation was much higher at the end of the last glacial period (>3 m/ky) relative to the deglaciation and Holocene (0.6 m/ky) reflecting an increase in terrigenous supply due to (1) closer proximity of the site to land during sea level low stand and (2) enhanced physical weathering due to the presence of permanent glaciers. Ice-rafted debris is expected below ~8 m. Site J1002 allows us to investigate variations in the Northern Patagonia ice sheet

during the last glacial period and Holocene using sedimentological and geochemical proxies. The core depth intersects PDW and we expect benthic foraminifera will record changes in PDW water mass properties over this time period.

## Operations

Hole locations, water depths, and the number of cores recovered are listed in Table T1. All times are local ship time (UTC -04 h) unless otherwise noted. Site J1002 (proposed Site CM-05) was the second site occupied during Expedition 379T (Figure F3). The plan for Site J1002 was to advanced piston corer (APC) triple core to ~100 mbsf while using stratigraphic correlation to construct a complete splice for a 100% record over the 100 m interval. Temperature measurements with the advanced piston corer temperature tool (APCT-3) were scheduled to be completed on the first hole.

### *Hole J1002A*

After the 71 nautical mile transit from Site J1001 averaging 10.4 knots, the vessel arrived at Site J1002 at 1830 h (UTC -03h) on 31 July 2019. The thrusters were lowered and secured, the dynamic positioning system was engaged and at 1908 h, the drill floor was cleared for operations, beginning Hole J1002A. We did not deploy an acoustic positioning beacon, but prepared one for immediate deployment if required.

The APC bottom-hole assembly (BHA) was made up and run to 135.62 m. While we waited on weather two 30’ knobbies were picked up and place on top of the BHA. After 13.5 h, the weather had subsided sufficiently where the remainder of the drill string could be run. The calculated precision depth recorder (PDR) depth for the site was 1543.4 mbrf. Based on the PDR, 1538.5 mbrf was selected as the shoot depth for the first core. A non-magnetic core barrel was

run to bottom and the mudline core (J1002A-1H) recovered 2.15 meters of sediment. The seafloor was estimated to be 1545.9 mbrf (1534.9 mbsl). Non-magnetic core barrels were used for all cores and temperature measurements were taken on Cores J1002A-5H, 7H, 9H and 11H with good results, despite the high vessel heave. Coring continued through Core J1002A-12H to a depth of 106.6 mbsf. From the 106.6 m cored in Hole J1002A, we recovered 110.95 m of core (104%). Hole J1002A ended at 0315 h on 2 August 2019 and the vessel was offset 20 m east.

### *Hole J1002B*

The drill pipe was spaced out to 1543.5 mbrf and Hole J1002B was spudded at 0405 h on 2 August. The mudline core (J1002B-1H) recovered 8.89 m of sediment and sea floor was calculated to be 1544.1 mbrf. Non-magnetic core barrels were used for APC coring. Coring continued through Core J1002B-7H to a depth of 65.9 mbsf. A routine inspection of the coring line revealed several broken strands in the wire. Coring was halted and a routine slip and cut of the coring line was performed, resulting in 1.5 h of productive time lost. After removing 150 m of coring line and re-terminating the wire rope socket, coring resumed. Coring terminated with Core J1002B-11H at a final depth of 103.9 mbsf. The bit was tripped back and cleared the seafloor at 1445 h ending Hole J1002B. From the 103.90 m cored in Hole J1002B, we recovered 110.77 m of core (107%).

### *Hole J1002C*

The vessel was repositioned 20 m south for the start of Hole J1002C. The drill pipe was spaced out to 1541.0 mbrf and Hole J1002C was spudded at 1550 h on 2 August 2019. The mudline core (J1002C-1H) recovered 6.9 m of sediment and sea floor was calculated to be 1543.6 mbrf. Non-magnetic core barrels were used for APC coring and coring continued through Core J1002C-11H to a depth of 101.9 mbsf. During the latter part of Hole J1002C we

experienced increasing heave and vessel motion (pitch and roll). The bit was tripped back and cleared the drill floor at 0930 h on 3 August 2019, ending Hole J1002C and Site J1002. From the 101.90 m cored in Hole J1002C, we recovered 108.59 m of core (106%).

A total of 34 cores were recorded for the Site J1002. Only the APC coring system was used, with 105.6% recovery over the 312.4 m cored. The three holes at Site J1002 consumed 2.64 days of expedition time. Of that time, 13.5 hours were lost because of weather related vessel motion and 1.5 h were lost when the core wire had to be slipped and cut (proactively repaired).

## Principal results

All depth references in meters in this section refer to the CSF-A depth scale.

The sediment cored at Site J1002 is assigned to a single lithologic unit composed of ~110.89 m of Pleistocene silty clay with sulfide precipitates interspersed throughout and regular thin layers of silty sand (Figure F7). The dominance of siliciclastics at the site reflects its location close to the South American continent. Volcanogenic particles are observed, but are usually less than 7% of the sediment due to the high influx of siliciclastic sediment. Microfossils are present, mainly in the upper two cores and in a short interval at ~85 m. Within these intervals, the sediment color is greener than the more common non-biogenic, gray siliciclastics. Among the biogenic particles, diatoms dominate, but foraminifera, nannofossils, and sponge spicules are also present in trace amounts. Below ~45 m, clay and silt-sized siliciclastics dominate, except between 79 – 86 m where the lithology changes to pure clay with occasional nannofossils but no sulfides. Prominent disturbances occur throughout the core randomly and include slight to heavy gas expansion, voids, and some up-arching. Bioturbation is slight, with burrows, some of which

are pyritized. Mineral clasts, which may be ice-rafted debris (IRD), occur in Samples J1002A-3H-CC and -4H-CC (61% and 58%, respectively),

Planktonic foraminifers, benthic foraminifers, calcareous nannofossils, and siliceous microfossils are present and show varying levels of preservation from very good to moderate. Planktonic foraminifers are generally abundant and well preserved. A total of 14 planktonic species identified. The most abundant planktonic foraminifer species in Hole J1002A were polar *Neogloboquadrina pachyderma (s)*, subpolar *Neogloboquadrina incompta* and *Turborotalita quinqueloba*, and transitional species such as *Globigerina bulloides*, *Globigerinita glutinata*, and *Globorotalia inflata*. Calcareous nannofossils are well preserved through Hole J1002A with abundances ranging from rare to abundant (Figure J1002-E-F1). Biostratigraphic control on Hole J1002A was limited due to the presence of *Emiliania huxleyi* throughout the entire sampled section, denoting an age younger than the *E. huxleyi* first appearance datum of 0.29 ka. Diatoms are most abundant in the uppermost section of the core, corresponding to the olive-green, diatom-rich silty clay interval (see J1002-D-Core Description). The diatom assemblage is dominated by *Chaetoceros* subgenus Hyalochaete resting spores and vegetative valves, indicative of upwelling conditions. *Thalassiosira eccentrica* and other species of the *Thalassiosira* genus are also present. Diatom abundances drop to trace amounts throughout most of the grey, silty clay interval of the core, but occasionally have moderate abundances. Unlike Site J1001, warm water species are observed at Site J1002. *Fragilariopsis kerguelensis*, a species associated with the Antarctic Circumpolar Current (ACC), is present in trace amounts, suggesting intermittent influence of the ACC to a lesser degree than that seen at Site J1001. 37 taxa of benthic foraminifera were identified. High abundances of infaunal species in almost all

core-catcher samples suggest high organic flux and low bottom water oxygen levels through Hole J1002A.

Paleomagnetic investigations on the recovered materials from Site J1002 involved the measurement of the natural remanent magnetization (NRM) of APC archive-half cores from Holes J1002A, J1002B, and J1002C before and after alternating field (AF) demagnetization. In addition, we generally took two discrete samples per core in Sections 3 and 5 (only one was taken in Core 379T-J1002A-1H) from Hole J1002A in order to more fully characterize the magnetic properties of the sediment, including anisotropy of magnetic susceptibility (AMS). In general, the NRM demagnetization behavior of the discrete samples are in agreement with the results from rock magnetism and point to a low coercive ferromagnetic mineral (e.g. magnetite or titanomagnetite) being the main carrier of the NRM in the majority of sediments recovered at Site J1002. Both SRM- and discrete-measured inclination fall around the values expected for the site latitude (around -64°) assuming the geocentric axial dipole (GAD) field model (e.g. Opdyke and Channel, 1996 and references therein). Thus, the majority of the paleomagnetic data appear stable enough to support magnetostratigraphic investigations but the intervals of low MS and NRM intensity should be interpreted with caution. Over shorter timescales both inclination and declination vary over a few tens of degrees suggesting that a paleosecular variation (PSV) record is preserved in the sediments deposited at Site J1002. We identify three paleomagnetic anomalies that are consistent across multiple holes and interpret these as excursions of the geomagnetic field. The deepest of these, E2, has similarities in form and timing to a PSV feature in ODP Site 1233 associated with the Laschamp excursion. Sedimentation rates at Site J1002 appear to be higher than those recorded at ODP Site 1233, suggesting that the PSV record over the radiocarbon era may be better resolved at J1002.

The physical property data collected for Site J1002 includes gamma ray attenuation (GRA) bulk density, magnetic susceptibility (MS), and natural gamma ray counts (NGR) collected on whole-round cores and additional measurements on split cores and discrete samples including P-wave velocity; porosity; thermal conductivity; and bulk, dry, and grain densities. Due to high gas content, cracks and voids are very common in all the three holes at Site J1002 (except for Cores J1002B-1H and 2H), causing anomalously low values of GRA, MS, and NGR. Nevertheless, the MS record shows real (not caused by cracks or voids), high-frequency and high-amplitude variability (decimeter-scale) throughout the record except for a low MS interval observed in all holes from ~80 to ~90 m CSF-A. The downhole NGR record also shows decimeter-scale variability, but varies inversely with MS (Figure F7). Formation temperature measurements made with the advanced piston corer temperature tool (APCT-3) indicate a strong geothermal gradient of 116°C/km for the upper ~100 m CSF-A, consistent with the young age of the underlying crust.

Tie points were established initially with Whole-Round Multisensor Logger magnetic susceptibility data, and these tie points were sufficiently robust to establish that a complete section was recovered. Subsequent scanning of the split cores indicated that it was possible to use the RGB green to blue ratio to refine the initial correlations, given the rich structure and evident reproducibility of the color signal among holes. The relative depth offset of each core was then assessed with NGR (10 cm resolution) and other products such as paleomagnetic inclination to provide additional cross-checks on the stratigraphic ties. The variable within-core expansion of sequences implies that single depth offsets will result in inevitable misalignment of features that are clearly correlative among holes. This variable expansion does not appear to be systematic with depth, and, therefore, the tie points were chosen carefully to maximize lengths of

cores in a spliced composite. Once the composite depth scale was created, selected sequences from all holes (Holes J1002A, J1002B and J1002C) were spliced together to create a complete section. The splice is continuous from 0 to ~129.53 m CCSF-A, but with a precision of ~20 cm owing to the differential expansion of individual cores.

We collected 66 interstitial water samples from Hole J1002A, 10 interstitial water samples from Hole J1002C, one mudline water sample for each hole, and surface seawater. We carried out routine shipboard analyses on one sample per core from J1002A, one sample from cores 1 and 2 of J1002C and each mudline sample, totaling 16 samples. Routine shipboard analyses included chloride (by titration and ion chromatography; IC), alkalinity (by titration), major and minor elements (by Inductively Coupled Plasma-Optical Emission Spectroscopy; ICP-OES), major cations and anions (by IC), and ammonium and phosphate (by UV/vis spectrophotometry). Chemical gradients at this site reflect the influence of microbially mediated oxidation of organic matter, authigenic mineralization reactions, and diffusive processes on pore water fluid composition. The observed chloride maxima at 13.67 m CCSF likely reflects the presence and subsequent diffusion of more saline Last Glacial Maximum seawater throughout the profile, indicating that porewaters from this site may be useful for determining LGM seawater properties. However, the lower concentrations deeper in the hole, coupled to the decrease of several major elements with depth such as Sr, Mg, and Na, may be caused by melting of gas hydrates, clay mineral dehydration (Kastner., 1995), or mixing with terrestrial meteoric melt water that penetrated to the continental shelf during the last glacial (Post et al., 2013).

Maximum methane concentrations (~46,000 ppmV) occur at 8.61 m CSF-A (Figure F19). Ethane is present in low concentrations (~10 ppmV) and covaried with methane from 83.92 m

CCSF to the bottom of the hole. The high concentrations of methane relative to other gases from 11.44 to 83.92 m CCSF suggest a biogenic source.

Calcium carbonate contents vary between 0 and 8% downhole, with an average value of 2%. Carbonate contents are slightly elevated, 5 to 8%, in the upper ~5 m of each Hole.

## J1003 Site Summary

### Background and Objectives

Site J1003 (proposed site CM-9) is located at 45° 28.5008'S, 75° 33.5020'W offshore of the Taitao Peninsula to the east of the Chile Triple Junction on the edge of the continental shelf at 670 m water depth (Figure F4). The site is located along the seismic line 743 of RC2901 near CMP 1950 (http://www-udc.ig.utexas.edu/sdc/cruise.php?cruiseIn=rc2901). The site is landward (east) of the ridge axis and the forearc basin, and situated on the accreted strata overlying the South American Plate in proximity to the Guamblin Fracture zone. A strong seismic reflector, seen at 1.1 sec sub-bottom below the core site, can be traced seaward and is interpreted to mark the continental basement in this region. A bottom-simulating reflector (BSR) can be seen in the seismic reflection data at Site J1003 at ~0.1-0.2 sec (Figure F9), presumably resulting from the presence of a zone of frozen gas hydrate in the shallow sub-bottom. High-resolution down hole sampling of interstitial waters completed here will offer information on the geochemical processes at this site.

At present the site is located at the northern extent of the Antarctic Circumpolar Current (ACC) and thus sensitive to shifts in the location of the polar fronts. Like at site J1002, surface water at site J1003 is influenced by the meltwater flow from the Patagonia ice sheet as reflected in the relative freshening of the surface at this location (Figure F1). The site was recovered from

670 m water depth and is therefore situated within the core of oxygen-rich Antarctic intermediate water (AAIW). No previous coring was done at this site.

## Operations

Hole locations, water depths, and the number of cores recovered are listed in Table T1. All times are local ship time (UTC -04 h) unless otherwise noted. Site J1003 (proposed Site CM-09) was the third site occupied during Expedition 379T. The plan for Site J1003 was to advanced piston corer (APC) triple core to ~100 mbsf while using stratigraphic correlation to construct a complete splice for a 100% record over the 100 m interval. Temperature measurements with the advanced piston corer temperature tool (APCT-3) were scheduled to be completed on the first hole.

### *Hole J1003A*

After departing Site J1002 in rough weather, the 41 nautical mile transit to Site J1003 required 6.5 h in cruise mode (average 6.5 knots) and another 5 h in dynamic positioning mode. In order to reduce the excessive rolling a course change was made, putting the vessel to the northwest of the site. The vessel arrived at Site J1003 at 2100 h on 3 August 2019. We arrived with the thrusters already lowered and the dynamic positioning system engaged. The vessel stabilized over the initial position at 2100 h and began to wait on weather (WOW). After a 19.5 h WOW, the drill floor was cleared to begin operations on Site J1003 at 1630 h on 4 August. We did not deploy an acoustic positioning beacon, but prepared one for immediate deployment if required.

The APC bottom-hole assembly (BHA) was made up and run to 135.62 m and the drill string was run to 648.6 mbrf. The calculated precision depth recorder (PDR) depth for the site was

680.4 mbrf. Based on the PDR, 675.0 mbrf was selected as the shoot depth for the first core. A non-magnetic core barrel was run to bottom and the mudline core (J1003A-1H) was spudded at 2150 h on 4 August, recovering 3.6 meters of sediment. The seafloor was estimated to be 680.9 mbrf (669.8 mbsl). Non-magnetic core barrels were used for all cores and temperature measurements were taken on Cores J1003A-5H, 7H, 9H with good results, despite the high vessel heave. Coring concluded on Core J1003A-9H at a depth of 79.6 mbsf. We terminated Hole J1003A based on the quality of the samples. The last core (J1003A-9H) had to be pumped out of the core barrel. From the 79.6 m cored in Hole J1003A, we recovered 79.58 m of core (100%). Hole J1003A ended at 0800 h on 5 August 2019 and the vessel was offset 20 m east.

### *Hole J1003B*

The drill pipe was spaced out to 678.0 mbrf, however, a routine inspection of the coring line found broken wire strands just above the rope socket so the coring line was slipped, cut, re-terminated and reinstalled. Hole J1003B was spudded at 1000 h on 5 August. The mudline core (J1003B-1H) recovered 5.69 m of sediment and sea floor was calculated to be 681.9 mbrf (670.8 mbsl). Non-magnetic core barrels were used for APC coring. Coring continued through Core J1003B-6H to a depth of 53.1 mbsf, terminating before the planned 100 m to ensure quality core recovery. The bit was tripped back and cleared the rigfloor at 1845 h ending Hole J1003B and Site J1003. From the 53.1 m cored in Hole J1003B, we recovered 54.16 m of core (102%).

A total of 15 cores were recorded for the Site J1003. Only the APC coring system was used, with 100.8% recovery over the 132.7 m cored. The two holes at Site J1003 consumed 1.91 days of expedition time. Of that time, 19.5 hours were lost because of weather related vessel motion and ~1 h was lost when the core wire had to be slipped and cut (proactively repaired).

## Principal results

All depth references in meters in this section refer to the CSF-A depth scale.

The sediment cored at Site J1003 is assigned to a single lithologic unit composed of ~80 m of clay minerals mixed with coarser siliciclastic grains (mainly silt size), with minor biogenic components (primarily calcareous nannofossils and secondarily diatoms) and volcaniclastic (ash) particles (Figure F8). The dominance of hemipelagic sediments over pelagic sediments is reflective of the close proximity to the South American continent. Situated on the edge of the continental shelf, this site receives cross-shelf transport of fluvial and glacial sediments. A prominent sand bed (about 1.5 m thick) is observed at ~40 m CSF-A. The texture and mineralogy of the ~1.5 m thick sand layer (Cores J1003A-5H and J1003B-5H) is characterized by sub-angular, moderately sorted grains of amphiboles, plagioclase, and biotite, indicating limited physical and chemical weathering of the (granitoid) protoliths. In addition, secondary precipitates occur in the form of sulfides throughout Hole J1003A and in the form of carbonate concretions. Bioturbation, indicated by burrows and an absence of clear sedimentary layering, is moderate to heavy throughout most of the cores. Drilling disturbances, mainly in the form of cracks, up-arches, gas expansion, and soupy intervals, are common.

Planktonic foraminifers, benthic foraminifers, calcareous nannofossils, and siliceous microfossils are present and show varying levels of preservation. Calcareous nannofossils are common to abundance and their preservation ranged from poor to good with minor to significant dissolution around the outer rim of the coccoliths. Biostratigraphic control on Hole J1003A was difficult due to poor preservation and the presence of reworked Pliocene/Miocene nannofossils throughout the entire set of core catchers observed in Hole A. Diatom assemblages at Site J1003 are characterized by high relative abundances of species indicative of upwelling. Their

abundances range from trace to common throughout Site J1003 and preservation in terms of dissolution ranges from good to moderate and fragmentation is consistently moderate. Planktonic foraminifers are generally abundant in all core catcher samples from Hole J1003A. Preservation is variable through Hole J1003A, and ranges from good to poor. Pyrite concretions are present in almost all core catcher samples from Hole J1003A, and pyrite and pyritized foraminifera are dominantly found in Samples J1003A-1H-CC and -7H-CC. The most abundant species in Hole J1003A are polar *Neogloboquadrina pachyderma (s)*, subpolar *Neogloboquadrina incompta* and *Turborotalita quinqueloba*, and transitional species such as *Globigerina bulloides*, *Globigerinita glutinata*, and *Globorotalia inflata*.

Paleomagnetic investigations on the recovered materials from Site J1003 involved the measurement of the natural remanent magnetization (NRM) of APC archive-half cores from Holes J1003A and J1003B before and after alternating field (AF) demagnetization. The drill string overprint is magnetically soft and is effectively removed after AF demagnetization in a 5–15 mT field. In addition, we generally took two discrete samples per core in Sections 3 and 6 (only one was taken in Core 379T-J1003A-1H) from Hole J1003A (17 samples) to more fully characterize the NRM demagnetization behavior and to investigate the rock magnetic properties of the sediment, including anisotropy of magnetic susceptibility (AMS). Inclination and declination measured on discrete samples are generally in good agreement with those measured on the archive-half sections. SRM- and discrete-measured inclination in the upper ~25-35 m CSF-A generally plot around the expected values of -64° for the site latitude assuming the geocentric axial dipole (GAD) field model (e.g. Opdyke and Channel, 1996 and references therein). Below ~35 m CSF-A, inclination is more variable and generally shallower than that predicted by a GAD, which potentially suggests that sediment diagenesis, compaction and/or

disturbance affects the record at depth. Nevertheless, magnetic lineation orientations are promising and may illustrate the evolution of depositional or even the early tectonic processes at the Site.

Sediments in Hole J1003B (terminated at 53.1 CSF-A) and in the upper ~65 m CSF-A of Hole J1003A possess negative values of inclination suggesting deposition within a normal polarity chron. Assuming that this period relates to the most recent normal polarity interval, the Bruhnes chron, then these sediments were deposited within the last ~781 kyrs through correlation to the Geomagnetic polarity Timescale (GPTS) (Cande and Kent, 1995; Ogg et al., 2012) of the Geologic Timescale (Hilgen et al., 2012). In Section 379T-J1003A-8H-5A, inclination shifts from negative to largely positive values and is accompanied by a corresponding ~180° shift in declination. Positive inclination values are then maintained to the bottom of the Hole. These reversed polarity intervals suggest that the sediments involved were deposited during a reversed polarity configuration, likely during the Matuyama chron.

The physical property data collected for Site J1003 includes gamma ray attenuation (GRA) bulk density, magnetic susceptibility (MS), and natural gamma ray counts (NGR) collected on whole-round cores and additional measurements on split cores and discrete samples including P-wave velocity; porosity; thermal conductivity; and bulk, dry, and grain densities. Due to high gas content, cracks and voids are very common in both holes at Site J1003, causing anomalously low values of GRA, MS, and NGR. Nevertheless, the MS and NGR records show real (not caused by cracks or voids), high-frequency (decimeter-scale) variability, that are reproducible between holes. Intervals (about 2–10 meters long) with persistent low MS values occur in both Hole A and Hole B, which likely reflect diagenetic impacts of strongly reducing sediments. Abnormally high MS values (around 1100 10-5 SI) were observed in the bottom of Section J1003A-5H (~40–

41 m CSF-A) that are associated with a sand layer (Figure F8). Formation temperature measurements made with the advanced piston corer temperature tool (APCT-3) indicate a geothermal gradient of 53°C/km for the upper ~100 m CSF-A.

Sequences from both holes were composited in near-real-time using magnetic susceptibility data from the WRMSL measured at 2.5 cm resolution to guide the coring by optimizing the core stagger between Holes J1003A and J1003B. Tie points were then established with Whole-Round Multisensor Logger (WRMSL) magnetic susceptibility and natural gamma radiation (NGR) data. These tie points were sufficiently robust to indicate that a complete stratigraphic section was recovered down to a depth of ~56 m CCSF-A. Subsequent scanning of the split cores suggested that it was possible to use red-green-blue color space (RGB) green to blue ratio to further refine some of the initial correlations. However, we have not defined a splice at this site because identifiable features often displayed large differences in thickness and signature between Holes J1003A and J1003B.

We collected 38 interstitial water samples from Hole J1003A, and one mudline water sample from both Holes J1003A and J1003B. We carried out routine shipboard analyses on one sample per core from J1002A, one sample from cores 1 and 2 of J1002C and each mudline sample, totaling 16 samples. Routine shipboard analyses included chloride (by titration and ion chromatography; IC), alkalinity (by titration), major and minor elements (by Inductively Coupled Plasma-Optical Emission Spectroscopy; ICP-OES), major cations and anions (by IC), and ammonium and phosphate (by UV/vis spectrophotometry). Chemical gradients at this site reflect the influence of microbially mediated oxidation of organic matter, authigenic mineralization reactions, and diffusive processes on porewater fluid composition. The decrease of several major elements with depth such as Sr, Mg, Na and Cl is probably caused by dilution,

which may be the result of melting of gas hydrates (Mix et al. 2003) or mixing with terrestrial meteoric melt water that penetrated to the continental shelf during the last glacial (Post et al., 2013).

Hydrocarbon monitoring shows that the maximum methane concentration (48,440 ppmV) was found at 20.22 m CSF-A (Figure F19). Ethane was found in low concentrations (up to 17 ppmV) and covaried with methane throughout the hole. The high concentrations of methane relative to other gases suggest a biogenic source.

## J1004 Site Summary

### Background and Objectives

Site J1004 (proposed site CM-4) is located at 44° 0.0300'S, 75° 9.0650'W within a small-scale sediment drift 60 km offshore of the Aysén Region of Chile at 1125 m water depth (Figure F4). The site lies northeast of the Chile Triple Junction on accreted strata overlying the South American Plate east of the ridge axis and forearc basin. The acoustic record for Site J1004 shows well-developed stratification down to at least 55 mbsf. Two cores (3.3 and 17.25 m) collected at this location by the R/V MARION DUFRESNE contain dominantly terrigenous material with limited marine biogenic components, including diatoms, sponge spicules, foraminifera, and occasional shell fragments (Kissel & Leau, 2007). Sedimentation rates are ~3 m/ky. Interstitial waters were sampled down-hole at high resolution (1 per section) and will offer information on the geochemical processes at this site.

Site J1004 is located north of the Antarctic Circumpolar Current and, like the previous three sites, will be sensitive to latitudinal shifts in the location of the polar front. Today the site is located just north of the ACC bifurcation point in the path of the Peru-Chile Current (PCC); the

ACC bifurcates at ~45°S sending Subantarctic surface water both north and south along the coast of S. America via the PCC and the Cape Horn Current, respectively. Preliminary data from this site suggest it is highly sensitive to meltwater events from the Patagonia Icefield. At 1125 m water depth, the Site sits at the boundary between AAIW and PDW and will be sensitive to changes in water mass geometry during the Holocene and late deglaciation.

## Operations

Hole locations, water depths, and the number of cores recovered are listed in Table T1. All times are local ship time (UTC -04 h) unless otherwise noted. Site J1004 (proposed Site CM-04) was the fourth site occupied during Expedition 379T. The plan for Site J1004 was to advanced piston corer (APC) triple core to ~100 mbsf while using stratigraphic correlation to construct a complete splice for a 100% record over the 100 m interval. Temperature measurements with the advanced piston corer temperature tool (APCT-3) were scheduled to be completed on the first hole.

### *Hole J1004A*

After the 82 nautical mile transit from Site J1003, averaging 10.1 knots, the vessel arrived at Site J1004 at 0324 h on 6 August 2019. The thrusters were lowered and secured, the dynamic positioning system was engaged, and at 0330 h the drill floor was cleared for operations, beginning Hole J1004A. We did not deploy an acoustic positioning beacon, but prepared one for immediate deployment if required.

The APC bottom-hole assembly (BHA) was made up and run to 135.62 m and the drill string was run to 1109.4 mbrf. The calculated precision depth recorder (PDR) depth for the site was 1135.2 mbrf. Based on the PDR, 1130.0 mbrf was selected as the shoot depth for the first core. A

non-magnetic core barrel was run to bottom and the mudline core (J1004A-1H) recovered 3.28 meters of sediment. The seafloor was estimated to be 1136.3 mbrf (1125.2 mbsl). Non-magnetic core barrels were used for all cores and temperature measurements were taken on Cores J1004A-5H and 7H with good results. At ~58.4 mbsf (Core J1004A-7H) the APC core barrel encountered a layer (underdetermined thickness) of gravel. After pulling back the APCT-3 temperature shoe filled with gravel, the hole was drilled out to 60.2 mbsf and another core was attempted. The next core barrel (J1004-8H) rebounded off the gravel formation and recovered 0.65 m of gravel. The driller advanced 9.5 m and attempted one more core with the same results (0.43 m gravel recovered) and coring in Hole J1004 was terminated. From the 70.1 m cored in Hole J1004A, we recovered 60.94 m of core (87%). Hole J1004A ended at 1821 h on 6 August 2019 and the vessel was offset 20 m east.

### *Hole J1004B*

The drill pipe was spaced out to 1132.5 mbrf and Hole J1004B was spudded at 1855 h on 6 August. The mudline core (J1004B-1H) recovered 6.80 m of sediment and the sea floor was calculated to be 1135.3 mbrf (1124.2 mbsl). Non-magnetic core barrels were used for APC coring. Coring continued through Core J1004B-7H to a depth of 58.0 mbsf. The final core (J1004B-7H) was shot from 54.2 mbsf and was a partial stroke. Gravel was again encountered stopping the coring at 58.0 mbsf. A single temperature measurement was taken on Core J1004B-6H to complete our temperature data set. The bit was tripped back and cleared the seafloor at 0000 h on 7 August ending Hole J1004B. From the 58.0 m cored in Hole J1004B, we recovered 55.35 m of core (95%).

### *Hole J1004C*

The vessel was repositioned 20 m east for the start of Hole J1004C. The drill pipe was spaced out to 1135.1 mbrf and Hole J1004C was spudded at 0050 h on 7 August. The mudline core (J1004C-1H) recovered 9.4 m of sediment and sea floor was calculated to be 1135.1 mbrf (1124.0 mbsl). Non-magnetic core barrels were used for APC coring and coring continued through Core J1004C-6H to a depth of 56.9 mbsf. The bit was tripped back and cleared the drill floor at 0954 h on 7 August 2019, ending Hole J1004C and Site J1004. From the 56.9 m cored in Hole J1004C, we recovered 56.70 m of core (99%).

A total of 22 cores were recorded for the Site J1004. Only the APC coring system was used, with 93.4% recovery over the 185.0 m cored. The three holes at Site J1004 consumed 1.27 days of expedition time.

## Principal results

All depth references in meters in this section refer to the CSF-A depth scale.

The sediment cored at Site J1004 is assigned to two lithologic units. Unit I (upper ~58 m) is composed of nannofossil-bearing diatom rich clay and ash-bearing clay and silty clay (Figure F10). All of the holes show a gradual color transition from olive gray to dark gray, reflecting lithological shifts from diatom-rich clay to silty clay. Numerous sandy layers are observed; some of the sandy layers have erosive bases and some appear graded, possibly indicating mass gravity flows, such as turbidites. The thicker (>10 cm) poorly sorted felsic sandy layers contain easily weathered primary minerals (e.g., quartz, feldspar, and opaque minerals), which suggests rapid deposition, of which one possible process could be glacial outflow. Unit II was assigned to sediment below ~58 m composed of large (5-10 cm-sized) gravel clasts. The dominance of siliciclastics at this site reflects the proximal location of the site to the South American continent.

Slight coring disturbances are found throughout, due to cracks caused by gas expansion. Bioturbation is slight to moderate with some burrows.

Calcareous nannofossils, siliceous microfossils, planktonic foraminifers, and benthic foraminifers are present and show varying levels of preservation. Calcareous nannofossils were well preserved and ranged from common to abundant. The presence of *Emiliania huxleyi* in all samples down to J1004A-7H-CC suggests that the age of this site is younger than the first appearance of *E. huxleyi* at 290 ka. Samples from Site J1004 are characterized by high abundance of siliceous microfossils. Diatom preservation is good in terms of both fragmentation and dissolution in the upper ~34 m in Hole J1004A and moderate below. The diatom flora is consistent throughout the site and is dominated by *Chaetoceros* subgenus *Hyalochaete* resting spores and vegetative valves, indicating upwelling conditions. Additionally, the Antarctic Circumpolar Current-associated species *Fragilariopsis kerguelensis* is present in trace to rare abundances throughout the site. Benthic species such as *Cocconeis* spp., *Delphineis* sp., and *Paralia sulcata* occur in few to trace abundances throughout the site, indicating sediment redeposition, although they do not accompany any significant changes in lithology. Planktonic and benthic foraminifers are present in all core catcher samples from Hole J1004A. The planktonic:benthic foraminifer ratio (%) ranges from 88:12 to 59:41. Preservation is very good for both planktonic and benthic foraminifers over the upper ~42 m in Hole J1004A, but drops to poor at the base of the Hole. The most abundant planktonic species in Hole J1004A were polar *Neogloboquadrina pachyderma* (s), subpolar *Neogloboquadrina incompta* and *Turborotalita quinqueloba*, and transitional species *Globigerina bulloides* and *Globigerinita glutinata*—indicating temperate/transitional conditions. The benthic foraminiferal assemblage in Hole J1004A is dominated mostly by *Bulimina mexicana, Cibicidoides* sp., *Fursenkoina bradyi,*

*Globocassudulina subglobosa, Globobulimina affinis*, *Globobulimina* sp., *Melonis* sp., *Uvigerina peregrina* and *Uvigerina* sp. Finally, lithic grains, which may be ice-rafted in origin, dominate Samples 7H-CC (97%) and 8H-CC (~50%) suggesting glacial-like conditions.

Paleomagnetic investigations on the recovered materials from Site J1004 involved the measurement of the natural remanent magnetization (NRM) of APC archive-half cores from Holes J1004A, J1004B, and J1004C before and after alternating field (AF) demagnetization. The drill string overprint was effectively removed after AF demagnetization in a 15 mT field. In addition, we generally took two discrete samples per core in Sections 3 and 6 (only one was taken in Core 379T-J1004A-1H) from Hole J1004A (13 samples) to more fully characterize the NRM demagnetization behavior and to investigate the rock magnetic properties of the sediment, including anisotropy of magnetic susceptibility (AMS). Inclination and declination measured on discrete samples are generally in good agreement with those measured on the archive-half sections. Inclination data average around the value predicted by a GAD field (-64°) for normal polarity suggesting that the sediment record recovered at Site J1004 was deposited during the Brunhes Chron and is younger than 780 ka. Over shorter timescales both inclination and declination vary over a few tens of degrees. These variations are generally consistent between all three holes suggesting that a paleosecular variation (PSV) record is preserved in the sediments deposited at Site J1004, which may be used to facilitate chronostratigraphy through correlation to independently dated records e.g. ODP Site 1233 (Lund et al., 2006). Fabric orientations in J1004 do not show similar orientation among different sections, and the changes do not follow a noticeable consistent pattern downhole.

The physical property data collected for Site J1004 includes gamma ray attenuation (GRA) bulk density, magnetic susceptibility (MS), and natural gamma ray counts (NGR) collected on

whole-round cores and additional measurements on split cores and discrete samples including P-wave velocity; porosity; thermal conductivity; and bulk, dry, and grain densities. High MS values mostly coincide with peaks in GRA bulk density. Concurrent highs in MS and GRA values are likely associated with the appearance of sand layers. NGR shows no noticeable trend with depth, but downhole decimeter-scale variability is observed. Formation temperature measurements made with the advanced piston corer temperature tool (APCT-3) indicate a geothermal gradient of 31°C/km for the upper ~60 m CSF-A.

The extremely high sedimentation rates and numerous high magnetic susceptibility spikes made the WRMSL data difficult to impossible to use for correlation purposes. However, stratigraphic correlation using the high-resolution split core scans (e.g., RGB green to blue ratio) was generally robust for the upper 58 m CSF-A (Figure J1004-I-F1). Incomplete recovery and disturbance in the sediments of Cores J1004A-8H and -9H led to the decision not to extend Holes J1004B and J1004C below ~58 meters CSF-A. Thus, the composited sections extend through Core J1004A-7H with Cores J1004A-8H and 9H appended. The splice is likely to be continuous from 0 to ~66 m CCSF-A, and the ties made with one variable (e.g. color) typically produce similar results to those made with another variable, with a precision of a few centimeters.

We collected 37 interstitial water samples from Hole J1004A and one mudline water sample from Holes J1004A and J1004B. We measured the routine shipboard analyses on one sample per core and each mudline sample, totaling 9 samples. Routine shipboard analyses included chloride (by titration and ion chromatography; IC), alkalinity (by titration), major and minor elements (by Inductively Coupled Plasma-Optical Emission Spectroscopy; ICP-OES), major cations and anions (by IC), and ammonium and phosphate (by UV/vis spectrophotometry). The elevated

values of the various products of organic matter degradation indicate that very high levels of organic matter oxidation are dominating the interstitial water chemistry at Site J1004. Interstitial water alkalinity shows a maximum value of 122 mM at 32.1 m CCSF, which is much higher than the alkalinity maxima observed at nearby Sites J1002, J1003 and ODP Site 1233 (this report, Mix et al. 2003).

Hydrocarbon monitoring shows that the maximum methane concentration (41,598 ppm) was found at 10.17 m CSF-A (Figure F19). Concentrations decrease with a local minimum of 6,859 ppmV at 41.77 m CCSF. The high methane values relative to those from other sites such as J1003 indicate that relatively more methanogenesis is occurring at this site.

Calcium carbonate contents vary between 3.7 and 8% downhole with an average of 6.4%. $CaCO_3$ content decreases steadily down hole. The lower values occur as magnetic susceptibility increases, in association with increasing siliciclastic inputs.

## J1005 Site Summary

### Background and Objectives

Site J1005 (proposed site CM-3A) is located at 41° 4.5800'S, 74° 26.7000'W on a bench in the upper continental slope 38 km offshore at 807 m water depth (Figure F11). The site is offset ~10 km to the southeast of ODP site 1233, which was cored during ODP Leg 202 to 116.3 mbsf and yielded a high-resolution climate record of the past ~70 ky (Kaiser et al., 2010). The main objective in re-coring this site was to recover the last interglacial (LIG) sediments. Given the very high sedimentation rates at Site 1233 (about 1-3 m/ky; Lamy et al., 2004) and the restriction of 100 meters coring depth of the JR100 program, we have targeted nearby sites with expected lower sedimentation rates. Parasound and 3.5 kHz depth recorder data acquired along a

N-S strike line from Site 1233 suggest that sediment packages are thinner upslope (Figure F12). Projected lower sedimentation rates at the upper part of the record would possibly enable recovery of sediment going further back in time, relative to ODP Site 1233. Sediments at ODP Site 1233 are primarily composed of homogeneous fine-grained terrigenous material with minor amounts of well-preserved biogenic components (Mix et al., 2003). Interstitial waters were sampled down-hole at high resolution (1 per section) and will offer information on the geochemical processes at this site.

Sediments collected at site J1005 should record latitudinal variations in the boundary between the ACC and the subtropical gyre. Today the site is in the path of the Peru-Chile Current (PCC; aka Humboldt Current), which brings sub-Antarctic surface water north along the coast of Chile. The regional precipitation is controlled by the shifts of the southern westerly wind belt, which is reflected in the terrigenous inputs to the Chilean shelf. The site should also record meltwater events from the Patagonia Icefield (e.g. Lamy et al., 2004). At 807 m water depth, the Site sits in the heart of AAIW (Figure F2) and will be sensitive to changes in its properties over the last glacial-interglacial cycle.

## Operations

Hole locations, water depths, and the number of cores recovered are listed in Table T1. All times are local ship time (UTC -04 h) unless otherwise noted. Site J1005 (proposed Site CM-03A) was the fifth site occupied during Expedition 379T. The plan for Site J1005 was to advanced piston corer (APC) triple core to ~100 mbsf while using stratigraphic correlation to construct a complete splice for a 100% record over the 100 m interval. Temperature measurements with the advanced piston corer temperature tool (APCT-3) were scheduled to be completed on the first hole.

### *Hole J1005A*

During the 224 nautical mile transit from Site J1004 (averaging 11.8 knots) the vessel dropped off the two Chilean pilots (Pilot 1 and Pilot 2) at the Ancud pilot station at 0040 h on 8 August 2019. The vessel arrived at Site J1005 at 0506 h on 8 August 2019. The thrusters were lowered and secured, the dynamic positioning system was engaged, and at 0533 h the drill floor was cleared for operations, beginning Hole J1005A. We did not deploy an acoustic positioning beacon, but prepared one for immediate deployment if required.

The APC bottom-hole assembly (BHA) was made up and run to 135.62 m and the drill string was run to 794.2 mbrf. The calculated precision depth recorder (PDR) depth for the site was 819.4 mbrf. Based on the PDR, 815.0 mbrf was selected as the shoot depth for the first core. A non-magnetic core barrel was run to bottom and the mudline core (J1005A-1H) recovered 6.92 meters of sediment. The seafloor was estimated to be 817.6 mbrf (806.5 mbsl). Non-magnetic core barrels were used for all cores and temperature measurements were taken on Cores J1005A-5H, 7H, and 9H with good results. Coring continued through Core J1005A-11H to a depth of 101.9 mbsf. From the 101.9 m cored in Hole J1005A, we recovered 108.54 m of core (106.5%). Hole J1005A ended at 1847 h on 8 August 2019 and the vessel was offset 20 m east.

### *Hole J1005B*

The drill pipe was spaced out to 811.0 mbrf and Hole J1005B was spudded at 1930 h on 8 August. The mudline core (J1005B-1H) recovered 2.52 m of sediment and the seafloor was calculated to be 818.0 mbrf (806.9 mbsl). Non-magnetic core barrels were used for APC coring. Coring continued through Core J1005B-12H to a depth of 107.0 mbsf. Core J1005B-12H was categorized as a slow bleed and was most likely a partial stroke, explaining the poor (51%) recovery on the final core of Hole J1005B. The bit was tripped back and cleared the seafloor at

0329 h on 9 August ending Hole J1005B. From the 107.0 m cored in Hole J1005B, we recovered 108.9 m of core (102%).

### *Hole J1005C*

The vessel was repositioned 20 m south for the start of Hole J1005C. The drill pipe was spaced out to 817.0 mbrf and Hole J1005C was spudded at 0410 h on 9 August. The mudline core (J1005C-1H) recovered 8.22 m of sediment and sea floor was calculated to be 818.3 mbrf (807.2 mbsl). Non-magnetic core barrels were used for APC coring and coring continued through Core J1005C-11H to a depth of 103.2 mbsf. The bit was tripped back to three pipe stands above the seafloor (85.5 m) to prepare for the dynamic positioning move to Site J1006. The drill floor was secured at 1209 h on 9 August 2019, ending Hole J1005C and Site J1005. From the 103.2 m cored in Hole J1005C, we recovered 111.7 m of core (108%).

A total of 34 cores were recorded for the Site J1005. Only the APC coring system was used, with 105.5% recovery over the 312.1 m cored. The three holes at Site J1005 consumed 1.28 days of expedition time.

## Principal results

All depth references in meters in this section refer to the CSF-A depth scale.

The sediment cored at Site J1005 is assigned to a single lithologic unit composed of ~108.87 m of Pleistocene clay mixed with varying amounts of biogenic tests, volcanic ash, and some intervals dominated by authigenic carbonate precipitates (Figure F13**).** Biogenic constituents vary in abundance and consist primarily of nannofossils, but diatoms, along with sponge spicules, foraminifers, and shell fragments, are also observed regularly. In addition, two whole bivalves, identified as marine mollusks belonging to the Lucinidae family of seawater clams,

indicative of cold seep environments where hydrogen sulfide, methane, and/or other hydrocarbon-rich fluid seepage occur. The sediments contain various types of authigenic precipitates including carbonates, both in the form of carbonate concretions and micron-sized particles scattered in the sediment. Sulfide minerals, including pyrite minerals, appear as discrete dark spots or as finely dispersed particles and cause a distinct dark-color mottling in the otherwise homogeneous greenish gray to dark-gray sediments. Rare, cm-scale layers of silty clay, sand, and volcanic ash occur. The ash layers are generally a few cm thick and some are traceable between holes. Except for rare sedimentary structures, including sand layers that may represent hybrid mass-gravity flows and tephra layers, the lithology at Site J1005 is relatively homogenous, suggesting moderate bioturbation throughout the site.

Calcareous nannofossils, siliceous microfossils, planktonic foraminifers, and benthic foraminifers are present and show varying levels of preservation. Calcareous nannofossils range from barren to abundance in Site J1005 and their preservation is good over the upper ~54 m CSF-A and moderate to poor below. Age constraints are difficult to assign due to the poor preservation, but appears to be within the total range of *E. huxleyi* in the NN21 nannofossil biozone (< 290 ka). Diatom microfossil abundance is consistently high at Site J1005, with all samples containing abundances of few or common. Preservation is good in terms of dissolution and fragmentation throughout most of Hole J1005A, with only Sample 11H-CC displaying moderate dissolution and Samples 9H-CC through 11H-CC displaying moderate fragmentation. Similar to previous sites, the diatom flora at Site J1005 is dominated by *Chaetoceros* subg. *Hyalochaete* resting spores and vegetative valves, which are indicative of upwelling. *Coscinodiscus radiatus* and *Nitzschia marina*, which are associated with warm waters, and *Coscinodiscus marginatus*, and *Rhizosolenia hebetata*, which are associated with cold waters,

occasionally occur in trace amounts. Planktonic and benthic foraminifers are present in all core catcher samples from Hole J1005A. In general, planktonic foraminifers were more abundant than benthics, ranging from 85:15 to 17:83. The benthic foraminiferal assemblage in Hole J1005 is characterized mostly by *Cassidulina teretis, Cibicidoides* sp.*, Ehrenbergina sp., Epistomella sp., Globobulimina affinis, Melonis* sp.*, Melonis affinis, Nonionella turgida, Uvigerina peregrina* and *Uvigerina* sp., which were present in almost all core catcher samples.

Paleomagnetic investigations on the recovered materials from Site J1005 involved the measurement of the natural remanent magnetization (NRM) of APC archive-half cores from Holes J1005A, J1005B, and J1005C before and after alternating field (AF) demagnetization. The drill string overprint is magnetically soft and is effectively removed after AF demagnetization in a 5–15 mT field. In addition, we generally took two discrete samples per core in Sections 3 and 6 from Hole J1005A (22 samples) to more fully characterize the NRM demagnetization behavior and to investigate the rock magnetic properties of the sediment, including anisotropy of magnetic susceptibility (AMS). Fabric orientations in J1005 share a similar orientation downhole and may be related to processes capable of regularizing the orientation of magnetic fabric (e.g. ocean currents). Inclination and declination measured on discrete samples are generally in good agreement with those measured on the archive-half sections. Inclination data average around the value predicted by a GAD field (-60°) but over shorter timescales both inclination and declination vary over a few tens of degrees suggesting that a PSV record is preserved in the sediments deposited at Site J1005. Several inclination and declination anomalies are present in the records from Holes J1005A, J1005B, and J1005C, but just two horizons have anomalies that are expressed in both inclination and declination and occur across all three holes. These intervals occur at ~10 m CSF-A, Event 1 (E1), and ~100 m, Event 2 (E2). We can tentatively associate E1

with the Laschamp excursion (~41 ka) identified as excursion 3β in ODP Site 1233 (Lund et al., 2006). However, inclination values at ODP Site 1233 have a predominantly positive expression during the 3β excursion (Lund et al., 2006), not the steeply negative expression as seen in the sediments deposited at Site J1005. Unlike E1 we cannot be certain that the directional anomalies associated with E2 are geomagnetic in origin.

The physical property data collected for Site J1005 includes gamma ray attenuation (GRA) bulk density, magnetic susceptibility (MS), and natural gamma ray counts (NGR) collected on whole-round cores and additional measurements on split cores and discrete samples including P-wave velocity; porosity; thermal conductivity; and bulk, dry, and grain densities. The amplitude of MS variability increases downhole, with a particularly noticeable amplification between ~65 and 90 m CSF-A in each hole (Figure F13). Recurring periods of low (<100 x $10^{-5}$ SI Instrument Units) and relatively invariable MS, which are potentially associated with sedimentary diagenesis, are also observed. NGR displays a slight increasing trend downhole at Site J1005. Formation temperature measurements made with the advanced piston corer temperature tool (APCT-3) indicate a geothermal gradient of 57°C/km for the upper ~100 m CSF-A.

Sequences from both holes were composited in near-real-time using magnetic susceptibility data from the WRMSL measured at 2.5 cm resolution to guide the coring by optimizing the core stagger between holes. Final compositing was accomplished using a combination of magnetic susceptibility measurements from the Whole-Round Multisensor Logger (WRMSL) and the ratio of Green/Blue channels from the Section Half Imaging Logger (SHIL). The splice is likely to be continuous from 0 to ~118 m core composite depth below seafloor (CCSF), and the ties made with one variable (e.g. magnetic susceptibility) typically produce similar results to those made with another variable, with a precision of a few centimeters.

We collected 65 interstitial water samples from Hole J1005A, and one mudline water sample from both Holes J1005A and J1005B. We measured the routine shipboard analyses on one sample per core from J1005A and from each mudline sample, totaling 13 samples. The rest of the samples were collected for high-resolution isotope and chlorinity measurements. Routine shipboard analyses included chloride (by titration and ion chromatography; IC), alkalinity (by titration), major and minor elements (by Inductively Coupled Plasma-Optical Emission Spectroscopy; ICP-OES), major cations and anions (by IC), and ammonium and phosphate (by UV/vis spectrophotometry). Chemical gradients at this site reflect the influence of microbially mediated oxidation of organic matter, authigenic mineralization reactions, water-rock interaction processes and diffusive processes on porewater fluid composition.

A methane headspace sample was collected from each core. The maximum methane concentration (60,313 ppmV) was found at 23.41 m CSF-A (Figure F19). Concentrations decrease with a local minimum of 6,238 ppmV at 69.55 m CSF-A. The high concentrations of methane relative to other gases suggest a biogenic source.

Calcium carbonate content of the hemipelagic sediments varies between 0.5 and 9.6 % downhole, with an average value of 4.3 %. The overall low concentrations are likely due to dilution of the mostly biogenic carbonate by siliciclastic sediments. Carbonate contents of discrete precipitates measured from 27.39 m and 115.25 m CCSF were high, at 58.2 and 45.1 wt%, respectively. The carbonate-rich precipitates occur in low magnetic susceptibility intervals consistent with authigenic carbonate precipitation associated with anaerobic methane oxidation.

# J1006 Site Summary

## Background and Objectives

Site J1006 (proposed site CM-3B) is located at 41°1.5600'S, 74° 26.7000'W on a bench in the upper continental slope 38 km offshore at 824 m water depth (Figure F11). The site is offset ~5 km to the southeast of ODP site 1233, which was cored during ODP Leg 202 to 116.3 mbsf, yielding a high-resolution climate record of the past ~70 Kyr (Kaiser et al., 2010). Parasound and PDR depth recorder data acquired on approach suggest that sediment packages are thinner upslope (Figure F12). Projected lower sedimentation rates may enable recovery of sediment going further back in time, relative to ODP Site 1233, with the goal of reaching Marine Isotope Stage 5e. Relative to Site J1005, we expect the uppermost sediment packages are thicker, but still accumulate more slowly than those collected at ODP Site 1233. Sediments at ODP Site 1233 are primarily composed of homogeneous fine-grained terrigenous material with minor amounts of well-preserved biogenic components (Mix et al., 2003). Sedimentation rates at ODP Site 1233 range from 1-3 m/ky (Lamy et al., 2004). Interstitial waters were sampled down-hole at high resolution (1 per section) and will offer information on the geochemical processes at this site.

Sediments collected at site J1006 should record latitudinal variations in the position of the ACC and the SWWs. Today the site is in the path of the Peru-Chile Current (PCC), which brings Subantarctic surface water north along the coast of Chile. The site should also record meltwater events from the Patagonia Icefield (e.g. Lamy et al., 2004). At 824 m water depth, the Site sits in the heart of AAIW (Figure F2) and will be sensitive to changes in its properties over the last glacial-interglacial cycle.

## Operations

Hole locations, water depths, and the number of cores recovered are listed in Table J1006-C-T1. All times are local ship time (UTC -04 h) unless otherwise noted. Site J1006 (proposed Site CM-03B) was the sixth site occupied during Expedition 379T. The plan for Site J1006 was to advanced piston corer (APC) triple core to ~100 mbsf while using stratigraphic correlation to construct a complete splice for a 100% record over the 100 m interval. Temperature measurements with the advanced piston corer temperature tool (APCT-3) were scheduled to be completed on the first hole.

### *Hole J1006A*

The 3 nautical mile transit from Site J1006 was made using the dynamic positioning (DP) system while the drill string remained suspended from the vessel at 723.5 mbrf. The vessel arrived at Site J1006 at 1506 h on 9 August 2019 and the drill floor was cleared for operations, beginning Hole J1006A. We did not deploy an acoustic positioning beacon, but prepared one for immediate deployment if required.

With the drill string already suspended, the bit was lowered to 794.2 mbrf. The calculated precision depth recorder (PDR) depth for the site was 833.4 mbrf. Based on the PDR, 828.5 mbrf was selected as the shoot depth for the first core. A non-magnetic core barrel was run to bottom to spud Hole J1006A. Unfortunately, the first attempt came back without any sediment. The shoot depth was lowered by 5 m to 833.5 mbrf and Hole J1006A was finally spudded at 1734 h. The mudline core (J1006A-1H) recovered 8.64 meters of sediment and the seafloor was estimated to be 834.4 mbrf (823.3 mbsl). Non-magnetic core barrels were used for all cores and temperature measurements were taken on Cores J1006A-5H, 7H, and 9H with good results. Coring continued through Core J1006A-11H to a depth of 103.6 mbsf. From the 103.6 m cored

in Hole J1006A, we recovered 105.62 m of core (106.6%). Hole J1006A ended at 0250 h on 10 August 2019 and the vessel was offset 20 m east.

### *Hole J1006B*

The drill pipe was spaced out to 830.5 mbrf and Hole J1006B was spudded at 0410 h on 10 August. The mudline core (J1006B-1H) recovered 4.41 m of sediment and the sea floor was calculated to be 835.6 mbrf (824.5 mbsl). Non-magnetic core barrels were used for APC coring. Coring continued through Core J1006B-12H to a depth of 108.9 mbsf. The bit was tripped back and cleared the seafloor at 1330 h on 10 August ending Hole J1006B. From the 108.9 m cored in Hole J1006B, we recovered 109.1 m of core (100.2%).

### *Hole J1006C*

The vessel was repositioned 20 m south for the start of Hole J1006C. The drill pipe was spaced out to 832.5 mbrf and Hole J1006C was spudded at 1420 h on 10 August. The mudline core (J1006C-1H) recovered 5.42 m of sediment and sea floor was calculated to be 836.6 mbrf (825.5 mbsl). Non-magnetic core barrels were used for APC coring and coring continued through Core J1006C-12H to a depth of 108.9 mbsf. There was a deliberate short core (8.5 m) on Core J1006C-6H to help improve the splice. There were some problems with biogenic gas expansion while curating core on the catwalk. The bit was tripped back and the drill floor was secured at 0415 h on 11 August 2019, ending Hole J1006C and Site J1006. From the 108.9 m cored in Hole J1006C, we recovered 106.23 m of core (97.5%).

A total of 35 cores were recorded for the Site J1006. Only the APC coring system was used, with 99.6% recovery over the 321.4 m cored. The three holes at Site J1006 consumed 1.55 days of expedition time.

## Principal results

All depth references in meters in this section refer to the CSF-A depth scale.

The sediment cored at Site J1006 is assigned to a single lithologic unit composed of 109.12 m of Pleistocene clay mixed with various amounts of biogenic tests, silt, and volcanic ash (Figure F14). Biogenic constituents vary in abundance and consist of roughly equal portions of nannofossils and diatoms, with foraminifers and small shell fragments frequently present. The sediment also contains authigenic precipitates, with the two main mineralogies being carbonate and sulfide. Slight to severe drilling disturbances occur throughout, most commonly in the form of cracks caused by gas expansion.

Calcareous nannofossils, siliceous microfossils, planktonic foraminifers, and benthic foraminifers are present and show very good to good preservation. The calcareous nannofossils ranged from common to abundant. The presence of *Emiliania huxleyi* down to 11H-CC suggests an age no older than 290 ka based on the FAD of *E. huxleyi*, placing the entire sampled section within the nannofossil biozone NN21. Diatom microfossils are present throughout the hole, but abundance is generally greater in younger sediments and decreases downcore. Preservation is good in terms of dissolution and fragmentation throughout most of Hole J1006A. *Chaetoceros* subgenus *Hyalochaete* resting spores and vegetative valves, along with other upwelling-related species *Delphineis* spp. and *Thalassionema nitzschioides* dominate the assemblage. A total of 15 taxa of planktonic foraminiera were identified in Hole J1006A. The most abundant species in Hole J1006A were polar *Neogloboquadrina pachyderma* (s), subpolar *Neogloboquadrina incompta* and *Turborotalita quinqueloba*, and transitional species *Globigerina bulloides*, *Globigerinita glutinata* and *Globorotalia inflata* —indicating subpolar to transitional conditions. Planktonic foraminifers are generally more abundant than benthic forms; planktonic/benthic

ratios range from 87:13 to 54:46. Benthic foraminifer preservation ranged from very good to good in Hole J1006A, although pyritized foraminifers were occasionally present. Despite the presence of epifaunal, oxic indicator species (e.g., *C. wuellerstorfi*, *Cibicidoides* spp., *Pyrgo* spp., *Quinqueloculina* spp., *Triloculina* sp. and *Triloculina tricarinata*) throughout Hole J1006A, the majority of the assemblage constitutes infaunal species that are characteristic of low oxygen environments and high organic matter flux.

Paleomagnetic investigations on the recovered materials from Site J1006 involved the measurement of the natural remanent magnetization (NRM) of APC archive-half cores from Holes J1006, J1006, and J1006 before and after alternating field (AF) demagnetization. The drill string overprint is magnetically soft and is effectively removed after AF demagnetization in a 5–15 mT field. In addition to the superconducting rock magnetometer (SRM) measured half core sections, two discrete samples were taken per core, generally from Sections 3 and 6 from Hole J1006A (22 samples in total) to provide a more detailed characterization of the paleomagnetic behavior and the rock magnetic properties of the sediment, including anisotropy of magnetic susceptibility (AMS). Inclination and declination measured on discrete samples are generally in good agreement with those measured on the archive-half sections. Magnetic inclination data average around the value predicted by a GAD field (-60°) but over shorter timescales both inclination and declination vary over a few tens of degrees, suggesting that a PSV record is preserved in the sediments deposited at Site J1006. The three holes at this site can be clearly correlated using the secular variation in inclination and declination particularly when viewed on the CCSF-A depth scale suggesting a robust PSV record can be derived from this site. Three anomalies have both inclination and declination expressions and occur over multiple holes. The shallowest of these events, named E1, occurs at ~22 m CSF-A in Holes J1006A and J1006C,

above a prominent marker in MS that occurs at ~42-43 m CSF-A in all three holes. If we correlate this marker to ODP (Oceanic Drilling Program) Site 1233 where it occurs at 89 meters composite depth (mcd) then we can tentatively associate E1 with the Laschamp excursion (~41 ka), identified as excursion 3β in ODP Site 1233 (Lund et al., 2006).

The physical property data collected for Site J1006 includes gamma ray attenuation (GRA) bulk density, magnetic susceptibility (MS), and natural gamma ray counts (NGR) collected on whole-round cores and additional measurements on split cores and discrete samples including P-wave velocity; porosity; thermal conductivity; and bulk, dry, and grain densities. High frequency variability in the MS data is apparent in all Site J1006 holes and the amplitude increases downhole (Figure F14). Recurring periods of low (<100 Instrument Units) and invariable MS, which are potentially associated with sedimentary diagenesis, are observed. NGR counts show a slight increasing trend and amplified variability downhole at Site J1006. Formation temperature measurements made with the advanced piston corer temperature tool (APCT-3) indicate a geothermal gradient of 76°C/km for the upper ~100 m CSF-A.

Sequences from both holes were composited in near-real-time using magnetic susceptibility data from the WRMSL measured at 2.5 cm resolution to guide the coring by optimizing the core stagger between holes. Final compositing was accomplished using a combination of magnetic susceptibility measurements from the Whole-Round Multisensor Logger (WRMSL) and the ratio of Green/Blue channels from the Section Half Imaging Logger. In general, the large amplitude signals in magnetic susceptibility resulted in relatively robust stratigraphic ties that could be verified and refined with the color data, despite the complication imposed by extreme stretching of some cores near the middle of the stratigraphic section.

We collected 68 interstitial water samples from Hole J1006A, and one mudline water sample from Holes J1006A, J1006B, and J1006C. We measured the routine shipboard analyses on one sample per core from J1006A, and from each mudline sample, totaling 15 samples. The rest of the samples were collected for high-resolution isotope and chlorinity measurements. Routine shipboard analyses included chloride (by titration and ion chromatography; IC), alkalinity (by titration), major and minor elements (by Inductively Coupled Plasma-Optical Emission Spectroscopy; ICP-OES), major cations and anions (by IC), and ammonium and phosphate (by UV/vis spectrophotometry). Chemical gradients at this site reflect the influence of microbially mediated oxidation of organic matter, authigenic mineralization reactions, water-rock interaction processes, dilution, and diffusive processes on porewater fluid composition.

A methane headspace sample was collected from each core. The maximum methane concentration (57,369 ppmV) was found at 15.6 m CSF-A (Figure F19). Concentrations decrease to a local minimum of 6,207 ppmV at 62.9 m CSF-A and remain low to the base of the hole. The high concentrations of methane relative to other gases suggest a biogenic source.

The calcium carbonate contents of the hemipelagic sediments at J1006 vary between 0.9 and 5.9 wt% downhole, with an average value of 4.0 wt%. Discrete precipitates, sampled from 51.2 and 79.1 m CCSF, contain 21.7 and 50.0 wt% carbonate, respectively. This suggests that the precipitates reflect authigenic carbonate formation, perhaps related to the anaerobic oxidation of methane.

# J1007 Site Summary

## Background and Objectives

Site J1007 (proposed site CM-7), located at 36° 32.5400'S, 73° 39.9900'W, lies 60 km offshore, shoreward of the Peru-Chile Trench, on continental crust at 786 m water depth (Figure F15). Two sediment cores, GeoB 7162-6 and GeoB 7165-1, were recovered at this location in 2001 during the SO-156 cruise (Hebbeln and cruise participants, 2001). Sediment core GeoB7165-1 is composed of strongly bioturbated dark olive green, hemipelagic, low carbonate, mud in the upper ~3m, reddish gray muddy clay from 3 to 6 m, and olive green clayey mud to the base of the core at 7.5 m. Age control was determined based on AMS $^{14}C$ dates and by comparing planktonic $\delta^{18}O$ data to the record from nearby site ODP 1233 (Mohtadi et al., 2008). The core may be missing part of the late Holocene and terminates at ~22 ka (Mohtadi et al., 2008). Estimated sedimentation rates are ~40 cm/ky during the LGM, ~75 cm/ky during the deglaciation, and ~35 cm/ky during the Holocene.

Sediments collected at Site J1007 will possibly provide records of surface and intermediate water variability over the last ~300 ky. At 36°S, the site is located south of the main upwelling region along the coast of Peru and Northern Chile but upwelling does occur seasonally, primarily during austral spring and summer driving high primary production, ~20 g C $m^{-2}$ $d^{-2}$ (e.g. Daneri et al., 2000). Nutrients are also supplied to the study area via the Itata and Biobío rivers, which carry weathering products and fresh water from the Andes and Coastal Ranges out into the open ocean. In the shallow subsurface, the Peru-Chile Undercurrent brings low oxygen water sourced from the oxygen minimum zone to the north. This site extends our transect of cores to the north enabling comparative studies with cores collected further south to assess N-S penetration of water masses in the eastern Pacific, including Subantarctic surface waters, low oxygen

Equatorial Subsurface Water, and AAIW (Figure F1, F2). Furthermore, as Site J1007 lies in the heart of AAIW, we can unambiguously tie its porewater signature to the water mass.

## Operations

Hole locations, water depths, and the number of cores recovered are listed in Table T1. All times are local ship time (UTC -04 h) unless otherwise noted. Site J1007 (proposed Site CM-07) was the seventh site occupied during Expedition 379T. The plan for Site J1007 was to advanced piston corer (APC) triple core to ~100 mbsf while using stratigraphic correlation to construct a complete splice for a 100% record over the 100 m interval. Temperature measurements with the advanced piston corer temperature tool (APCT-3) were scheduled to be completed on the first hole.

### *Hole J1007A*

During the 273 nautical mile transit from Site J1007 the vessel averaged 11.3 knots. We arrived at Site J1007 at 0441 h on 12 August 2019. The thrusters were lowered and secured, the dynamic positioning system was engaged, and at 0510 h the drill floor was cleared for operations, beginning Hole J1007A. We did not deploy an acoustic positioning beacon, but prepared one for immediate deployment if required.

The APC bottom-hole assembly (BHA) was made up and run to 135.62 m and the drill string was run. The calculated precision depth recorder (PDR) depth for the site was 799.4 mbrf. Based on the PDR and estimated tides, 795.5 mbrf was selected as the shoot depth for the first core. A non-magnetic core barrel was run to bottom and the mudline core (J1007A-1H) recovered 6.80 meters of sediment. The seafloor was estimated to be 798.2 mbrf (787.1 mbsl). Non-magnetic core barrels were used for all cores and temperature measurements were taken on Cores J1007A-

5H, 7H, and 9H with good results. Coring continued through Core J1007A-11H to a depth of 101.8 mbsf. From the 101.8 m cored in Hole J1007A, we recovered 103.77 m of core (102%). Hole J1007A ended at 1700 h on 12 August 2019 and the vessel was offset 20 m east.

### *Hole J1007B*

Hole J1007B was spudded at 1820 h on 12 August. The mudline core (J1007B-1H) recovered 4.37 m of sediment and the sea floor was calculated to be 797.6 mbrf (786.5 mbsl). Non-magnetic core barrels were used for APC coring. Coring continued through Core J1007B-12H to a depth of 108.9 mbsf. The bit was tripped back and cleared the seafloor at 0100 h on 13 August ending Hole J1007B. From the 108.9 m cored in Hole J1007B, we recovered 105.03 m of core (96.4%).

### *Hole J1007C*

The vessel was repositioned 20 m south for the start of Hole J1007C. The drill pipe was spaced out to 797.0 mbrf and Hole J1007C was spudded at 0200 h on 13 August. The mudline core (J1007C-1H) recovered >9.5 m of sediment and sea floor was calculated to be 797.0 mbrf (785.9 mbsl). Non-magnetic core barrels were used for APC coring and coring continued through Core J1007C-11H to a depth of 95.1 mbsf. The bit was tripped back and the drill floor was secured at 1230 h on 13 August 2019, ending Hole J1007C and Site J1007. From the 95.1 m cored in Hole J1007C, we recovered 95.86 m of core (100.8%).

A total of 34 cores were recorded for the Site J1007. Only the APC coring system was used, with 99.6% recovery over the 305.8 m cored. The three holes at Site J1007 consumed 1.30 days of expedition time.

## Principal results

All depth references in meters in this section refer to the CSF-A depth scale.

The sediment cored at Site J1007 is assigned to a single lithologic unit composed of 108.9 m of Pleistocene silty clay and clay mixed with various amounts of biogenic tests, volcanic ash, and authigenic precipitates (Figure F16). Biogenic constituents vary in abundance and mostly consist of nannofossils and diatoms, though sponge spicules, bivalve shell fragments, and foraminifers are also observed throughout the site. The sediments contain carbonate precipitates in the form of concretions and micron-sized particles scattered in the sediment. Sulfide minerals, including pyrite appearing as discrete dark spots or as finely dispersed particles, cause a distinct dark-color mottling in sediments. Slight to severe drilling disturbances occur throughout, mostly in the form of cracks caused by gas expansion.

Calcareous nannofossils, siliceous microfossils, planktonic foraminifers, and benthic foraminifers are present and show moderate to good preservation. The calcareous nannofossils ranged from few to abundant. *Emiliania huxleyi* is observed throughout the sampled section, suggesting this site is no older than the first appearance datum of 290 ka. There is frequent Pliocene/Miocene reworking observed at this site, including intermediate to large *Reticulofenestra spp., Coccolithus miopelagicus, Cyclicargolithus floridanus, Dictyococcites bisectus,* and *Discoaster deflandrei.* Diatom microfossils are common throughout Site J1007 and their preservation ranges from moderate to good in terms of dissolution and fragmentation. The diatom flora is characterized by an upwelling-related assemblage composed mainly of *Chaetoceros* subgenus *Hyalochaete* (resting spores and vegetative valves) and secondarily of *Delphineis* spp., *Pseudonitzschia* spp., and *Thalassionema nitzschioides*. Planktonic foraminifers were more abundant than benthic foraminifers in almost all core catcher samples in Hole

J1007A; with the planktonic:benthic ratio ranging from 74:26 to 30:70. A total of 14 planktonic taxa were identified in Hole J1007A. The most abundant species in Hole J1007A were polar *Neogloboquadrina pachyderma* (s), subpolar *Neogloboquadrina incompta* and *Turborotalita quinqueloba*, and transitional species *Globigerina bulloides*, *Globigerinita glutinata* and *Globorotalia inflata* —indicating subpolar to transitional conditions. The benthic foraminiferal assemblage in Hole J1007A is characterized mostly by *Bulimina mexicana, Cibicidoides* sp., *Ehrenbergina sp., Epistominella sp., Fursenkoina bradyi, Globobulimina affinis, Melonis affinis, Nonionella turgida, Oridorsalis umbonatus, Uvigerina peregrina* and *Uvigerina* sp., which were present in almost all core catcher samples.

Paleomagnetic investigations on the recovered materials from Site J1007 involved the measurement of the natural remanent magnetization (NRM) of APC archive-half cores from Holes J1007A, J1007B, and J1007C before and after alternating field (AF) demagnetization. The drill string overprint is magnetically soft and is effectively removed after AF demagnetization in a 15 mT field. In addition to the superconducting rock magnetometer (SRM) measured half core sections, two discrete samples were taken per core, generally from Sections 3 and 6 from Hole J1007A (22 samples in total) to provide a more detailed characterization of the paleomagnetic behavior and the rock magnetic properties of the sediment, including anisotropy of magnetic susceptibility (AMS). Inclination and declination measured on discrete samples are generally in good agreement with those measured on the archive-half sections. Magnetic inclination data average around the value predicted by a GAD field (-56°) suggesting that the sediment was deposited during a period of normal polarity during the Brunhes chron and is < 780 ka in age. Over shorter timescales both inclination and declination vary over a few tens of degrees, suggesting that a paleosecular variation (PSV) record is preserved in the sediments deposited at

Site J1007. Three anomalies (E1, E2, E3) in both inclination and declination occur over multiple holes. The shallowest of these events, E1, occurs around 22 m CSF-A in all three holes whereas E2 occurs in just Holes J1007A and J1007C. E3 occurs in Holes J1007B and J1007C at around 87 m CSF-A but, unlike E1 and E2, it coincides with an interval of very low values of WRMSL MS. Based on evidence from changes in sediment composition coupled with rock magnetic evidence we suggest the ferromagnetic mineral assemblage across the E3 anomaly may have been affected by diagenesis, and thus sedimentological or geochemical factors are more likely responsible for the E3 anomaly rather than geomagnetic variability. However, E1 and E2 could reflect excursions of the geomagnetic field recorded in the sediments deposited at Site J1007.

The physical property data collected for Site J1007 includes gamma ray attenuation (GRA) bulk density, magnetic susceptibility (MS), and natural gamma ray counts (NGR) collected on whole-round cores and additional measurements on split cores and discrete samples including P-wave velocity; porosity; thermal conductivity; and bulk, dry, and grain densities. The MS signature is characterized by high-frequency (decimeter-scale), high-amplitude variability interrupted by intervals of low MS (<100 x $10^{-5}$ SI) (Figure F16), in which authigenic alteration was observed. NGR counts show a slight increasing trend downhole at Site J1007. Formation temperature measurements made with the advanced piston corer temperature tool (APCT-3) indicate a geothermal gradient of 37°C/km for the upper ~100 m CSF-A.

Sequences from the three holes were composited in near-real-time using magnetic susceptibility data from the WRMSL measured at 2.5 cm resolution to guide the coring by optimizing the core stagger between holes. Final compositing was accomplished using a combination of magnetic susceptibility measurements from the Whole-Round Multisensor Logger (WRMSL) and the ratio of Green/Blue channels from the Section Half Imaging Logger.

In general, the large amplitude signals in magnetic susceptibility resulted in relatively robust stratigraphic ties that could be verified and refined with the color data, despite the complication imposed by extreme stretching of some cores near the middle of the stratigraphic section.

We collected 66 interstitial water samples from Hole J1007A, and one mudline water sample from Holes J1007A and J1007B. We measured the routine shipboard analyses on one sample per core from J1007A, and from each mudline sample, totaling 13 samples. The rest of the samples were collected for high-resolution isotope and chlorinity measurements. Routine shipboard analyses included chloride (by titration and ion chromatography; IC), alkalinity (by titration), major and minor elements (by Inductively Coupled Plasma-Optical Emission Spectroscopy; ICP-OES), major cations and anions (by IC), and ammonium and phosphate (by UV/vis spectrophotometry). Chemical gradients at this site reflect the influence of microbially mediated oxidation of organic matter, authigenic mineralization reactions, water-rock interaction processes, and diffusive processes on porewater fluid composition.

A methane headspace sample was collected from each core. The maximum methane concentration (95,606 ppmV) was found at 14.0 m CSF-A (Figure F19). Methane concentrations then decrease sharply until 31.4 m CSF-A and then gradually increase towards the bottom of the hole (~6,150 ppmV). The high concentrations of methane relative to other gases suggest a biogenic source.

The calcium carbonate contents of the hemipelagic sediments at J1007 vary between 1 and 4 wt% downhole, with an average value of 2.6 wt%. Carbonate contents are slightly elevated around or within low magnetic susceptibility intervals e.g. around 5, 50, 70, and 95 m CCSF. This suggests that $CaCO_3$ enrichment at these depths reflects authigenic carbonate precipitation.

# J1008 Site Summary

## Background and Objectives

Site J1008 (proposed site CM-8), located at 36° 27.1906'S, 73° 54.4651'W, lies ~80 km offshore, shoreward of the Peru-Chile Trench, on continental crust at 2032 m water depth (Figure F15). A 663 cm sediment core was recovered here in 2001 by the R/V Sonne, GeoB 7167-6 (Hebbeln and cruise participants, 2001). Sediments here are composed of strongly bioturbated clayey mud. Foraminifers are widespread and abundant in some intervals. Clay content increases downcore transitioning to muddy clay at 577 cm. The high terrigenous content of the sediment core likely reflects its proximity to the outflow of the Biobío River. Parasound data indicate well stratified sediment down to at least ~60 mbsf.

Sediments collected at Site J1008 will provide records of surface and Pacific Deep Water variability over the last ~600 ky. At 36°S, the site is located south of the main upwelling region along the coast of Peru and Northern Chile but upwelling does occur seasonally, primarily during austral spring and summer driving high primary production, ~20 g C m-2 d-2 (e.g. Daneri et al., 2000). Nutrients are also supplied to the study area via the Itata and Biobío rivers, which carry weathering products and fresh water from the Andes and Coastal Ranges out into the open ocean. In the shallow subsurface (70 and 400 m), the Gunter Undercurrent brings low oxygen water sourced from the oxygen minimum zone located to the north. Nitrogen isotopes, foraminifer I/Ca, and redox sensitive metals may be used at this location to track changes in the strength of the OMZ. This site is our northernmost site and will therefore enable comparative studies with cores collected further south to assess N-S penetration of water masses in the eastern Pacific, including sub-Antarctic surface waters, low oxygen Equatorial Subsurface Water carried by the GUC, and PDW (Figure F2).

## Operations

Hole locations, water depths, and the number of cores recovered are listed in Table T1. All times are local ship time (UTC -04 h) unless otherwise noted. Site J1008 (proposed Site CM-08) was the eighth site occupied during Expedition 379T. The plan for Site J1008 was to advanced piston corer (APC) triple core to ~100 mbsf while using stratigraphic correlation to construct a complete splice for a 100% record over the 100 m interval. Temperature measurements with the advanced piston corer temperature tool (APCT-3) were scheduled to be completed on the first hole.

### *Hole J1008A*

During the 13 nautical mile transit from Site J1007 the vessel averaged 8.1 knots. We arrived at Site J1008 at 1418 h on 13 August 2019. The thrusters were lowered and secured, the dynamic positioning system was engaged, and at 1433 h the drill floor was cleared for operations, beginning Hole J1008A. We did not deploy an acoustic positioning beacon, but prepared one for immediate deployment if required.

The APC bottom-hole assembly (BHA) was made up and run to 135.62 m and the drill string was run to 2039.0 mbrf. The calculated precision depth recorder (PDR) depth for the site was 2043.9 mbrf. Based on the PDR, 2039.0 mbrf was selected as the shoot depth for the first core. A non-magnetic core barrel was run to bottom and the mudline core (J1008A-1H) recovered 4.04 meters of sediment. The seafloor was estimated to be 2044.5 mbrf (2033.4 mbsl). Non-magnetic core barrels were used for all cores and coring continued through Core J1008A-11H to a depth of 99.0 mbsf. From the 99.0 m cored in Hole J1008A, we recovered 104.90 m of core (106%). Hole J1008A ended at 0530 h on 14 August 2019 and the vessel was offset 20 m east.

### *Hole J1008B*

Hole J1008B was spudded at 0625 h on 14 August. The mudline core (J1008B-1H) recovered 9.42 m of sediment and the sea floor was calculated to be 2043.1 mbrf (2031.9 mbsl). Non-magnetic core barrels were used for APC coring. Coring continued through Core J1008B-12H to a depth of 104.4 mbsf. The bit was tripped back and cleared the seafloor at 1415 h on 14 August ending Hole J1008B. From the 104.4 m cored in Hole J1008B, we recovered 109.91 m of core (105%).

### *Hole J1008C*

The vessel was repositioned 20 m south for the start of Hole J1008C. The drill pipe was spaced out to 2041.0 mbrf and Hole J1008C was spudded at 1525 h on 14 August. The mudline core (J1008C-1H) recovered 6.96 m of sediment and the seafloor was calculated to be 2043.6 mbrf (2032.3 mbsl). Non-magnetic core barrels were used for APC coring and temperature measurements were taken on Cores J1008C-5H, 7H, and 10H with good results. Coring continued through Core J1008C-12H to a depth of 109.4 mbsf. There was one short advance on Core J1008C-9H of 7.5 m to assist in correlation. The bit was tripped back and the drill floor was secured at 0630 h on 15 August 2019, ending Hole J1008C and Site J1008. From the 109.4 m cored in Hole J1008C, we recovered 117.84 m of core (108%).

A total of 34 cores were recorded for the Site J1008. Only the APC coring system was used, with 106% recovery over the 312.8 m cored. The three holes at Site J1008 consumed 1.67 days of expedition time.

## Principal results

All depth references in meters in this section refer to the CSF-A depth scale.

The sediment cored at Site J1008 is assigned to a single lithologic unit composed of 109.9 m of Pleistocene nannofossil-rich clay mixed with varying amounts of biogenic tests and coarser siliciclastics (Figure F17). Biogenic constituents vary in abundance and mostly consist of nannofossils and diatoms, though sponge spicules, bivalve shell fragments, and foraminifers are also observed throughout the site. Minor constituents include intermittent thin (cm-scale) silty, sandy-silt, and vitric ash-bearing intervals scattered throughout. The silty or sandy silt layers always contain volcanogenic material, often volcanoclastic (reworked, rounded and partially altered) ash and lava pieces, and they also nearly always contain significant fractions of pyroclastic ash (tephra, i.e. first cycle, angular and vitric). In addition, the section contains tephra layers, ~3-6 cm in thickness. Three of these tephra layers can be traced across all three holes and serve as potential time-marker layers.

Calcareous nannofossils, planktonic foraminifers, and benthic foraminifers are present and show good to very good preservation. Siliceous microfossils exhibit moderate to good preservation. The calcareous nannofossils ranged from few to dominant. The last downhole occurrence of *Emiliania huxleyi* is observed within the sample at 49.7 m CSF-A. The first downhole occurrence of *Pseudoemiliania lacunosa,* which marks the top of nannofossil biozone NN19 and corresponds to an age of 400 ka, is observed at 64.4 m CSF-A and persists to the base of the hole (Figure F18). There is a minor amount of Pliocene/Miocene reworking observed at this site, noted by the presence of intermediate to large *Reticulofenestra spp., Dictyococcites bisecta,* and *Discoaster variabilis.* Diatom microfossils are common throughout Site J1008 with good preservation in terms of dissolution and moderate preservation in terms of fragmentation. The diatom flora is characterized by an upwelling-related assemblage composed mainly of *Chaetoceros* subgenus *Hyalochaete* (resting spores and vegetative valves) and secondarily of

*Delphineis* spp., *Pseudonitzschia* spp., and *Thalassionema nitzschioides*. Planktonic foraminifers were more abundant than benthic foraminifers in almost all core catcher samples in Hole J1008A, with the planktonic:benthic ratio ranging from 82:18 to 59:41. A total of 15 planktonic taxa were identified in Hole J1008A. The most abundant species in Hole J1008A were polar *Neogloboquadrina pachyderma* (s), subpolar *Neogloboquadrina incompta*, and transitional species *Globigerina bulloides, Globigerinita glutinata* and *Globorotalia inflata* —indicating subpolar to transitional conditions. The benthic foraminiferal assemblage in Hole J1007A is characterized mostly by *Bulimina mexicana, Cibicidoides* sp., *Fursenkoina bradyi, Globobulimina affinis, Oridorsalis umbonatus, Uvigerina peregrina* and *Uvigerina* sp.

Paleomagnetic investigations on the recovered materials from Site J1008 involved the measurement of the natural remanent magnetization (NRM) of APC archive-half cores from Holes J1008A, J1008B, and J1008C before and after alternating field (AF) demagnetization. The drill string overprint is magnetically soft and is effectively removed after AF demagnetization in a 5-15 mT field. In addition to the superconducting rock magnetometer (SRM) measured half core sections, two discrete samples were taken per core, generally from Sections 3 and 6 from Hole J1008A (21 samples in total) to provide a more detailed characterization of the paleomagnetic behavior and the rock magnetic properties of the sediment, including anisotropy of magnetic susceptibility (AMS). Inclination and declination measured on discrete samples are generally in good agreement with those measured on the archive-half sections. Magnetic inclination data average around the value predicted by a GAD field (-56°) suggesting that the sediment was deposited during a period of normal polarity during the Brunhes chron and is < 780 ka in age. Over shorter timescales both inclination and declination vary over a few tens of degrees, suggesting that a paleosecular variation (PSV) record is preserved in the sediments

deposited at Site J1008. Several inclination and/or declination anomalies are present throughout the records of Holes J1008A, J1008B, and J1008C, but only one anomaly, occurring at ~14.5 m CSFA-A has inclination and declination expressions that can be correlated across holes. Lower NRM intensity values during a period of relatively constant MS suggests that the observed variability does not coincide with decreases in magnetic mineral concentration that could be related to changes in lithology or sediment geochemistry. Following this initial evaluation, we suggest the anomaly could reflect an excursion of the geomagnetic field recorded in the sediments deposited at Site J1008. However, with no independent chronology or stratigraphic markers currently available for Site J1008 it is unclear which geomagnetic excursions this horizon might be associated with.

The physical property data collected for Site J1008 includes gamma ray attenuation (GRA) bulk density, magnetic susceptibility (MS), and natural gamma ray counts (NGR) collected on whole-round cores and additional measurements on split cores and discrete samples including P-wave velocity; porosity; thermal conductivity; and bulk, dry, and grain densities. The MS signature is characterized by decimeter-scale variability interrupted by intervals of low MS ($<100 \times 10^{-5}$ SI), in which authigenic alteration was observed. NGR counts show a slight decreasing trend downhole at Site J1008 and decimeter-scale variability. Formation temperature measurements made with the advanced piston corer temperature tool (APCT-3) indicate a geothermal gradient of 37°C/km for the upper ~100 m CSF-A.

Sequences from the three holes were composited in near-real-time using magnetic susceptibility data from the WRMSL measured at 2.5 cm resolution to guide the coring by optimizing the core stagger between holes. Final compositing was accomplished using a combination of magnetic susceptibility measurements from the Whole-Round Multisensor

Logger (WRMSL) and the ratio of Green/Blue channels from the Section Half Imaging Logger. In general, the large amplitude signals in magnetic susceptibility resulted in relatively robust stratigraphic ties that could be verified and refined with the color data, despite the complication imposed by extreme stretching of some cores near the middle of the stratigraphic section.

We collected 45 interstitial water samples from Hole J1008B, 24 interstitial water samples from Hole J1008C, and one mudline water sample from Holes J1008A, J1008B, and J1008C. We measured the routine shipboard analyses on one sample per core from J1008A, and from each mudline sample, totaling 13 samples. The rest of the samples were collected for high-resolution isotope and chlorinity measurements. Routine shipboard analyses included chloride (by titration and ion chromatography; IC), alkalinity (by titration), major and minor elements (by Inductively Coupled Plasma-Optical Emission Spectroscopy; ICP-OES), major cations and anions (by IC), and ammonium and phosphate (by UV/vis spectrophotometry). Chemical gradients at this site reflect the influence of microbially mediated oxidation of organic matter, authigenic mineralization reactions, water-rock interaction processes, and diffusive processes on porewater fluid composition.

A methane headspace sample was collected from each core. The maximum methane concentration (145,151 ppmV) was found at 58.7 m CSF-A (Figure F19). Methane concentrations then decrease towards the bottom of the hole (8,120 ppmV). The high concentrations of methane relative to other gases suggest a biogenic source. Low concentrations (<1 ppmV) of Ethene were detected below 58.7 m CSF-A. C1:C2 values generally decrease downhole from ~ 50,000 towards 11, 000 at the base. This trend is interrupted by a large spike, to >180,000 at 58.7 m CSF-A, corresponding to the methane peak.

The calcium carbonate contents of the hemipelagic sediments at J1008 vary between 1 and 16.4 wt% downhole, with an average value of 4.2 wt%. Generally, carbonate content is low, below 7 wt% and it is largely biogenic, with lesser amounts of inorganic carbonate. A distinctly higher value, of the 16.4 wt% at 84.5 m CCSF, comes from a foraminiferal-bearing nannofossil ooze. The increase in biogenic carbonate around this horizon may reflect either enhanced surface ocean productivity or improved carbonate preservation in the seafloor.

# Tables and Figures

*Table T1. Expedition 379T hole summary. DSF=drilling depth below seafloor. APC=advanced piston corer*

| Hole | Latitude | Longitude | Water depth (m) | Penetration DSF (m) | Interval cored (m) | Core recovered (m) | Recovery (%) | Drilled interval (m) | Drilled interval (N) | Total cores (N) | APC cores (N) | Date started (2019) | Time started (h UTC) | Date finished (2019) | Time finished (h UTC) | Time on hole (h) | Time on hole (days) |
|---|---|---|---|---|---|---|---|---|---|---|---|---|---|---|---|---|---|
| J1001A | 46° 24.3201'S | 77° 19.4362'W | 3054.93 | 9.5 | 9.5 | 9.66 | 101.68 | | | 1 | 1 | 28 Jul | 1406 | 29 Jul | 0720 | 17.28 | 0.72 |
| J1001B | 46° 24.3198'S | 77° 19.4343'W | 3056.23 | 100.7 | 100.7 | 101.25 | 100.55 | | | 11 | 11 | 29 Jul | 0720 | 30 Jul | 0600 | 22.56 | 0.94 |
| J1001C | 46° 24.3278'S | 77° 19.4333'W | 3056.94 | 102.5 | 99.5 | 102.61 | 103.13 | 3 | 1 | 11 | 11 | 30 Jul | 0600 | 30 Jul | 1915 | 13.20 | 0.55 |
| J1001D | 46° 24.3289'S | 77° 19.4652'W | 3056.91 | 6.1 | 6.1 | 6.13 | 100.49 | | | 1 | 1 | 30 Jul | 1915 | 30 Jul | 2015 | 0.96 | 0.04 |
| J1001E | 46° 24.3319'S | 77° 19.4639'W | 3054.61 | 90.9 | 85.4 | 87.76 | 102.76 | 5.5 | 2 | 9 | 9 | 30 Jul | 2015 | 31 Jul | 1500 | 18.72 | 0.78 |
| J1002A | 46° 4.2964'S | 75° 41.2300'W | 1534.85 | 106.6 | 106.6 | 110.95 | 104.08 | | | 12 | 12 | 31 Jul | 2208 | 02 Aug | 0715 | 33.12 | 1.38 |
| J1002B | 46° 4.3017'S | 75° 41.2146'W | 1533.05 | 103.9 | 103.9 | 110.77 | 106.61 | | | 11 | 11 | 02 Aug | 0715 | 02 Aug | 1845 | 11.52 | 0.48 |
| J1002C | 46° 4.3107'S | 75° 41.2151'W | 1532.53 | 101.9 | 101.9 | 108.59 | 106.57 | | | 11 | 11 | 02 Aug | 1845 | 03 Aug | 1330 | 18.72 | 0.78 |
| J1003A | 45° 28.5008'S | 75° 33.5020'W | 669.81 | 79.6 | 79.6 | 79.58 | 99.97 | | | 9 | 9 | 04 Aug | 0100 | 05 Aug | 1200 | 35.04 | 1.46 |
| J1003B | 45° 28.4993'S | 75° 33.4836'W | 670.81 | 53.1 | 53.1 | 54.16 | 102.00 | | | 6 | 6 | 05 Aug | 1200 | 05 Aug | 2245 | 10.80 | 0.45 |
| J1004A | 44° 9.0306'S | 75° 9.0651'W | 1125.23 | 70.1 | 70.1 | 60.94 | 86.93 | | | 9 | 9 | 06 Aug | 0730 | 06 Aug | 2221 | 14.88 | 0.62 |
| J1004B | 44° 9.0306'S | 75° 9.0478'W | 1124.23 | 58.0 | 58.0 | 55.35 | 95.43 | | | 7 | 7 | 06 Aug | 2221 | 07 Aug | 0400 | 5.76 | 0.24 |
| J1004C | 44° 9.0304'S | 75° 9.0328'W | 1124.03 | 56.9 | 56.9 | 56.70 | 99.65 | | | 6 | 6 | 07 Aug | 0400 | 07 Aug | 1354 | 9.84 | 0.41 |
| J1005A | 41° 4.5798'S | 74° 26.0998'W | 806.54 | 101.9 | 101.9 | 108.54 | 106.52 | | | 11 | 11 | 08 Aug | 0933 | 08 Aug | 2247 | 13.20 | 0.55 |
| J1005B | 41° 4.5796'S | 74° 26.0852'W | 806.94 | 107.0 | 107.0 | 108.90 | 101.78 | | | 12 | 12 | 08 Aug | 2247 | 09 Aug | 0729 | 8.64 | 0.36 |
| J1005C | 41° 4.5912'S | 74° 26.0855'W | 807.18 | 103.2 | 103.2 | 111.70 | 108.24 | | | 11 | 11 | 09 Aug | 0729 | 09 Aug | 1609 | 8.64 | 0.36 |
| J1006A | 41° 1.5646'S | 74° 26.7036'W | 823.28 | 103.6 | 103.6 | 105.62 | 101.95 | | | 11 | 11 | 09 Aug | 1906 | 10 Aug | 0650 | 11.76 | 0.49 |
| J1006B | 41° 1.5608'S | 74° 26.6856'W | 824.48 | 108.9 | 108.9 | 109.10 | 100.18 | | | 12 | 12 | 10 Aug | 0650 | 10 Aug | 1730 | 10.56 | 0.44 |
| J1006C | 41° 1.5726'S | 74° 26.6851'W | 825.44 | 108.9 | 108.9 | 106.23 | 97.55 | | | 12 | 12 | 10 Aug | 1730 | 11 Aug | 0815 | 14.64 | 0.61 |
| J1007A | 36° 32.5396'S | 73° 39.9894'W | 787.11 | 101.8 | 101.8 | 103.77 | 101.94 | | | 11 | 11 | 12 Aug | 0910 | 12 Aug | 2130 | 12.24 | 0.51 |
| J1007B | 36° 32.5393'S | 73° 39.9766'W | 786.51 | 108.9 | 108.9 | 105.03 | 96.45 | | | 12 | 12 | 12 Aug | 2130 | 13 Aug | 0500 | 7.44 | 0.31 |
| J1007C | 36° 32.5510'S | 73° 39.9756'W | 785.90 | 95.1 | 95.1 | 95.86 | 100.80 | | | 11 | 11 | 13 Aug | 0500 | 13 Aug | 1630 | 11.52 | 0.48 |
| J1008A | 36° 27.1902'S | 73° 54.4796'W | 2033.40 | 99.0 | 99.0 | 104.90 | 105.96 | | | 11 | 11 | 13 Aug | 1833 | 14 Aug | 0930 | 14.88 | 0.62 |
| J1008B | 36° 27.1906'S | 73° 54.4651'W | 2031.95 | 104.4 | 104.4 | 109.91 | 105.28 | | | 11 | 11 | 14 Aug | 0930 | 14 Aug | 1815 | 8.64 | 0.36 |
| J1008C | 36° 27.2012'S | 73° 54.4794'W | 2032.45 | 109.4 | 109.4 | 117.84 | 107.71 | | | 12 | 12 | 14 Aug | 1815 | 15 Aug | 1030 | 16.32 | 0.68 |
| | | Totals: | | 2191.9 | 2183.4 | 2231.85 | 2544.21 | 8.5 | 3 | 241 | 241 | | | | | 350.88 | 14.62 |

*Figure F1. Mean annual sea surface temperature and salinity along the Chile Margin with locations of sites cored (blue circles) and sites skipped (white circles). Modern extent of the Patagonia icefields are shown in light blue and their Last Glacial Maximum extent is shown in white. Data souce: ODV World Ocean Atlas, 2013 (https://odv.awi.de/de/data/ocean/world_ocean_atlas_2013/).*

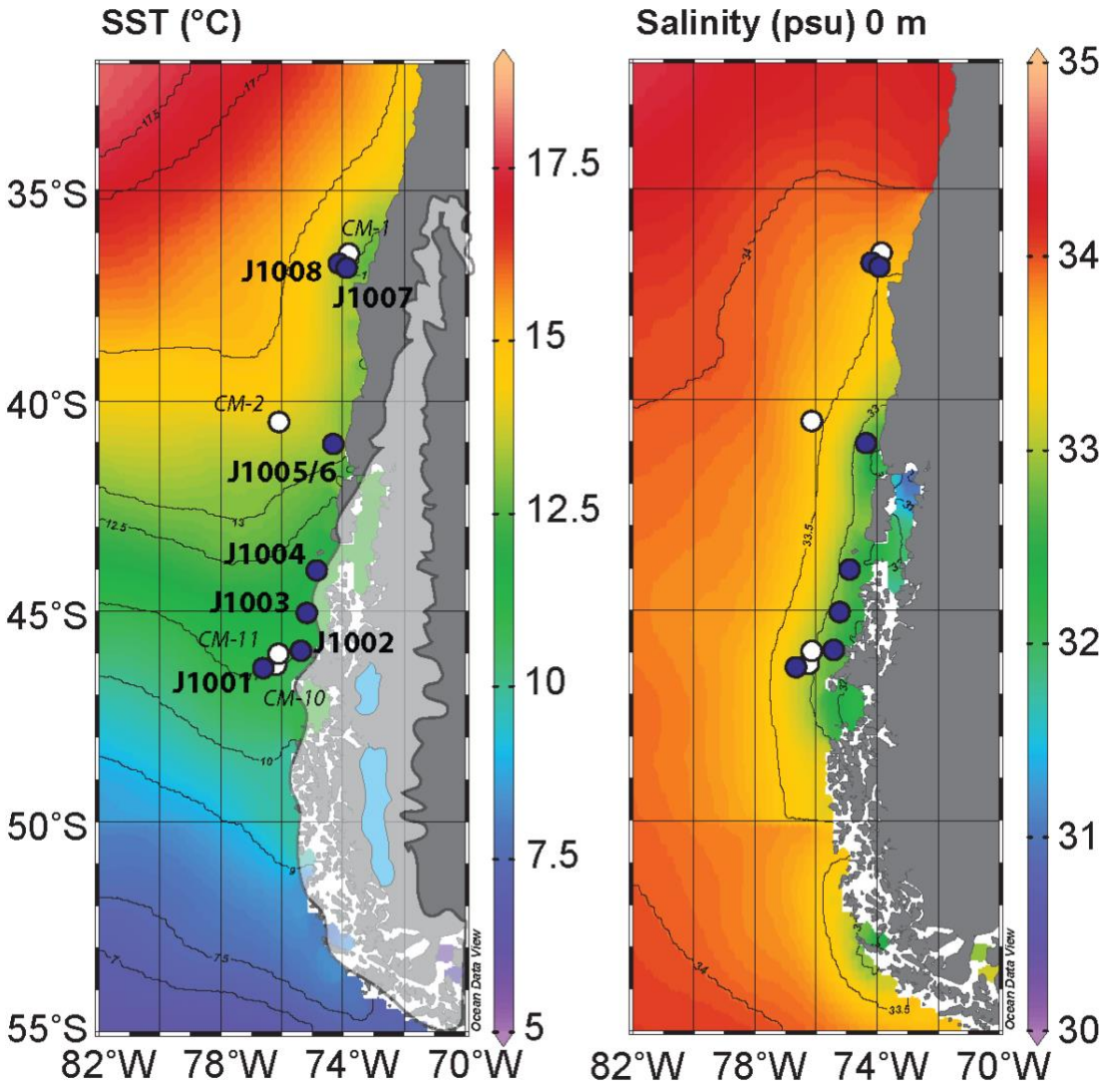

*Figure F2. Dissolved oxygen content along WOCE line P19 showing the main water masses in the southeast Pacific with locations of sites cored (blue circles) and sites skipped (white circles).*

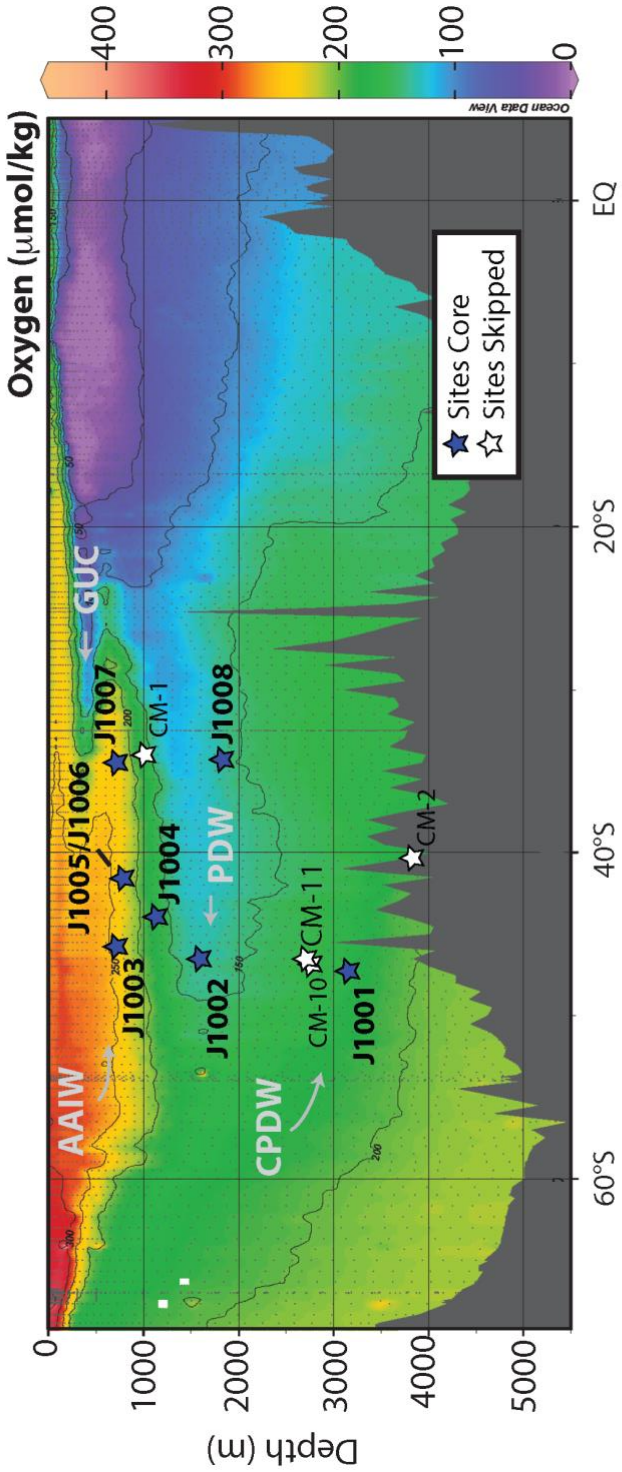

*Figure F3. Summary of coring operations and temporal resolution of Expedition 379T/JR100 core sites.*

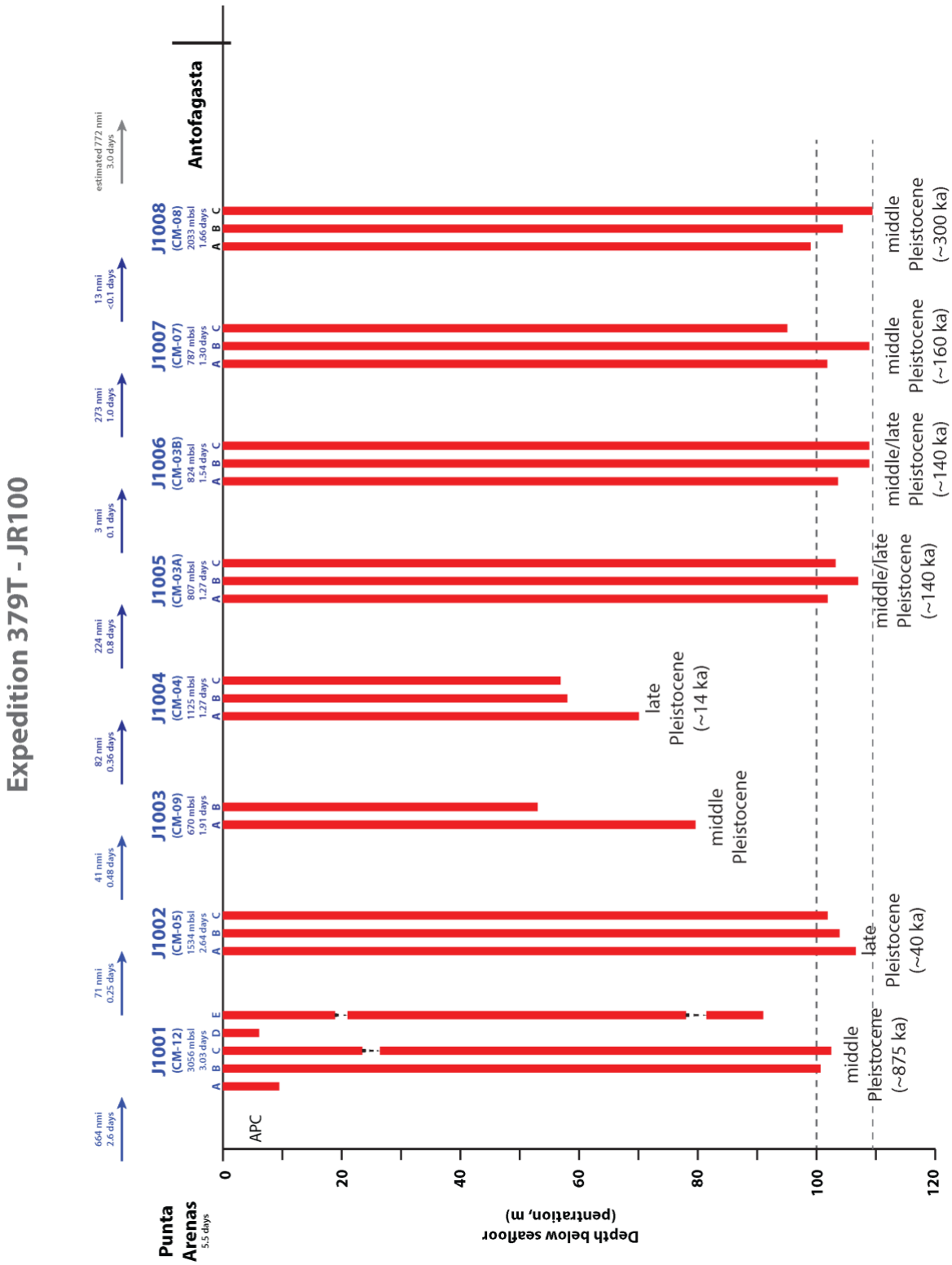

*Figure F4. South central Chilean Margin offshore of the Taitao Peninsula showing the location of Sites J1001, J1002, J1003, and J1004 (blue circles) as well as two proposed sites that were not cored during the Expedition (white circles).*

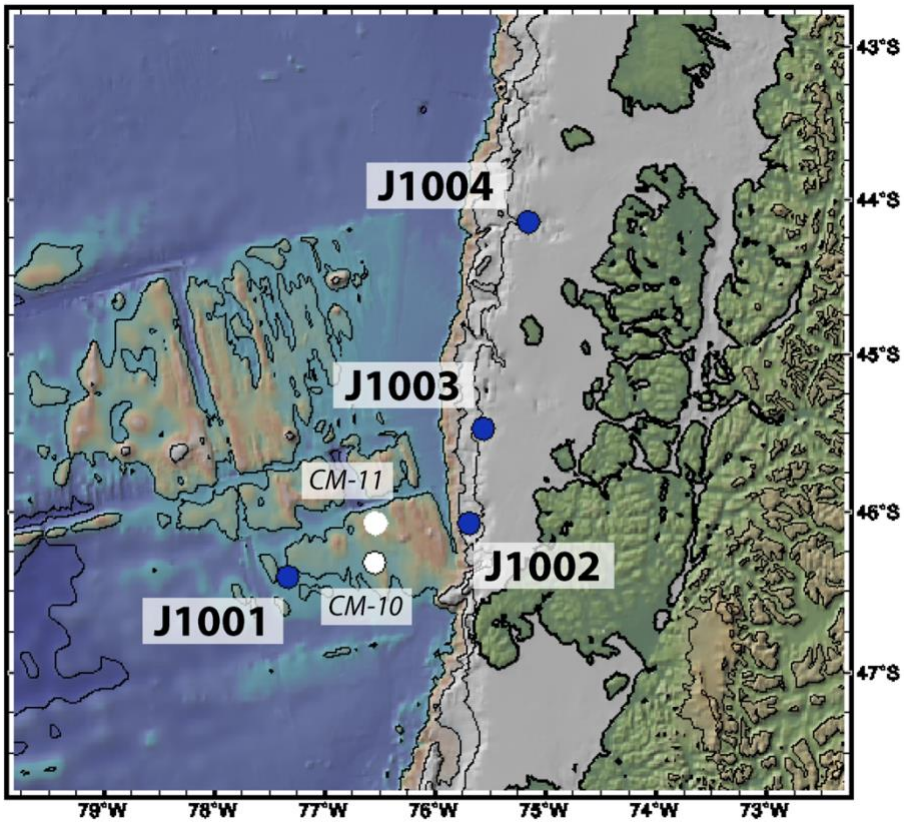

*Figure F5. Summary of Site J1001 results.*

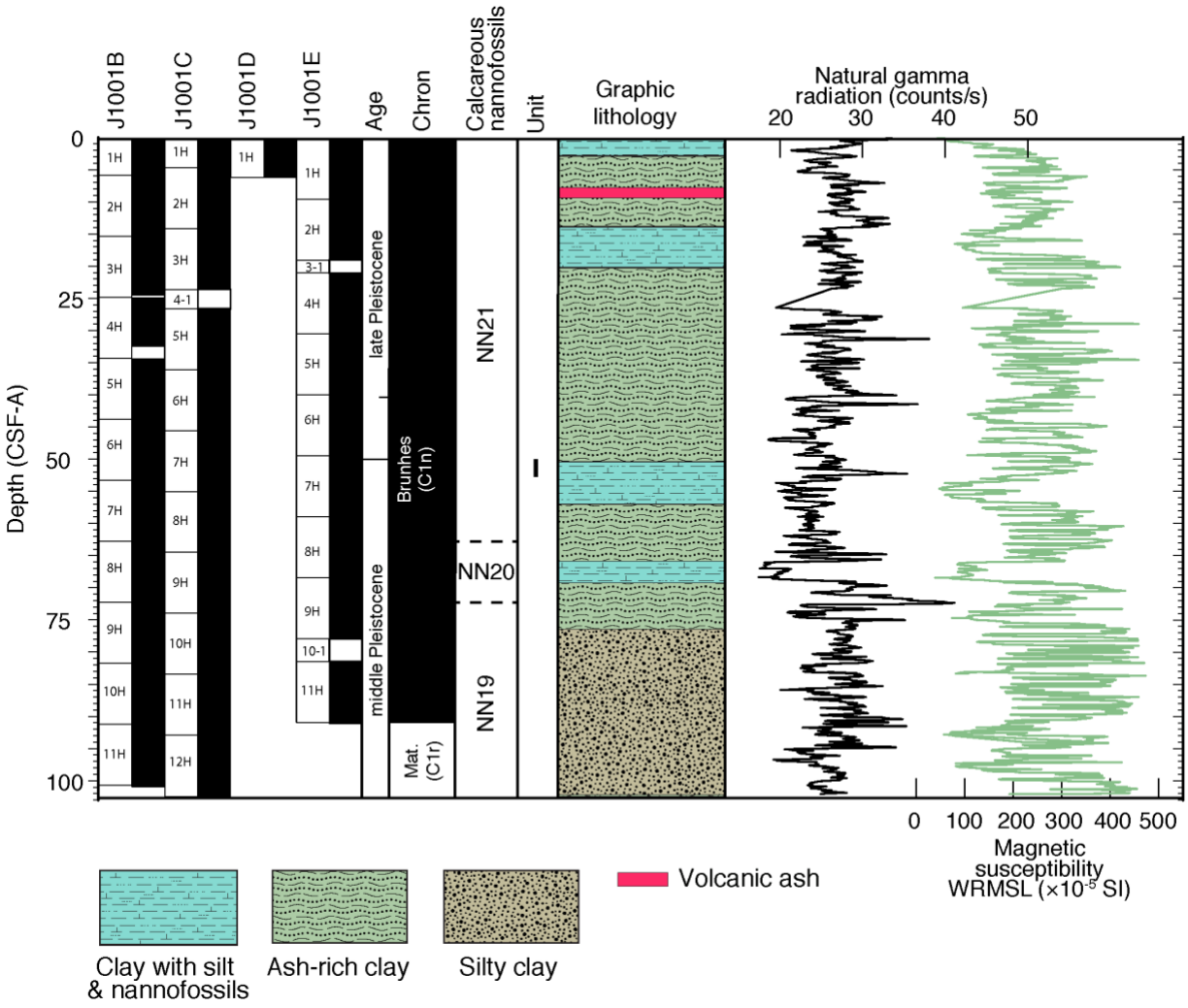

*Figure F6. Age-depth plot for calcareous nannofossil biohorizons and the Brunhes-Matuyama paleomagnetic datum, Site J1001. Average sedimentation rates are estimated at ~15 cm/ky during the last ~400 ky and <10 cm/ky to ~850 ky.*

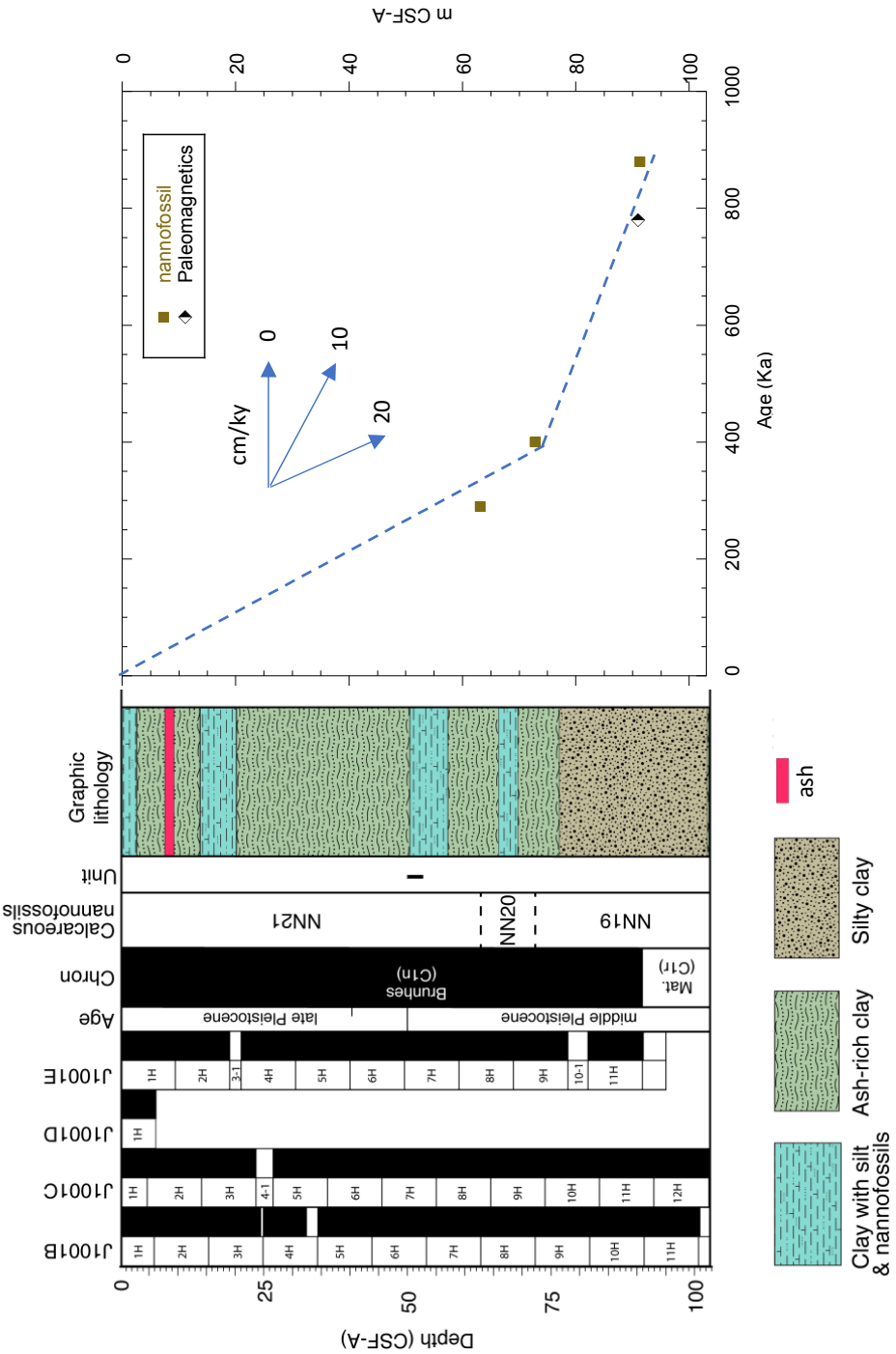

*Figure F7. Summary of Site J1002 results.*

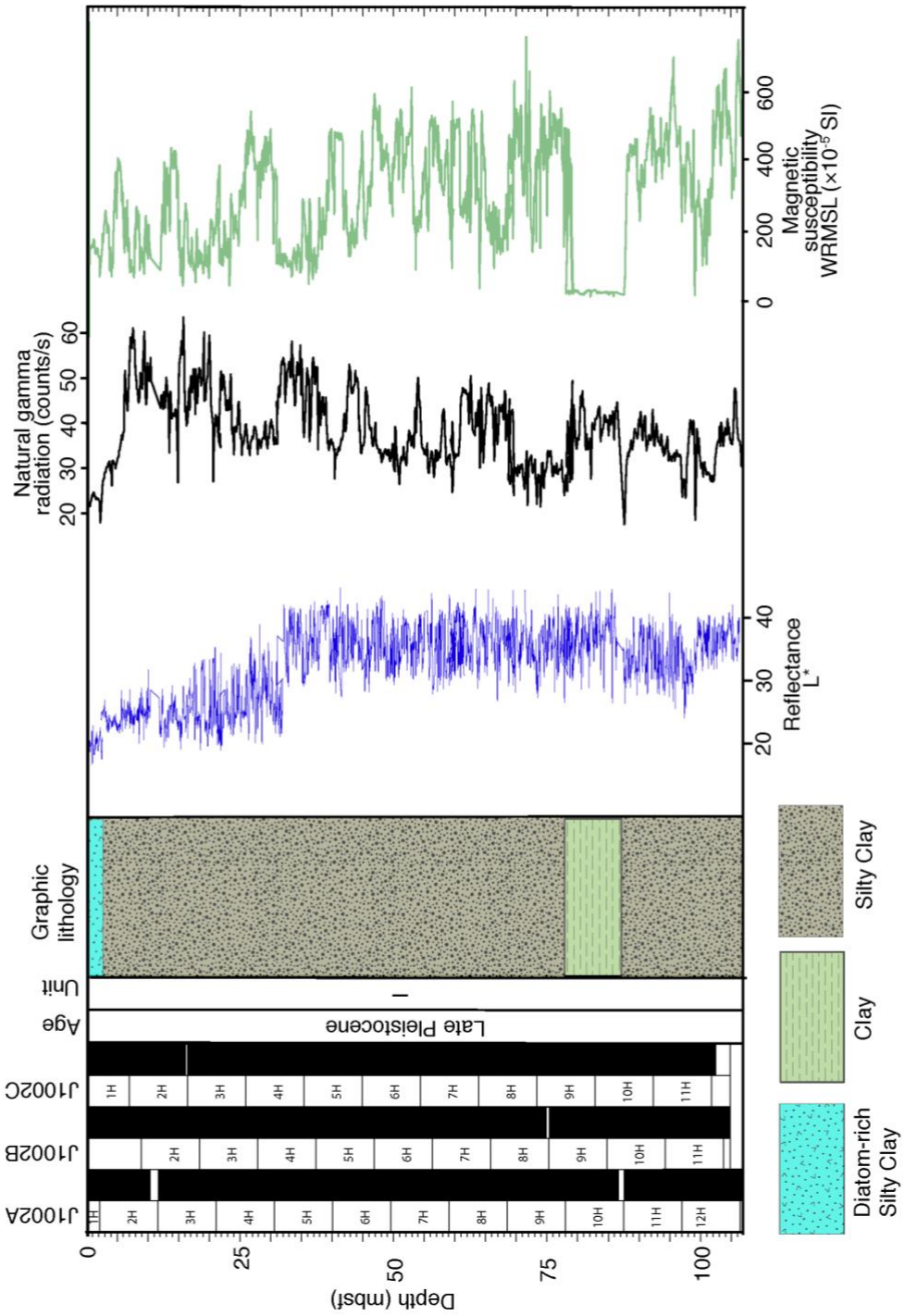

*Figure F8. Summary of J1003 results.*

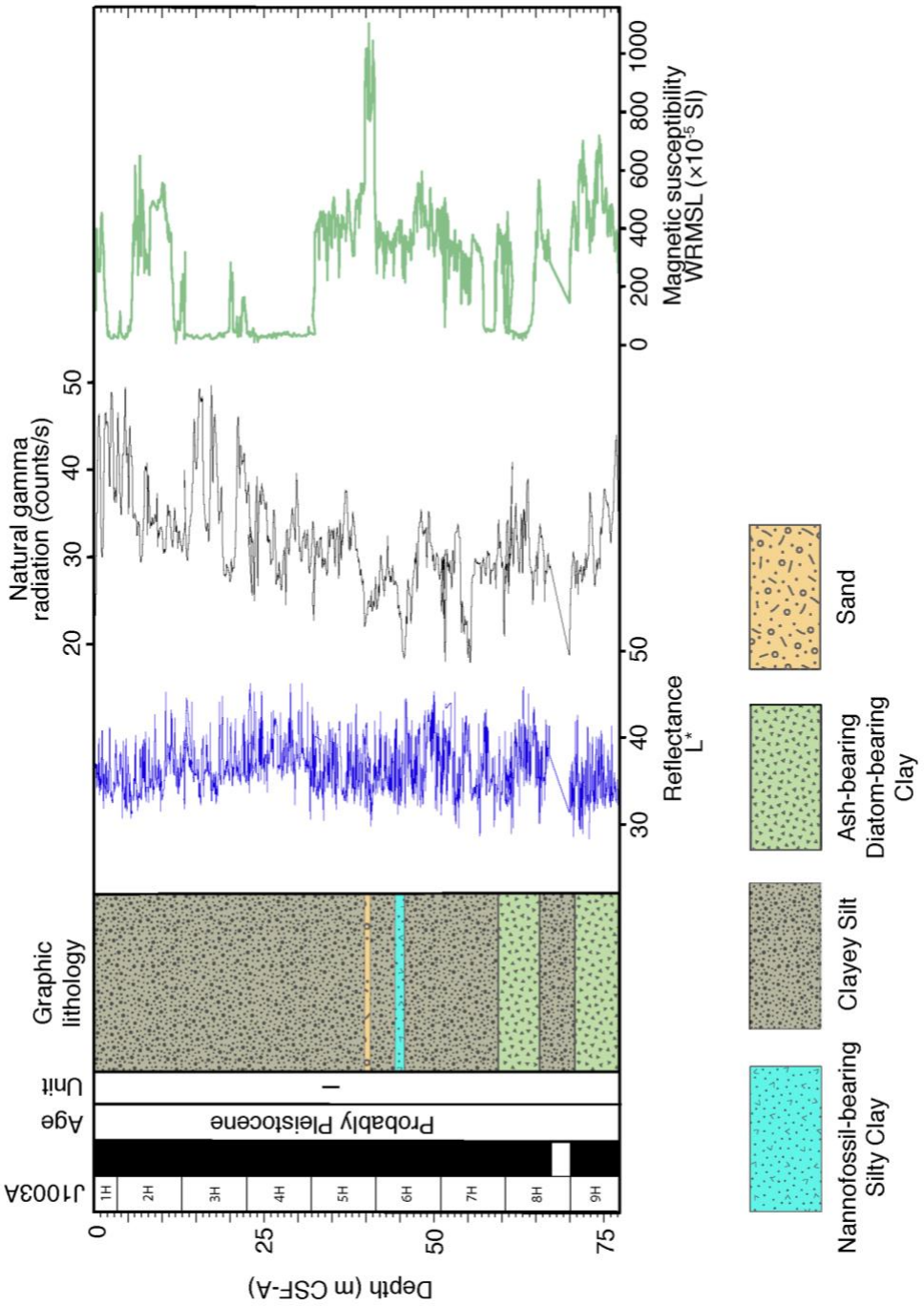

*Figure F9. Seismic Line 745 shown with line drawing interpretation showing the Nazca Plate subducting under the S. American plate. A prominent bottom seismic reflector can also be observed at~0.1-0.2 sec below the seafloor.*

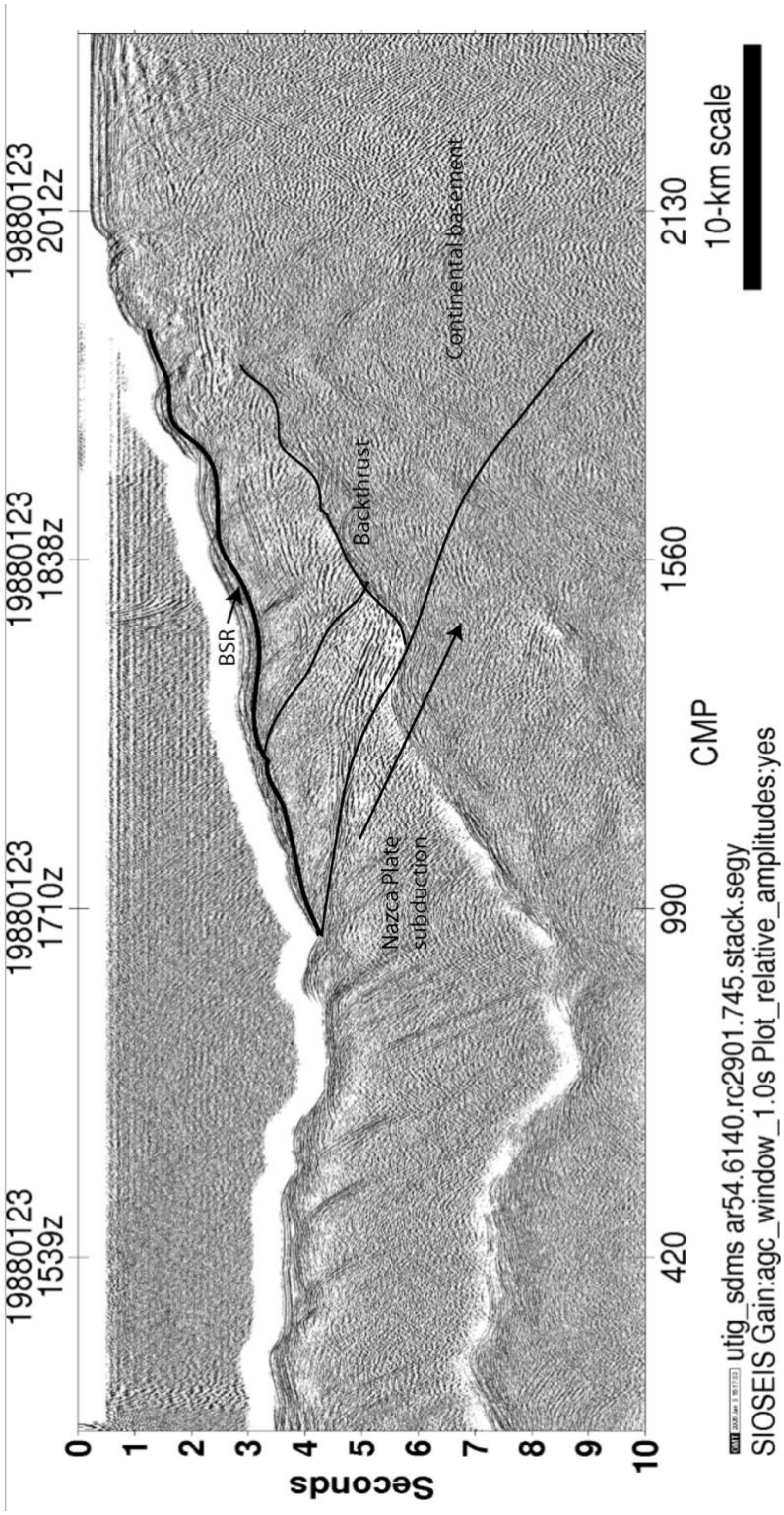

*Figure F10. Summary of J1004 results.*

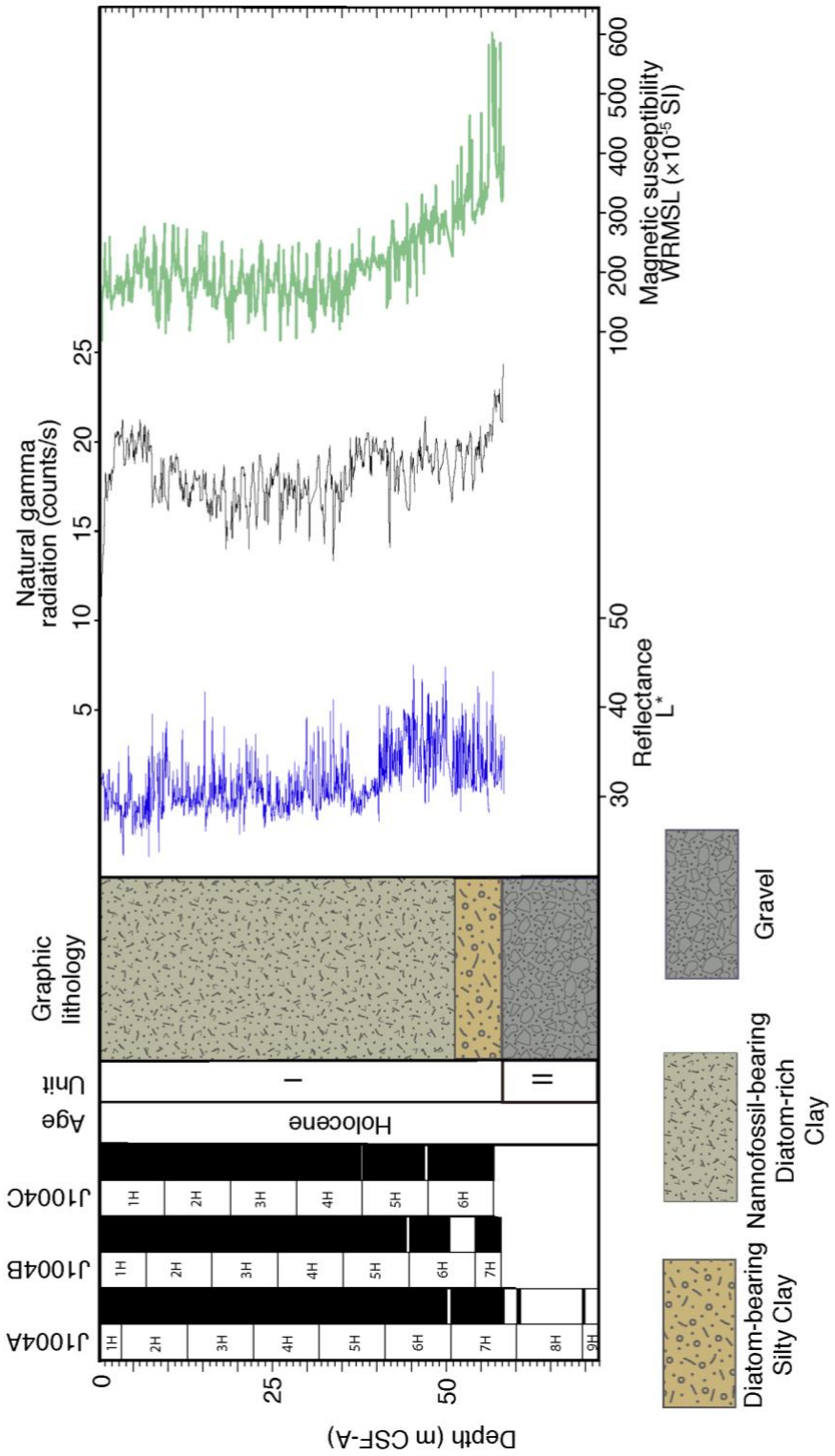

*Figure F11. Central Chilean Margin offshore just north of Chiloe Island showing the location of Sites J1005 and J1006 (blue circles) as that of ODP Site 1233 cored during ODP Leg 202 ias well as one alternate site that were not cored during the Expedition (white circles). Figure constructed using GeoMapApp. Contour interval = 100 m.*

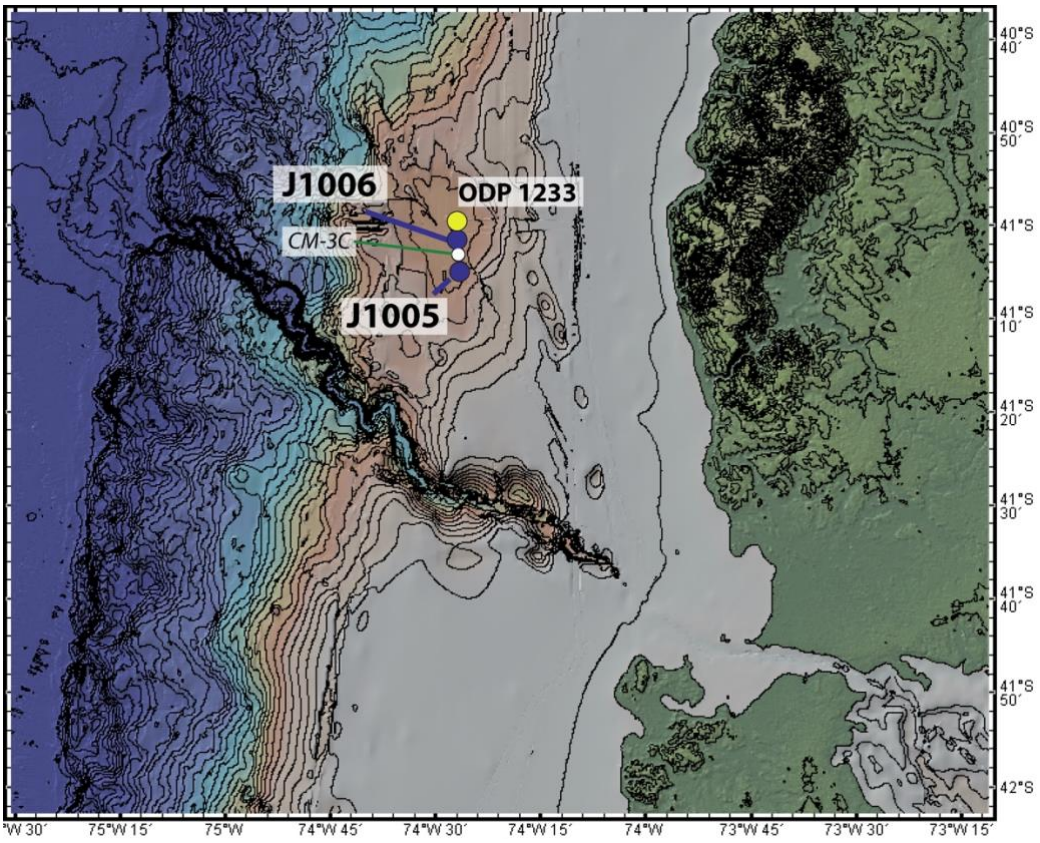

*Figure F12. (A.) Digital parasound data used to target ODP Site 1233, cored during Leg 202, and JR100/Exp. 379T sites J1005 and J1006. Site J1005 and J1006 were offset from ODP Site 1233 to target lower sedimentation rates. (B.) Analog 3.5-kHz profile collected during the approach to Site 1233 on Leg 202. Visible reflectors are traced between the Parasound and 3.5 kHz profiles.*

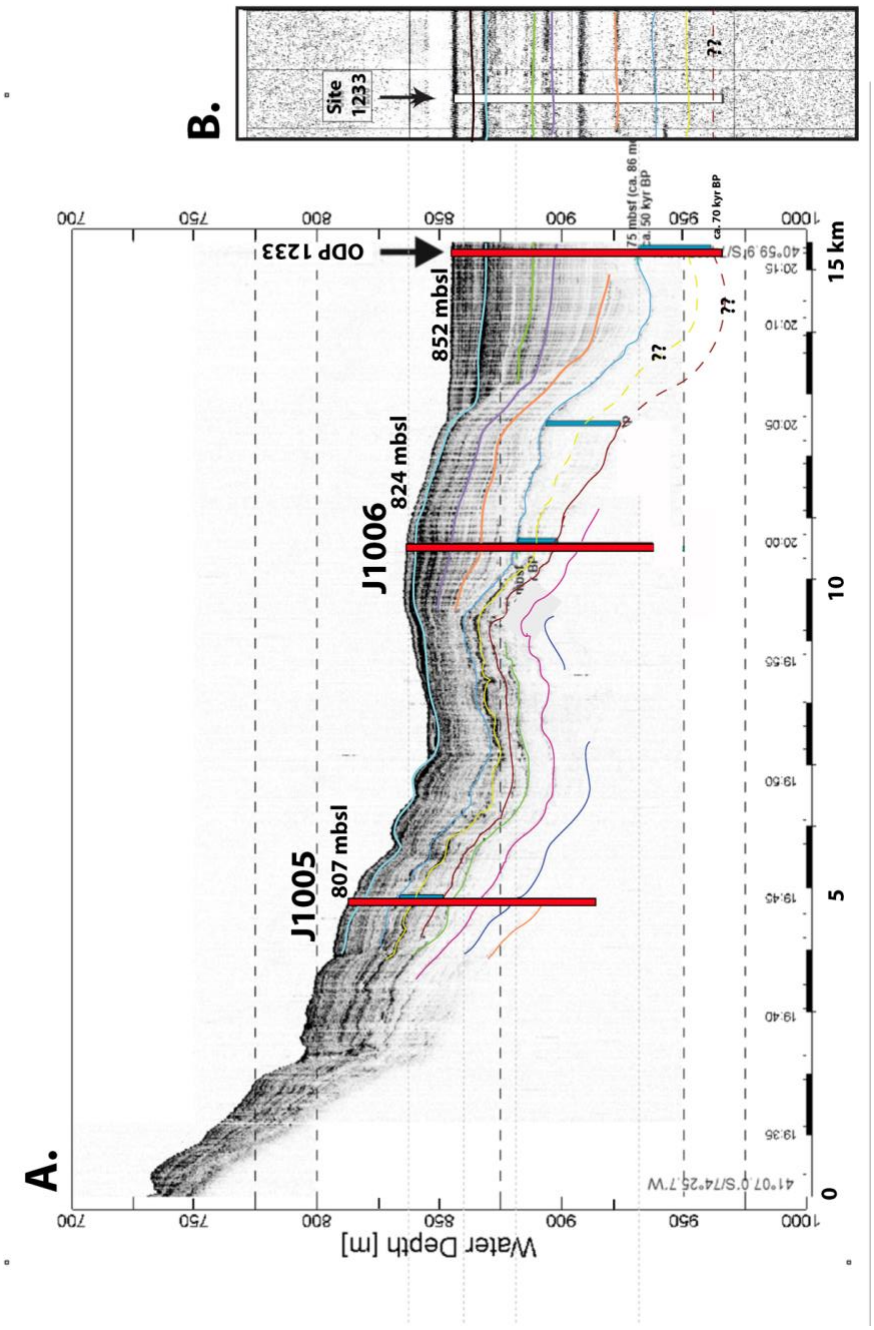

*Figure F13. Summary of J1005 results.*

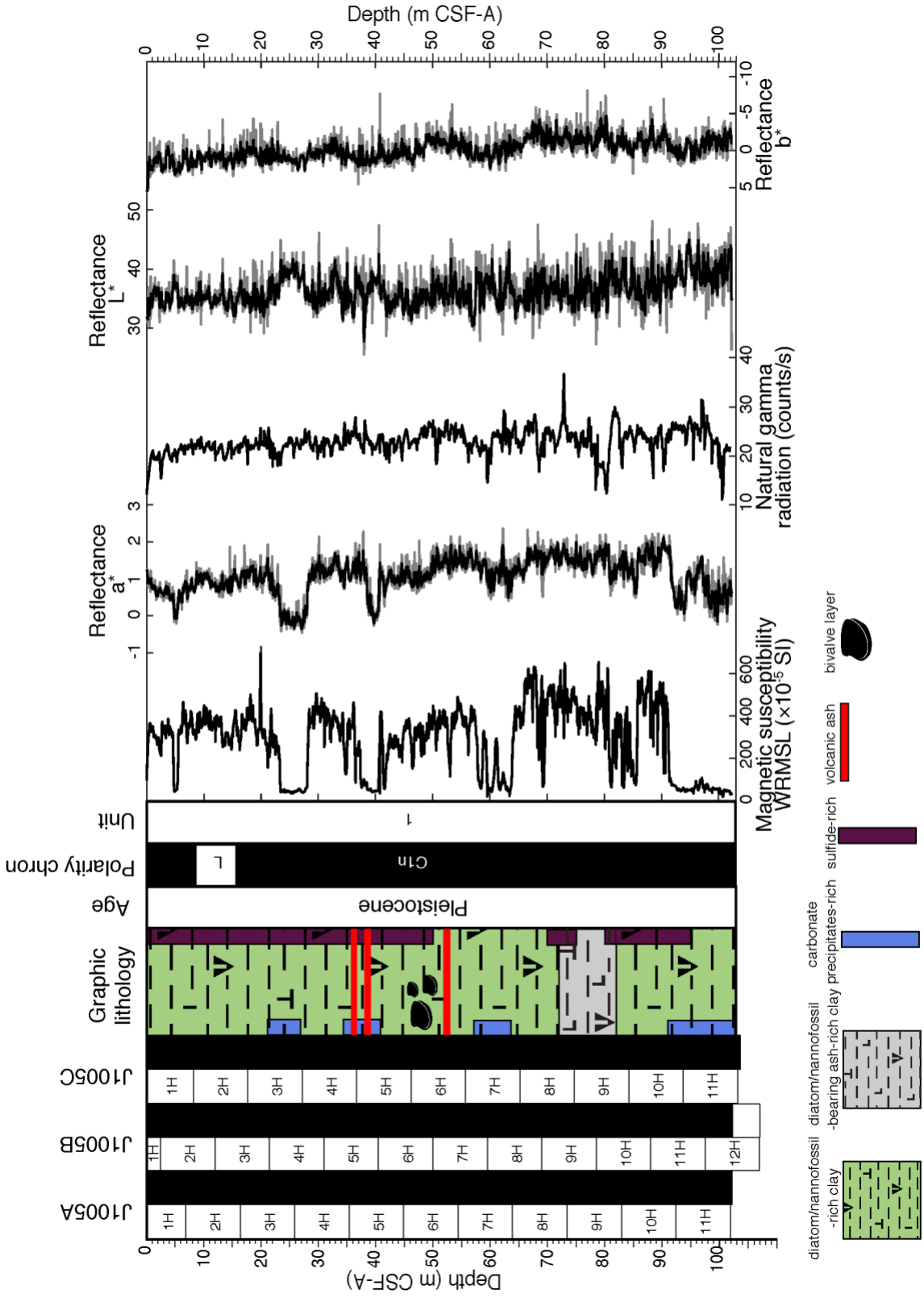

*Figure F14. Summary of J1006 results.*

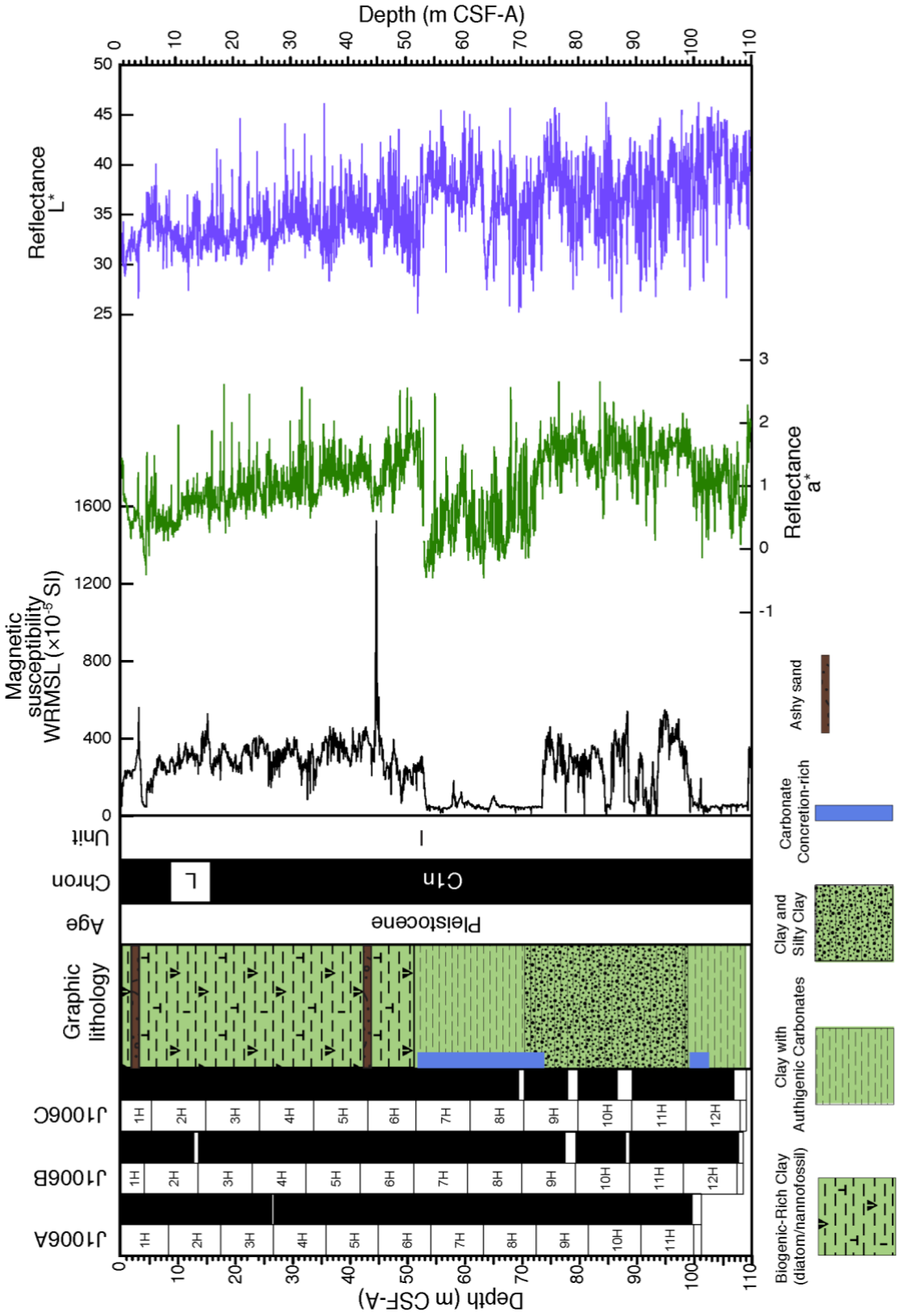

*Figure F15. Region offshore of the Arauco Peninsula showing the locations of Sites J1007 and J1008 (blue circles) and planned site CM-1 that was not cored during the expedition.*

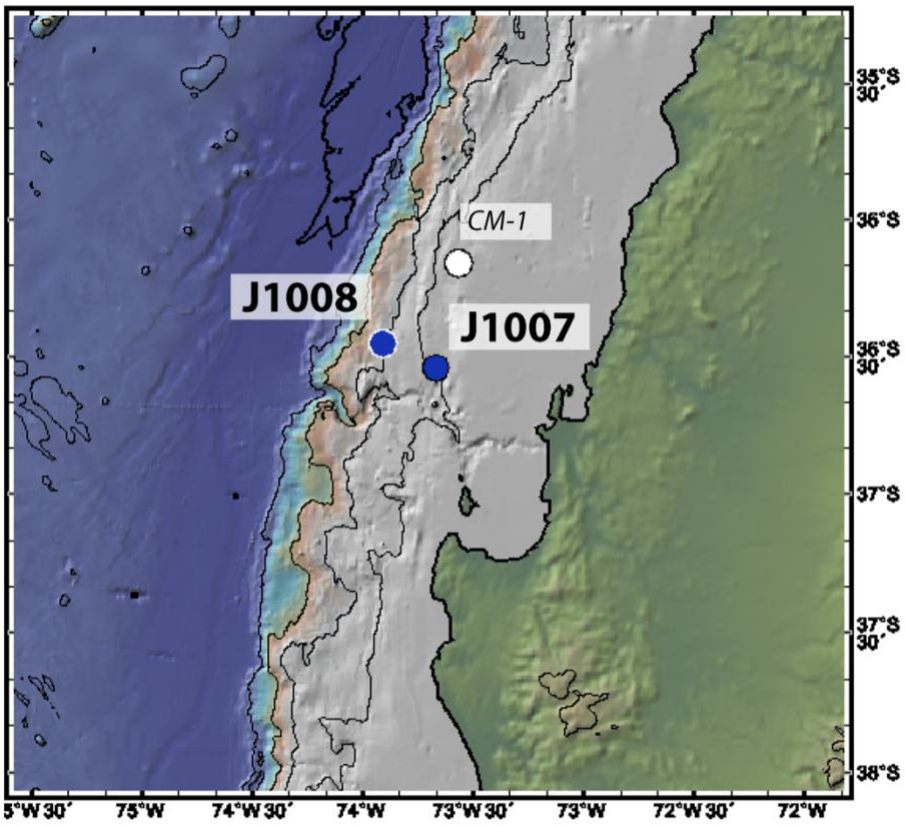

*Figure F16. Summary of J1007 results.*

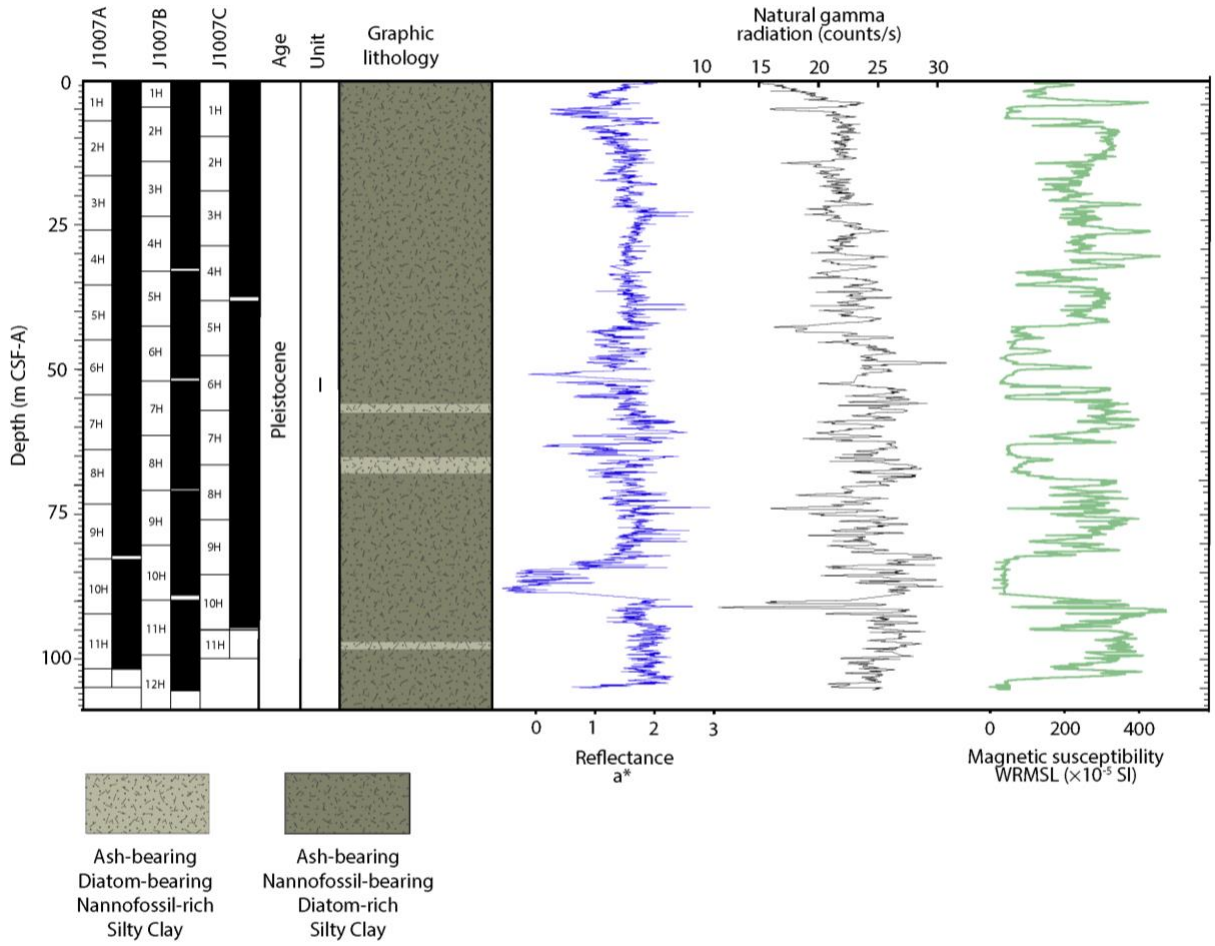

*Figure F17. Summary of J1008 results.*

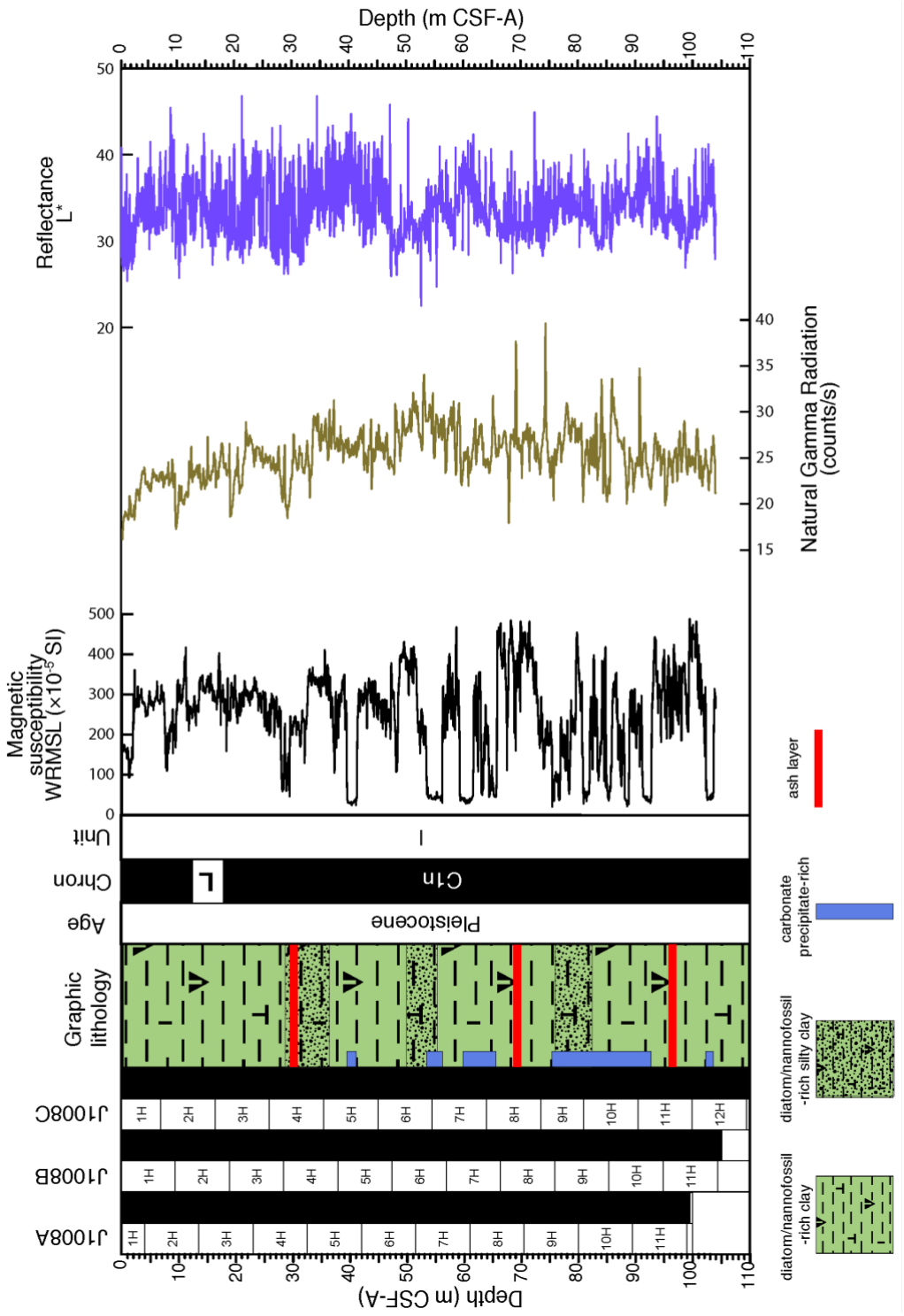

*Figure F18. Age-depth plot for calcareous nannofossil biohorizons, Site J1008. Average sedimentation rates are estimated at ~16 cm/ky.*

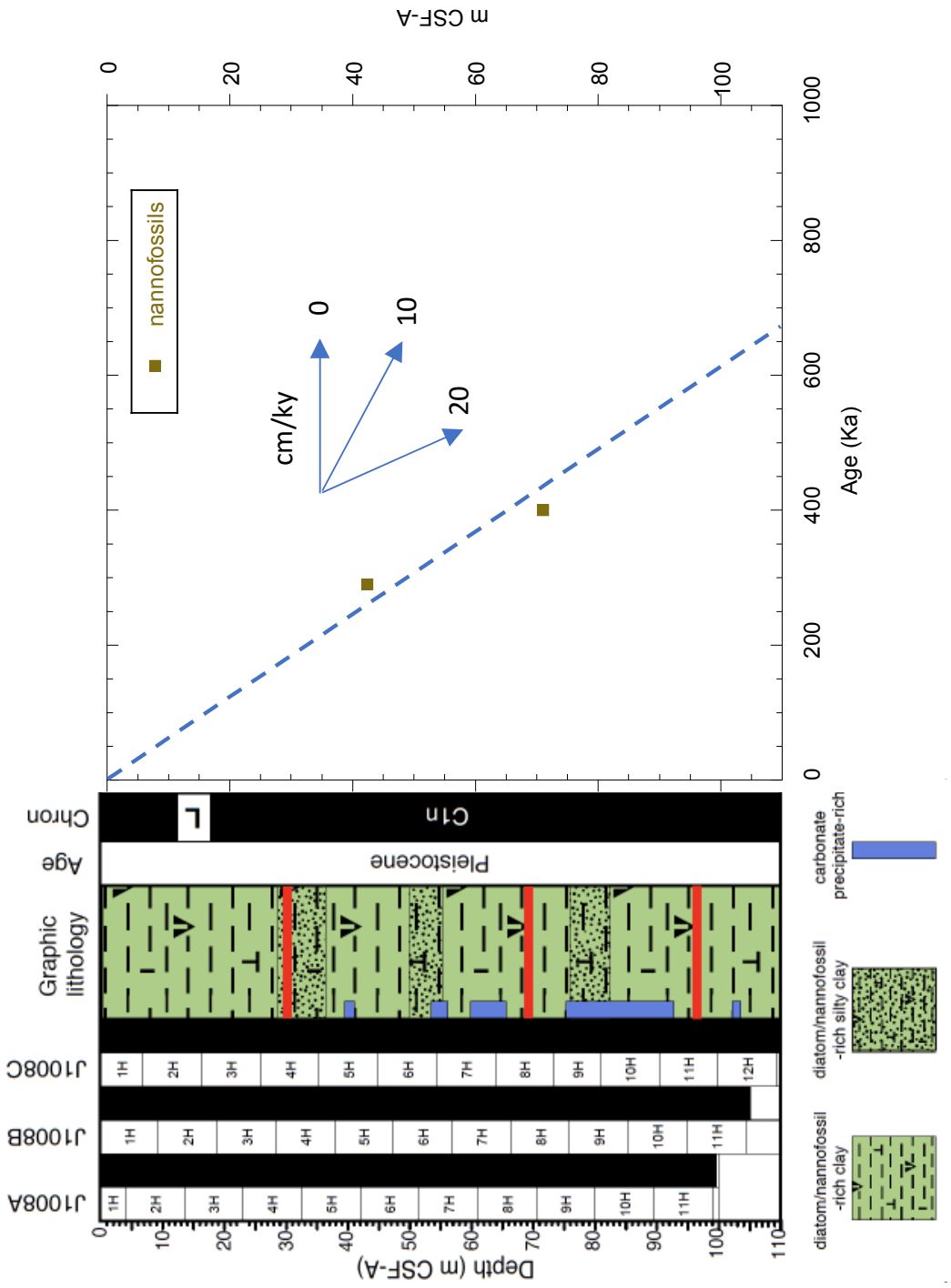

*Figure F19. Headspace methane concentrations at all eight sites cored during Expedition 379T.*

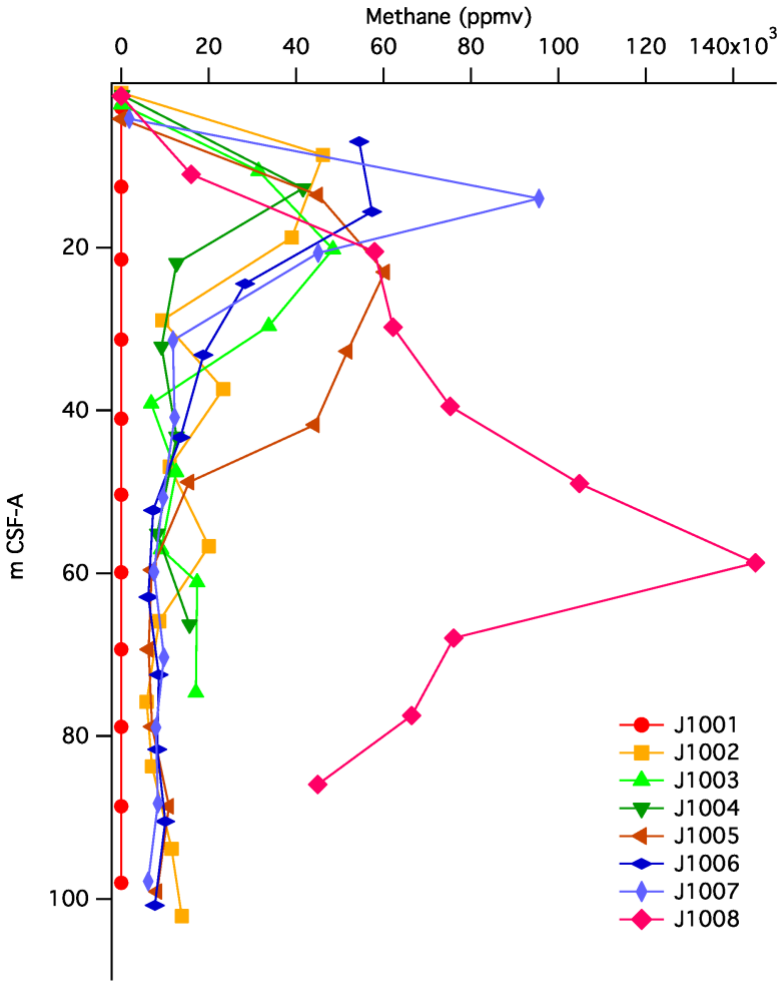

## References

Adkins, J.F., 2013. The role of deep ocean circulation in setting glacial climates. Paleoceanography 28, 539-561.

Adkins, J.F., McIntyre, K., Schrag, D.P., 2002. The salinity, temperature, and $\delta^{18}O$ of the glacial deep ocean. Science 298, 1769-1773.

Anderson, R.F., Ali, S., Bradtmiller, L.I., Nielsen, S.H.H., Fleisher, M.Q., Anderson, B.E., Burckle, L.H., 2009. Wind-Driven Upwelling in the Southern Ocean and the Deglacial Rise in Atmospheric $CO_2$. Science 323, 1443-1448.

Bendle, J. M., Palmer, A. P., Thorndycraft, V. R., and Matthews, I. P., 2019. Phased Patagonian Ice Sheet response to Southern Hemisphere atmospheric and oceanic warming between 18 and 17 ka. Scientific Reports, 9:4133. https://doi.org/10.1038/s41598-019-39750-w.

Bertrand, S., Hughen, K.A., Lamy, F., Stuut, J.B.W., Torrejon, F., Lange, C.B., 2012a. Precipitation as the main driver of Neoglacial fluctuations of Gualas glacier, Northern Patagonian Icefield. Clim Past 8, 519-534.

Bertrand, S., Hughen, K.A., Sepulveda, J., Pantoja, S., 2012b. Geochemistry of surface sediments from the fjords of Northern Chilean Patagonia (44-47° S): Spatial variability and implications for paleoclimate reconstructions. Geochim Cosmochim Ac 76, 125-146.

Bostock, H.C., Opdyke, B.N., Williams, M.J.M., 2010. Characterising the intermediate depth waters of the Pacific Ocean using $\delta^{13}C$ and other geochemical tracers. Deep-Sea Res Pt I 57, 847-859.

Bostock, H.C., Sutton, P.J., Williams, M.J.M., Opdyke, B.N., 2013. Reviewing the circulation and mixing of Antarctic Intermediate Water in the South Pacific using evidence from geochemical tracers and Argo float trajectories. Deep-Sea Res Pt I 73, 84-98.

Bova, S.C., Herbert, T., Rosenthal, Y., Kalansky, J., Altabet, M., Chazen, C., Mojarro, A., Zech, J., 2015. Links between eastern equatorial Pacific stratification and atmospheric $CO_2$ rise during the last deglaciation. Paleoceanography 30, 1407-1424.

Bova, S.C., Herbert, T.D., Fox-Kemper, B., 2016. Rapid variations in deep ocean temperature detected in the Holocene. Geophys Res Lett 43, 12190-12198.

Bova, S.C., Herbert, T.D., Altabet, M.A., 2018. Ventilation of Northern and Southern Sources of Aged Carbon in the Eastern Equatorial Pacific During the Younger Dryas Rise in Atmospheric $CO_2$. Paleoceanography and Paleoclimatology 33, 1151-1168. https://doi/full/10.1029/2018PA003386.

Cabre, M.F., Solman, S.A., Nunez, M.N., 2010. Creating regional climate change scenarios over southern South America for the 2020's and 2050's using the pattern scaling technique: validity and limitations. Climatic Change 98, 449-469.

Cande, S. C., and Kent, D. V., 1995. Revised calibration of the geomagnetic polarity timescale for the Late Cretaceous and Cenozoic. Journal of Geophysical Research: Solid Earth, 100(B4):6093–6095. https://doi.org/10.1029/94JB03098

Caniupan, M., Lamy, F., Lange, C.B., Kaiser, J., Arz, H., Kilian, R., Urrea, O.B., Aracena, C., Hebbeln, D., Kissel, C., Laj, C., Mollenhauer, G., Tiedemann, R., 2011. Millennial-scale sea surface temperature and Patagonian Ice Sheet changes off southernmost Chile (53°S) over the past similar to 60 kyr. Paleoceanography 26, PA3221.

Carrasco, J.F., Casassa, G., Rivera, A., 2002. Meteorological and climatological aspects of the southern Patagonia icefield, in: Casassa, G. (Ed.), The Patagonian Icefields: A Unique Natural Laboratory for Envrionmental and Climate Change Studies. Kluwer Academic/Plenum Publishers.

Channell, J. E. T., Xuan, C., and Hodell, D. A., 2009. Stacking paleointensity and oxygen isotope data for the last 1.5 Myr (PISO-1500). Earth and Planetary Science Letters, 283, 14-23.

Chase, Z., McManus, J., Mix, A.C., Muratli, J., 2014. Southern-ocean and glaciogenic nutrients control diatom export production on the Chile margin. Quaternary Sci Rev 99, 135-145.

Clark, P.U., Alley, R.B., Pollard, D., 1999. Northern hemisphere ice-sheet influences on global climate change. Science's Compass Review 286, 1104-1111.

Clark, P.U., Pisias, N.G., Stocker, T.F., Weaver, A.J., 2002. The role of the thermohaline circulation in abrupt climate change. Nature 415, 863-869.

Collins, J. A., Lamy, F., Kaiser, J., Ruggieri, N., Henkel, S., De Pol-Holz, R., Garreaud, R., and Arz, H. W. (2019). Centennial-Scale SE Pacific Sea Surface Temperature Variability Over the Past 2,300 Years. *Paleoceanography and Paleoclimatology*, *34*(3), 336-352.

Curry, W.B., Crowley, T.J., 1987. The $\delta_{13}C$ of equatorial Atlantic surface waters: implications for ice age $pCO_2$ levels. Paleoceanography 2, 489-517.

Daneri, G. Dellarossa, V., Quiñones, R., Jacob, B., Montero, P., and Ulloa, O., 2000. Primary production and community respiration in the Humboldt current system off Chile and associated oceanic areas. Mar Ecol Prog Ser 197, 41-49.

Denton, G.H., Heusser, C.J., Lowell, T.V., Moreno, P.I., Andersen, B.G., Heusser, L.E., Schluchter, C., Marchant, D.R., 1999. Interhemispheric linkage of paleoclimate during the last glaciation. Geografiska Annaler: Series A, Physical Geography, 81, 107-153.

De Pol-Holz, R., Ulloa, O., Lamy, F., Dezileau, L., Sabatier, P., Hebbeln, D., 2007. Late Quaternary variability of sedimentary nitrogen isotopes in the eastern South Pacific Ocean. Paleoceanography 22, PA2207.

Euler, C., Ninnemann, U.S., 2010. Climate and Antarctic Intermediate Water coupling during the late Holocene. Geology 38, 647-650.

Ferrari, R., Jansen, M.F., Adkins, J.F., Burke, A., Stewart, A.L., Thompson, A.F., 2014. Antarctic sea ice control on ocean circulation in present and glacial climates. P Natl Acad Sci USA 111, 8753-8758.

Fujiyoshi, Y., Kondo, H., Inoue, J., Yamada, T., 1987. Characteristics of precipitation and vertical structure of air temperature in Northern Patagonia. Bull. Glacial Res. 4, 15-24.

Ganopolski, A., Rahmstorf, S., 2001. Rapid changes of glacial climate simulated in a coupled climate model. Nature 409, 153-158.

Garreaud, R.D., 2007. Precipitation and circulation covariability in the extratropics. J Climate 20, 4789-4797.

Garreaud, R., Lopez, P., Minvielle, M., Rojas, M. 2013. Large-scale control on the Patagonian Climate. Jrnl. of Climate. 26, 215-230.

Glasser, N.F., Harrison, S., Jansson, K.N., Anderson, K., Cowley, A., 2011. Global sea-level contribution from the Patagonian Icefields since the Little Ice Age maximum. Nat Geosci 4, 303-307.

Glasser, N.F., Jansson, K.N., Duller, G.A.T., Singarayer, J., Holloway, M., Harrison, S., 2016. Glacial lake drainage in Patagonia (13-8 kyr) and response of the adjacent Pacific Ocean. Sci Rep 6, 21064.

Graham, J.A., Stevens, D.P., Heywood, K.J., Wang, Z.M., 2011. North Atlantic climate responses to perturbations in Antarctic Intermediate Water. Clim Dynam 37, 297-311.

Hall, A., Visbeck, M., 2002. Synchronous variability in the southern hemisphere atmosphere, sea ice, and ocean resulting from the annular mode. J Climate 15, 3043-3057.

Hayes, C.T., Anderson, R.F., Fleisher, M.Q., 2011. Opal accumulation rates in the equatorial Pacific and mechanisms of deglaciation. Paleoceanography 26, PA1207.

Hebbeln, D. and cruise participants, 2001. PUCK, Report and Preliminary Results of R/V SONNE cruise SO 156, Valparaiso (Chile) – Talcahuano (Chile), March 29 – May 14, 2001, Berichte, Fachbereich Geowissenschaften, Universitat Bremen, No. 182, 195 pages, Bremen.

Heusser, L., Heusser, C., Mix, A., McManus, J., 2006. Chilean and Southeast Pacific paleoclimate variations during the last glacial cycle: directly correlated pollen and $\delta_{18}O$ records from ODP Site 1234. Quaternary Sci Rev 25, 3404-3415.

Hilgen, F. J., Lourens, L.J., and Van Dam, J.A., 2012. The Neogene period. With contributions by A.G. Beu, A.F. Boyes, R.A. Cooper, W. Krijgsman, J.G. Ogg, W.E. Piller, and D.S. Wilson. In: Gradstein, F.M., Ogg, J.G., Schmitz, M.D., and Ogg, G.M. (Eds.), The Geologic Time Scale: Oxford, United Kingdom (Elsevier), 923–978. https://doi.org/10.1016/B978-0-444-59425-9.00029-9

Kaiser, J., Lamy, F., Arz, H.W., Hebbeln, D., 2007. Dynamics of the millennial-scale sea surface temperature and Patagonian Ice Sheet fluctuations in southern Chile during the last 70kyr (ODP Site 1233). Quatern Int 161, 77-89.

Kaiser, J., Lamy, F., Hebbeln, D., 2005. A 70-kyr sea surface temperature record off southern Chile (Ocean Drilling Program Site 1233). Paleoceanography 20, PA4009.

Kaiser, J., Schefuss, E., Lamy, F., Mohtadi, M., Hebbeln, D., 2008. Glacial to Holocene changes in sea surface temperature and coastal vegetation in north central Chile: high versus low latitude forcing. Quaternary Sci Rev 27, 2064-2075.

Kalansky, J., Rosenthal, Y., Herbert, T., Bova, S., Altabet, M., 2015. Southern Ocean contributions to the Eastern Equatorial Pacific heat content during the Holocene. Earth Planet Sc Lett 424, 158-167.

Kastner, M., Kvenvolden, K.A., Whiticar, M.J., Camerlenghi, A. and Lorenson, T.D., 1995. 10. Relation between pore fluid chemistry and gas hydrates associated with bottom-simulating reflectors at the Cascadia margin, Sites 889 and 892. 1995. Proceedings of the Ocean Drilling Program, Scientific Results, 146(Pt 1), 175-187.

Kim, J.H., Schneider, R.R., Hebbeln, D., Muller, P.J., Wefer, G., 2002. Last deglacial sea-surface temperature evolution in the Southeast Pacific compared to climate changes on the South American continent. Quaternary Sci Rev 21, 2085-2097.

Kissel, C., Leau, H., and Shipboard Participants, 2007. MD159-PACHIDERME IMAGES XV Cruise Report, Punta Arenas (Chile) – Punta Arenas (Chile), Feb. 2 – Feb. 28, 2007.

Knorr, G., Lohmann, G., 2003. Southern Ocean origin for the resumption of Atlantic thermohaline circulation during deglaciation. Nature 424, 532-536.

Knox, F., Mcelroy, M.B., 1984. Changes in Atmospheric $CO_2$ - Influence of the Marine Biota at High-Latitude. J Geophys Res-Atmos 89, 4629-4637.

Lamy, F., Anderson, R., Cortese, G., Esper, O., Gohl, K., Arz, H., Hall, I., Hillenbrand, C., Hubscher, C., Lange, C., Lembke-Jene, L., Ninnemann, U., Pahnke, K., Polonia, A., Stoner, J., Nurnberg, D., Martinez-Garcia, A., Tiedemann, R., Uenzelmann-Nebe, G., and Winckler, G, 2016. Plio-Pleistocene Dynamics of the Pacific Antarctic Circumpolar Current, IODP Proposal Cover Sheet.

Lamy, F., Arz, H.W., Kilianc, R., Lange, C.B., Lembke-Jene, L., Wengler, M., Kaiser, J., Baeza-Urrea, O., Hall, I.R., Harada, N., Tiedemann, R., 2015. Glacial reduction and millennial-scale variations in Drake Passage throughflow. P Natl Acad Sci USA 112, 13496-13501.

Lamy, F., Hebbeln, D., Rohl, U., Wefer, G., 2001. Holocene rainfall variability in southern Chile: a marine record of latitudinal shifts of the Southern Westerlies. Earth Planet Sc Lett 185, 369-382.

Lamy, F., Hebbeln, D., Wefer, G., 1998. Late quaternary precessional cycles of terrigenous sediment input off the Norte Chico, Chile (27.5°S) and palaeoclimatic implications. Palaeogeogr Palaeocl 141, 233-251.

Lamy, F., Kaiser, J., Ninnemann, U., Hebbeln, D., Arz, H.W., Stoner, J., 2004. Antarctic timing of surface water changes off Chile and Patagonian ice sheet response. Science 304, 1959-1962.

Lamy, F., Kilian, R., Arz, H.W., Francois, J.P., Kaiser, J., Prange, M., Steinke, T., 2010. Holocene changes in the position and intensity of the southern westerly wind belt. Nat Geosci 3, 695-699.

Lamy, F., Ruhlemann, C., Hebbeln, D., Wefer, G., 2002. High- and low-latitude climate control on the position of the southern Peru-Chile Current during the Holocene. Paleoceanography 17(2), PA0727.

Lea, D.W., Pak, D.K., Belanger, C.L., Spero, H.J., Hall, M.A., Shackleton, N.J., 2006. Paleoclimate history of Galapagos surface waters over the last 135,000 yr. Quaternary Sci Rev 25, 1152-1167.

Liu, Z.Y., Alexander, M., 2007. Atmospheric bridge, oceanic tunnel, and global climatic teleconnections. Rev Geophys 45, RG2005.

Lowell, T.V., Heusser, C.J., Andersen, B.G., Moreno, P.I., Hauser, A., Heusser, L.E., Schluchter, C., Marchant, D.R., Denton, G.H., 1995. Interhemispheric Correlation of Late Pleistocene Glacial Events. Science 269, 1541-1549.

Lund, S.P., Stoner, J.S., and Lamy, F. 2006. Late Quaternary paleomagnetic secular variation and chronostratigraphy from ODP Sites 1233 and 1234. In Tiedemann, R., Mix, A.C., Richter, C., and Ruddiman, W.F. (Eds.), Proc. ODP, Sci. Results, 202: College Station, TX (Ocean Drilling Program), 1-22.

Mann, M.E., Zhang, Z.H., Hughes, M.K., Bradley, R.S., Miller, S.K., Rutherford, S., Ni, F.B., 2008. Proxy-based reconstructions of hemispheric and global surface temperature variations over the past two millennia. P Natl Acad Sci USA 105, 13252-13257.

Martinez, P., Lamy, F., Robinson, R.R., Pichevin, L., Billy, I., 2006. Atypical delta(15)N variations at the southern boundary of the East Pacific oxygen minimum zone over the last 50 ka. Quaternary Sci Rev 25, 3017-3028.

McManus, J.F., Francois, R., Gherardi, J.M., Keigwin, L.D., Brown-Leger, S., 2004. Collapse and rapid resumption of Atlantic meridional circulation linked to deglacial climate changes. Nature 428, 834-837.

Mix, A.C., Tiedemann, Blum, P. and Shipboard Scientific Party, 2002. Ocean Drilling Program Leg 202 Preliminary Report, Southeast Pacific Paleoceanographic Transects, March 29 – May 30, 2002.

Mix, A.C. and Cruise Participants, 2003. Proceedings of the Ocean Drilling Program, Initial Reports. Volume 202.

Moffa-Sanchez, P., Rosenthal, Y., Babila, T. L., Mohtadi, M., & Zhang, X. (2019). Temperature evolution of the Indo-Pacific Warm Pool over the Holocene and the last deglaciation. *Paleoceanography and Paleoclimatology*.

Mohtadi, M., Rossel, P., Lange, C.B., Pantoja, S., Boning, P., Repeta, D.J., Grunwald, M., Lamy, F., Hebbeln, D., Brumsack, H.J., 2008. Deglacial pattern of circulation and marine productivity in the upwelling region off central-south Chile. Earth Planet Sc Lett 272, 221-230.

Moreno, P.I., Jacobson, G.L., Lowell, T.V., Denton, G.H., 2001. Interhemispheric climate links revealed by a late-glacial cooling episode in southern Chile. Nature 409, 804-808.

Moreno, P.I, Denton, G. H., Moreno, H., Lowell, T.V., Putnam, A. E., and Kaplan, M. R., 2015. Radiocarbon chronology of the last glacial maximum and its termination in northwest Patagonia. Quaternary Sci Rev 122, 233-249.

Murata, Harada, Abe, Uchida, 2017. Mirai Cruise Report, MR16-09: Trans South Pacific Project., JAMSTEC.

Muratli, J.M., Chase, Z., McManus, J., Mix, A., 2010a. Ice-sheet control of continental erosion in central and southern Chile (36°-41°S) over the last 30,000 years. Quaternary Sci Rev 29, 3230-3239.

Muratli, J.M., Chase, Z., Mix, A.C., McManus, J., 2010b. Increased glacial-age ventilation of the Chilean margin by Antarctic Intermediate Water. Nat Geosci 3, 23-26.

Ninnemann, U.S., Charles, C.D., 1997. Regional differences in Quaternary Subantarctic nutrient cycling: Link to intermediate and deep water ventilation. Paleoceanography 12, 560-567.

Ogg, J. G., 2012. Geomagnetic Polarity Time Scale. *In:* Gradstein, F.M., Ogg, J.G., Schmitz, M.D., and Ogg, G.M. (Eds.), *The Geologic Time Scale: Oxford, United Kingdom (Elsevier)*, 85-114. https://doi.org/10.1016/B978-0-444-59425-9.00029-9

Opdyke, M. D., Channel, J. E. T., 1996. Magnetic Stratigraphy Vol 64. Academic Press, London, 346pp.

PAGES 2k Consortium, 2013. Continental-scale temperature variability during the past two millennia. Nat Geosci 6, 339-346.

Pena, L.D., Cacho, I., Ferretti, P., Hall, M.A., 2008. El Niño-Southern Oscillation-like variability during glacial terminations and interlatitudinal teleconnections. Paleoceanography 23, PA3101.

Pisias, N.G., Heusser, L., Heusser, C., Hostetler, S.W., Mix, A.C., Weber, M., 2006. Radiolaria and pollen records from 0 to 50 ka at ODP Site 1233: continental and marine climate records from the Southeast Pacific. Quaternary Sci Rev 25, 455-473.

Post, V.E.A., Groen, J., Kooi, H., Person, M., Ge, S., Edmunds, W.M, 2013, Offshore fresh Groundwater reserves as a global phenomenon, Nature, 504, 71-78

Rignot, E., Rivera, A., Casassa, G., 2003. Contribution of the Patagonia Icefields of South America to sea level rise. Science 302, 434-437.

Robinson, R.S., Martinez, P., Pena, L.D., Cacho, I., 2009. Nitrogen isotopic evidence for deglacial changes in nutrient supply in the eastern equatorial Pacific. Paleoceanography 24, PA4213.

Robinson, R.S., Mix, A., Martinez, P., 2007. Southern Ocean control on the extent of denitrification in the southeast Pacific over the last 70 ka. Quaternary Sci Rev 26, 201-212.

Roemmich, D., Church, J., Gilson, J., Monselesan, D., Sutton, P., Wijffels, S., 2015. Unabated planetary warming and its ocean structure since 2006. Nat Clim Change 5, 240-245.

Rosenthal, Y., Kalansky, J., Morley, A., Linsley, B., 2017. A paleo-perspective on ocean heat content: Lessons from the Holocene and Common Era. Quaternary Sci Rev 155, 1-12.

Rosenthal, Y., Linsley, B.K., Oppo, D.W., 2013. Pacific Ocean Heat Content During the Past 10,000 Years. Science 342, 617-621.

Ruddiman, W.F., 2003. The anthropogenic greenhouse era began thousands of years ago. Climatic Change 61, 261-293.

Russell, J.L., Dixon, K.W., Gnanadesikan, A., Stouffer, R.J., Toggweiler, J.R., 2006a. The Southern Hemisphere westerlies in a warming world: Propping open the door to the deep ocean. J Climate 19, 6382-6390.

Russell, J.L., Stouffer, R.J., Dixon, K.W., 2006b. Intercomparison of the Southern Ocean circulations in IPCC coupled model control simulations. J Climate 19, 4560-4575.

Sarmiento, J.L., Toggweiler, J.R., 1984. A New Model for the Role of the Oceans in Determining Atmospheric Pco2. Nature 308, 621-624.

Schmidtko, S., Johnson, G.C., 2012. Multidecadal Warming and Shoaling of Antarctic Intermediate Water. J Climate 25, 207-221.

Shackleton, N.J., Pisias, N.G., 1985. Atmospheric carbon dioxide, orbital forcing, and climate, The Carbon Cycle and Atmospheric $CO_2$: Natural Variations Archean to Present, pp. 303-317.

Shakun, J.D., Clark, P.U., He, F., Lifton, N.A., Liu, Z.Y., Otto-Bliesner, B.L., 2015. Regional and global forcing of glacier retreat during the last deglaciation. Nat Commun 6, 8059.

Shakun, J.D., Clark, P.U., He, F., Marcott, S.A., Mix, A.C., Liu, Z.Y., Otto-Bliesner, B., Schmittner, A., Bard, E., 2012. Global warming preceded by increasing carbon dioxide concentrations during the last deglaciation. Nature 484, 49-54.

Siani, G., Colin, C., Michel, E., Carel, M., Richter, T., Kissel, C., Dewilde, F., 2010. Late Glacial to Holocene terrigenous sediment record in the Northern Patagonian margin: Paleoclimate implications. Palaeogeogr Palaeocl 297, 26-36.

Siegenthaler, U., Wenk, T., 1984. Rapid Atmospheric Co2 Variations and Ocean Circulation. Nature 308, 624-626.

Sijp, W. P., & England, M. H. (2009). Southern Hemisphere westerly wind control over the ocean's thermohaline circulation. *Journal of Climate*, *22*(5), 1277-1286.

Spero, H.J., Lea, D.W., 2002. The cause of carbon isotope minimum events on glacial terminations. Geochim Cosmochim Ac 66, A731-A731.

Stern, C. 2010, Active Andean volcanism: its geologic and tectonic setting. Revista Geológica de Chile 31 (2): 161-206. [doi:http://dx.doi.org/10.5027/andgeoV31n2-a01]

Stoner, J. S., and St-Onge, G., 2007. Magnetic stratigraphy in paleooceanography: reversal, excursion, paleointensity and secular variation. In Hillaire-Marcel, C., and de Vernal, A. (Eds.), Developments in Marine Geology (Volume 1): Proxies in Late Cenozoic Paleoceanography. R. Stein (Series Ed.): Amsterdam (Elsevier B.V.), 99–138. https://doi.org/10.1016/S1572-5480(07)01008-1

Toggweiler, J.R., Russell, J.L., Carson, S.R., 2006. Midlatitude westerlies, atmospheric $CO_2$, and climate change during the ice ages. Paleoceanography 21, PA2005.

Toggweiler, J.R., Samuels, B., 1993. Is the magnitude of the deep outflow from the Atlantic Ocean actually governed by Southern Hemisphere winds?, The Global Carbon Cycle. NATO ASI (Series I: Global Environmental Change). Springer, Berlin, Heidelberg.

Toggweiler, J.R., Samuels, B., 1995. Effect of Drake Passage on the Global Thermohaline Circulation. Deep-Sea Res Pt I 42, 477-500.

Umling, N. E., & Thunell, R. C. (2017). Synchronous deglacial thermocline and deep-water ventilation in the eastern equatorial Pacific. *Nature communications*, *8*, 14203.

Vera, C., Silvestri, G., Liebmann, B., Gonzalez, P., 2006. Climate change scenarios for seasonal precipitation in South America from IPCC-AR4 models. Geophys Res Lett 33, L13707.